Earth-Science Reviews 250 (2024) 104711

Contents lists available at ScienceDirect

Earth-Science Reviews

journal homepage: www.elsevier.com/locate/earscirev

Invited Review

The Samail subduction zone dilemma: Geochronology of high-pressure rocks from the Saih Hatat window, Oman, reveals juxtaposition of two subduction zones with contrasting thermal histories

Uwe Ring [a,*], Johannes Glodny [b], Reuben Hansman [a,1], Andreas Scharf [c,g], Frank Mattern [c], Ivan Callegari [d], Douwe J.J. van Hinsbergen [e], Arne Willner [f], Yangbaihe Hong [a]

[a] Department of Geological Sciences, Stockholm University, Stockholm, Sweden
[b] Deutsches GeoForschungsZentrum (GFZ), Potsdam, Germany
[c] Department of Earth Sciences, Sultan Qaboos University, Al-Khod, Oman
[d] Department of Applied GeoSciences, GUTech, Halban, Oman
[e] Department of Earth Sciences, Utrecht University, Utrecht, the Netherlands
[f] Institut für Geologie, Mineralogie und Geophysik, Ruhr-Universität, Bochum, Germany
[g] UNESCO Chair on Ophiolite Studies, Sultan Qaboos University, Al-Khod, Oman

ARTICLE INFO

Keywords:
Subduction-zone processes
High-pressure metamorphism
Rb-Sr geochronology
Exhumation, Oman

ABSTRACT

The Samail Ophiolite in the Oman Mountains formed at a Cretaceous subduction zone that was part of a wider Neo-Tethys plate-boundary system. The original configuration and evolution of this plate-boundary system is hidden in a structurally and metamorphically complex nappe stack below the Samail Ophiolite. Previous work provided evidence for high-temperature metamorphism high in the nappe pile (in the metamorphic sole of the Samail Ophiolite), and high-pressure metamorphism in the deepest part of the nappe pile (Saih Hatat window), possibly reflecting a downward younging, progressive accretion history at the Samail subduction zone. However, there is evidence that the two subduction-related metamorphic events are disparate, but temporally overlapping during the mid-Cretaceous.

We present the first geochronologic dataset across the entire high-pressure nappe stack below the Samail Ophiolite, and the shear zones between the high-pressure nappes. Our 22 new Rb—Sr multimineral isochron ages from the Saih Hatat window, along with independent new field mapping and kinematic reconstructions, constrain the timing and geometry of tectonometamorphic events. Our work indicates the existence of a high-pressure metamorphic event in the nappes below the ophiolite that was synchronous with the high-temperature conditions in the metamorphic sole. We argue that the thermal conditions of these synchronous metamorphic events can only be explained through the existence of two Cretaceous subduction zones/segments that underwent distinctly different thermal histories during subduction infancy. We infer that these two subduction zones initially formed at two perpendicular subduction segments at the Arabian margin and subsequently rotated relative to each other and, as a consequence, their records became juxtaposed: (1) The high-temperature metamorphic sole and the Samail Ophiolite both formed above the structurally higher, outboard, 'hot' and rotating Samail subduction zone and, (2) the high-pressure nappes developed within the structurally lower, inboard, 'cold' Ruwi subduction zone. We conclude that the formation and evolution of both subduction zones were likely controlled by the density structure of the mafic-rock-rich Arabian rifted margin and outermost Arabian Platform, and the subsequent arrival of the buoyant, largely mafic-rock-free, full-thickness Arabian lithosphere, which eventually halted subduction at the southern margin of Neo-Tethys.

* Corresponding author.
E-mail address: uwe.ring@geo.su.se (U. Ring).
[1] Now at: Northern Territory Geological Survey, Alice Springs, Australia.

https://doi.org/10.1016/j.earscirev.2024.104711
Received 15 September 2023; Received in revised form 16 January 2024; Accepted 4 February 2024
Available online 10 February 2024

1. Introduction

Understanding how subduction zones initiate and interact with each other in space and time is a fundamental topic in the Earth Sciences. In favourable cases, there are remnants of small segments of oceanic lithosphere exposed on-land, preserved as ophiolites with underlying metamorphic soles. More commonly, high-pressure (P) metamorphic complexes delineate convergent plate boundaries. A challenging task is to reconstruct how fragments of ophiolites and high-P complexes are connected to each other and to the global mosaic of convergent plate boundaries, which is important for understanding past plate interactions and subduction-zone evolution (e.g., Dewey and Bird, 1971; Dewey, 1976a, 1976b; Burke, 2011; Dilek and Furnes, 2011; Stern, 2018).

The Arabian Samail subduction zone, above which the iconic mid-Cretaceous (~96–94 Ma) Samail Ophiolite and its underlying high-temperature (T), 'hot', metamorphic sole formed (105–96 Ma), is considered a prime example for subduction-zone initiation (e.g., Stern and Gerya, 2018; Guilmette et al., 2018). Structurally below the Samail Ophiolite, its sole, and weakly to non-metamorphosed nappes containing deep-sea sediments, is the 'cold' high-P complex of the Saih Hatat window. Extensive metamorphic and structural work focused on the base of the high-P nappe stack and high-quality geochronologic data of the high-P metamorphic rocks yielded late Cretaceous (~80–76 Ma) ages (e.g., El-Shazly et al., 2001; Warren et al., 2003, 2005; Garber et al., 2021). Therefore, the high-P nappe stack has been considered to have formed distinctly (~20 Ma) later than the ophiolite-sole association. Thus, high-P metamorphism is widely viewed as being entirley related to a younger accreted nappe stack that formed when the Samail subduction zone had equilibrated to 'cold' P-T conditions (e.g., Searle et al., 2004; Agard et al., 2010; Garber et al., 2020; Goscombe et al., 2020; Hansman et al., 2021).

Age information, especially in conjunction with structural and metamorphic data, is important for better understanding the formation, exhumation and overall tectonics of subduction complexes along with associated (ultra)high-P and ophiolitic rocks. Therefore, age data are critical for testing the one-subduction-zone interpretation for the convergent margin of Arabia. Most well-studied high-P terranes show simple, structurally downward-propagating younging of the age of high-P metamorphism (e.g., Duchêne et al., 1997; Ring and Layer, 2003; Liu et al., 2009; Vitale Brovarone and Herwartz, 2013; Glodny and Ring, 2022) reflecting progressive underthrusting, accretion and exhumation towards the incoming (downgoing) plate. In line with this are a few observations from the Oman high-P nappes that suggest a more complicated convergent history between the ophiolite and the Arabian margin. Montigny et al. (1988) reported preliminary K-Ar-based white-mica ages of ~95 Ma from the top of the high-P nappe stack suggesting that 'hot' and 'cold' may be of the same age.

However, the K—Ar and $^{40}Ar/^{39}Ar$ data obtained from the Saih Hatat high-P rocks are not easy to interpret. The wide ranges of apparent K—Ar and $^{40}Ar/^{39}Ar$ ages reported by Montigny et al. (1988; 239 to 58 Ma), El-Shazly and Lanphere (1992) (111 to 72 Ma) and El-Shazly et al. (2001) (136 to 85 Ma) suggest that these ages are, at least in part, compromised by excess ^{40}Ar. Warren et al. (2011) conducted a systematic and detailed $^{40}Ar/^{39}Ar$ study on high-P phengite from the Saih Hatat window. The authors reported $^{40}Ar/^{39}Ar$ white-mica ages between 132 and 66 Ma. In some samples, mica cores yielded older ages than the crystal rims, but white-mica rims yielding older ages than cores also occur. Warren et al. (2011) concluded that "the range of $^{40}Ar/^{39}Ar$ ages measured in Oman micas are best interpreted as being related to excess argon" and that "excess argon contamination of metamorphic white micas in high-P terranes is probably the rule rather than the exception". Ring et al. (2020) discussed excess ^{40}Ar problems from the Cycladic Blueschist Unit in the Aegean Sea region and showed that the youngest age of a set of $^{40}Ar/^{39}Ar$ ages variably contaminated by excess ^{40}Ar, as demonstrated by Warren et al. (2011) for the Oman high-P rocks, is possibly close to the true age of the high-P overprint as independently confirmed by other geochronologic data sets. K—Ar and $^{40}Ar/^{39}Ar$ deformation ages from shallow-level (upper middle crust) rocks are often not affected by excess ^{40}Ar, as long as recrystallization processes were penetrative and occurred under open-system conditions allowing the 'old' Ar to escape. Nonetheless, some mid-crustal shear zones incorporated abundant excess ^{40}Ar from fluids derived from devolatization processes in deep crustal levels (Kelley, 2002). In the remainder of this article, we only use a few reported K—Ar and $^{40}Ar/^{39}Ar$ ages from the Oman Mountains, which agree with independent ages obtained by other isotopic dating methods.

Ring et al. (2023) reported Rb—Sr multimineral isochron ages of 99–96 Ma from the highest high-P nappe of the Saih Hatat window suggesting that high-P metamorphism is of the same mid-Cretaceous age as the high-T rocks of the metamorphic sole. Ages of 99–96 Ma make it difficult to form the high-P and the high-T rocks side by side at the same subduction interface. This evidence supports the hypothesis that two different subduction zones/segments became juxtaposed at a later stage (El-Shazly et al., 2001; Breton et al., 2004; Ring et al., 2023). The proposition of two different subduction zones, one 'hot' and one 'cold', of the same age, whose records became juxtaposed within ~20 Ma after their formation needs to be corroborated.

The discovery of mid-Cretaceous high-P metamorphism at the top of the Saih Hatat high-P nappe stack and the proposition of two subduction zones raise two important questions: (1) Is there a near-continuous age progression from the structurally highest nappe down to the base of the high-P stack? This is what might be expected if a single subduction system is envisaged. (2) In which of the two subduction zones did the younger, late Cretaceous high-P rocks form?

In this article, we review (section 2) and discuss (section 3) field and geochronologic evidence for the evolution of the sub-ophiolite nappe stack of Oman. This includes the kinematic context of the Arabian plate boundary, where the non-high-P Samail Ophiolite with its hot subduction-related metamorphic sole and the cold, also subduction-related high-P rocks are located. We also present a comprehensive set of 22 new Rb—Sr multimineral isochron ages for high-P metamorphism and decompression across the entire nappe stack and major shear zones of the Saih Hatat window (section 4) to assess how the timing of subduction initiation, 'hot' sole metamorphism, emplacement of the Samail Ophiolite and 'cold' high-P metamorphism relate to one another. Finally, we interpret the tectonic history of the sub-ophiolitic nappe stack in the context of recent plate kinematic reconstructions and paleomagnetic datasets of Cretaceous southern Neo-Tethys (van Hinsbergen et al., 2019, 2021).

2. Review of existing work defining the tectonic setting

Plate convergence between Arabia and Eurasia since the Jurassic/Cretaceous boundary has mainly been accommodated by northward subduction of Neo-Tethys lithosphere along a 'proto-Zagros/Makran' subduction system (see review by Burg, 2018) (Fig. 1). In the Iranian sector of the subduction system, Holtmann et al. (2022) suggested that the northern Neo-Tethyan ridge entered the subduction zone shortly after 120 Ma, in line with plate reconstructions (Stampfli and Borel, 2002). A mature magmatic arc at the Eurasian side of Neo-Tethys was established by 110 Ma (Burg, 2018). Plate-convergence rates were initially ~1–2 cm a^{-1}, increased to ~5–6 cm a^{-1} at ~118 Ma, and peaked when Arabia rotated counterclockwise between 92 and 80 Ma leading to maximum convergence rates of ~8 cm a^{-1} (Müller et al., 2019; Gürer et al., 2022). After ~80 Ma, convergence rates dropped to ~3 cm a^{-1} and remained nearly constant since.

At the southern end of 'Arabian' Neo-Tethys, mid/late-Cretaceous convergence was accomplished in its early stages by inferred short-lived (~30 Ma) subduction/obduction processes at the northern margin of Arabia in Oman (Hacker, 1991; Searle et al., 1994; Hacker et al., 1996). A regional kinematic reconstruction of this subduction system traced it from a trench-trench-trench triple junction with the Eurasian subduction zone in the eastern Mediterranean to the western Indian Ocean, where it

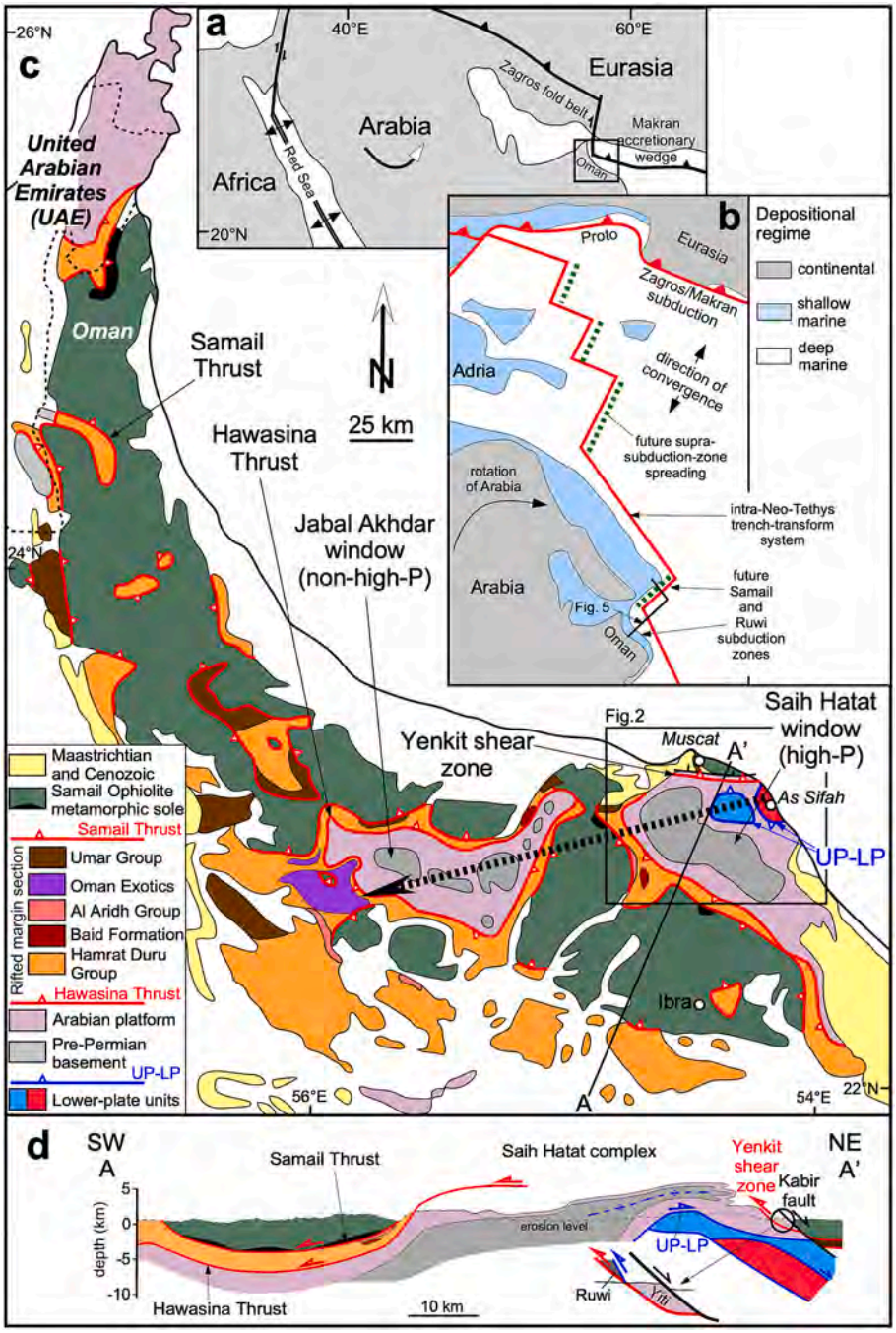

Fig. 1. (a) Current plate-tectonic setting of Arabian Plate. (b) Early Cretaceous plate-tectonic configuration, paleogeography and 'proto' Zagros/Makran subduction system of Neo-Tethys (from van Hinsbergen et al., 2021); position of future Samail subduction zone along transform zone of Neo-Tethys trench-transform system (Hacker et al., 1996; van Hinsbergen et al., 2019, 2021). Black line marks trace of rift-margin section shown in Fig. 5. (c) Geology of Oman Mountains at NE margin of Arabia; Saih Hatat high-pressure (high-P) window at base overlain by non-high-P Samail Ophiolite and Hawasina nappes (rifted-margin section in legend); note scattered outcrops of metamorphic sole (small black patches) below ophiolite. Metamorphic grade in windows decreases towards SW (dashed line with arrowhead), lower plate units below Upper/Lower Plate (UP-LP) Discontinuity (blueschist-facies (blue) and eclogite-facies (red) rocks). Location of Fig. 2 indicated. (d) Simplified NE-SW cross section showing high-P units below non-high-P Samail Ophiolite and Hawasina nappes (modified from Searle et al., 2022); complicated geometry of Ruwi Nappe highlighted; Hawasina Thrust separates high-P from non-high-P rocks in Saih Hatat window. Mid Cretaceous (~110–90 Ma) thrusts in red, late Cretaceous (<~90–70 Ma) thrusts, fold nappe and normal faults in blue, postorogenic faults in black. (For interpretation of the references to colour in this figure legend, the reader is referred to the web version of this article.)

connected to the Mascarene Basin ridge that ended in a ridge-ridge-ridge triple junction in the southern Indian Ocean (van Hinsbergen et al., 2021). This plate boundary accommodated counterclockwise rotation of India relative to Arabia (Gaina et al., 2015), and as a result, the Samail subduction zone at its onset accommodated ~E-W convergence (van Hinsbergen et al., 2021). Paleomagnetic data from the Samail Ophiolite revealed that the Samail subduction zone subsequently rotated >90° clockwise due to subduction rollback (Morris et al., 2016; van Hinsbergen et al., 2019). The rate of oceanic spreading in the ophiolite, as constrained from high-resolution dating of the Samail sheeted dyke sections, revealed full-spreading rates of 10–20 cm a^{-1} (Rioux et al., 2013), far higher than Arabian absolute plate-motion rates (van

Hinsbergen et al., 2021). Therefore, extension must have resulted from rollback, facilitating ocean spreading and the formation of the Samail oceanic lithosphere at 96–94 Ma (Tilton et al., 1981; Rioux et al., 2013, 2021). The ophiolite and underlying accreted units were subsequently underthrust by, and obducted onto the Arabian Platform.

2.1. Architecture of convergent margin

The convergent margin in northeast Oman is lithologically and tectonometamorphically made up of two main divisions: (1) The 'cold' high-P nappes of the Saih Hatat window are structurally at the base, (2) the far-travelled Samail Ophiolite, which together with its metamorphic sole and the underlying remnants of a former deep-sea marine basin (Hawasina nappes) constitute the 'hot' non-high-P overriding plate.

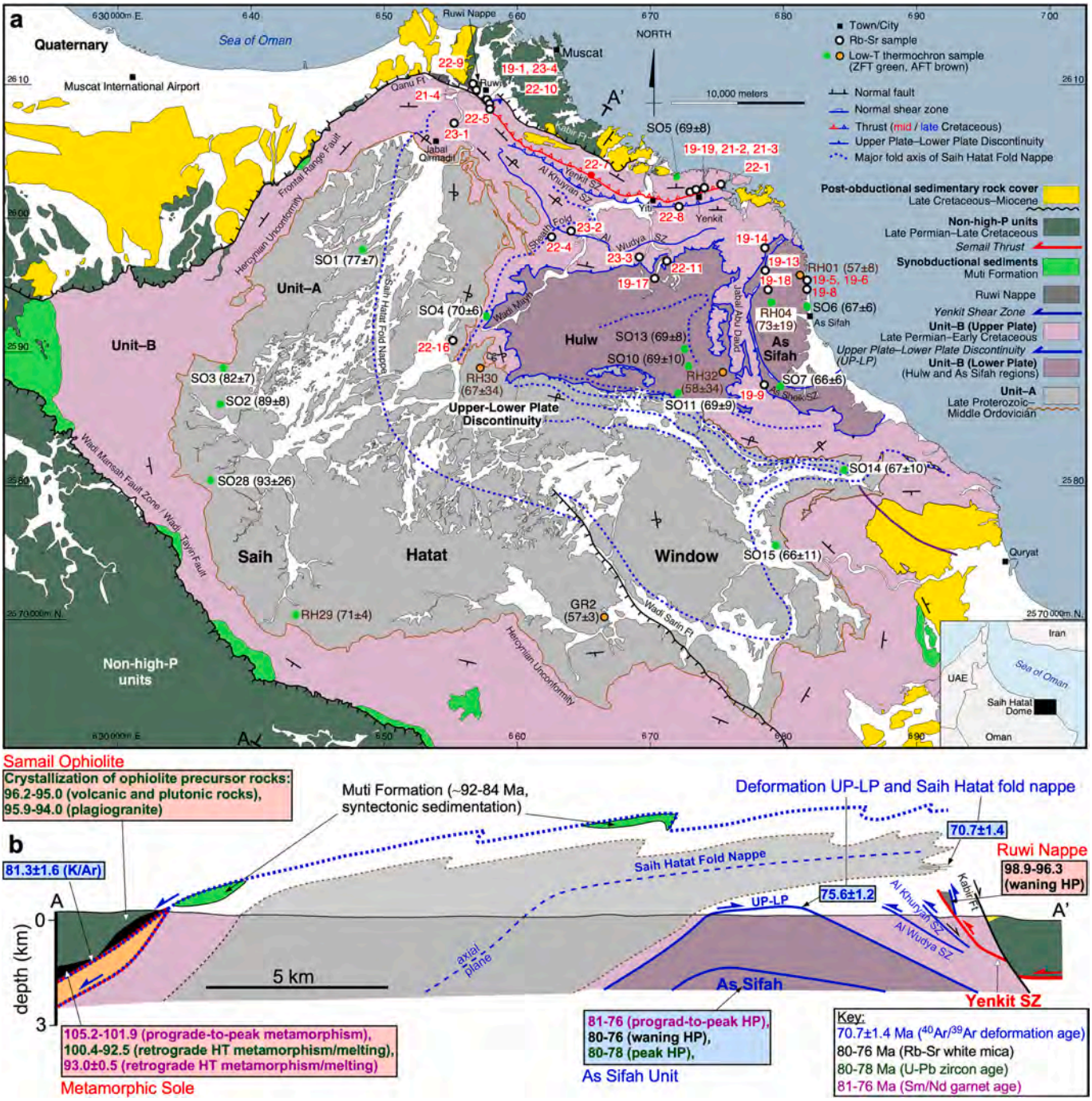

Fig. 2. (a) Simplified geologic map of Saih Hatat window (modified from Hansman et al., 2021) with localities of samples for Rb—Sr geochronology and published zircon- (green dots) and apatite-fission-track (brown dots) ages (Saddiqi et al., 2006; Hansman et al., 2017). Saih Hatat window separated into mid-Cretaceous high-P rocks of Ruwi Nappe (WSW of Muscat) and underlying late Proterozoic to early Cretaceous units high-P metamorphosed in late Cretaceous; non-high-P rocks of overriding plate undivided; Muti Formation shown in lighter green. (b) Schematic cross section showing overall structure and isotopic ages discussed in text. Note waning high-P in Ruwi Nappe largely contemporaneous with high-T metamorphism and subsequent partial melting of metamorphic sole and ophiolite crystallization (reddish boxes with mid Cretaceous ages); ages <82 Ma (blue boxes) in Saih Hatat window and single age at Samail Thrust; colour code for planar structures as Fig. 1. See text for more explanation. (For interpretation of the references to colour in this figure legend, the reader is referred to the web version of this article.)

2.1.1. Saih Hatat high-P window

Because of its almost complete exposure and the lack of a subsequent collision orogeny (Agard et al., 2010), the dome-like Saih Hatat window (Figs. 1, 2) is an outstanding example of a high-P subduction complex. Hence, the Saih Hatat window provides a one-of-a-kind natural laboratory important for understanding the architecture of high-P complexes, their deep exhumation, and the relation of the high-P rocks with the non-high-P overriding plate.

The overall architecture of the Saih Hatat window is complicated and different subdivisions exist (see Fig. 6 in Hansman et al., 2021). We slightly modified the tectonic scheme of Yamato et al. (2007) distinguishing five major high-P nappes, from bottom to top, the As Sifah, Hulw, Al Khuryan-Quryat-Mayh-Saih Hatat (KQMS), Yiti and Ruwi nappes (Fig. 3). Each of the five nappes has an internally coherent P-T history and is surrounded by tectonic boundaries. The nappes may encompass units, which are not necessarily divided by continuous tectonic boundaries (Fig. 3).

The As Sifah Nappe at the bottom of the nappe stack consists of the As Sifah Unit separated by the As Sifah shear zone from the overlying Diqdah Unit (Fig. 3). The As Sheik shear zone occurs between the As Sifah and Hulw nappes. The latter units are separated from the KQMS nappe by the crosscutting Upper Plate–Lower Plate (UP–LP) Discontinuity. Gregory et al. (1998) and Miller et al. (1998) identified this fault as a distinct and spectacular planar surface that truncates structures along a major subhorizontal shear zone (Fig. 4). The UP-LP Discontinuity is associated with a 500–1000-m-thick mylonite zone in its hanging- and footwall. Gray et al. (2005) documented a pronounced strain gradient towards the UP-LP Discontinuity shear zone. Agard et al. (2010) showed that there is no detectable P-T gap across the discontinuity. The large-scale (>2000 km^2) NE-closing, anticlinal, recumbent Saih Hatat fold nappe (Fig. 2) formed in its hanging wall (Gregory et al., 1998; Miller et al., 1998; Gray et al., 2005). All these mid-crustal shear zones and associated folds returned $^{40}Ar/^{39}Ar$ ages between ~80 and 70 Ma (see below).

Above the UP-LP Discontinuity follows the KQMS Nappe. The Yenkit shear zone separates the KQMS Nappe from the overlying Yiti Nappe. Rb—Sr multimineral isochron dating revealed a ~104-≥93 Ma deformation history (Ring et al., 2023). The Yenkit shear zone is the oldest Cretaceous shear zone in the Saih Hatat window and its movement started before the crystallization of the Samail Ophiolite, and synchronously with prograde metamorphism of its sole at ~105–102 Ma (Guilmette et al., 2018). Hence, the Yenkit shear zone is a critical structure. For most of its extent, it separates the Yiti and KQMS nappes. At its western end, the Ruwi Nappe crops out between the Yiti and KQMS nappes (Agard et al., 2010; Searle et al., 2022). Directly beneath the Yenkit shear zone are the Al Khuryan and Al Wudya shear zones, which are prominent shear zone within the KQMS Nappe (Fig. 3).

Except for the Ruwi Nappe, the composite stratigraphy of the nappes of the Saih Hatat window is coherent as shown by the detailed mapping of the French Bureau de Recherches Géologiques et Minières (BRGM) at the scale of 1:100,000 (Le Métour et al., 1986a, 1986b; Villey et al., 1986a, 1986b). It consists of: (1) >2500 m of Neoproterozoic schists of the Hatat Formation, overlain by ~400 m of gray and yellow dolostones (Hijam Formation) and up to 3400-m-thick massive Cambro-Ordovician siliciclastics of the Amdeh Formation (Lovelock et al., 1981) (Unit-A in Fig. 2). (2) Above a late Paleozoic (Hercynian) unconformity follows the Hajar Supergroup, a sequence of Permo-Triassic to Jurassic/Cretaceous carbonates (commonly dolomitic) and minor clastics of the Arabian Platform, intruded by widespread mafic rocks associated with Neo-Tethyan rifting (Chauvet et al., 2009; Weidle et al., 2022, 2023). This sequence encompasses ~1000 m of Permian Saiq Formation, ~700–800 m of Triassic Mahil Formation, ~100 m of Jurassic Sahtan Formation, and ~500 m of the early Cretaceous Kamah Group (Unit-B in Fig. 2).

The Ruwi Nappe does not consist of rocks of the platform sequence. Its lithology is dominated by red, partly gray-green, carpholite-bearing calcareous phyllite. Embedded in the phyllite are carbonate, chert, metaconglomerate, peridotite/serpentinite and lawsonite-bearing mafic lenses giving the Ruwi Nappe a mélange-like internal structure (El-Shazly and Coleman, 1990). With the exception of a ~5000-m^2-sized peridotite peridotite body all blocks are <100 m^2 in size.

Unconformably above the nappes of the Saih Hatat window follows the late Turonian to Coniacian (~92–86 Ma) Muti Formation of the Aruma Group, which represents a foreland basin interpreted to be associated with thrusting of the non-high-P overriding plate onto the Arabian Platform (Robertson, 1987). At the northern and eastern flanks of the Saih Hatat window, the entire Cretaceous and large parts of the Jurassic strata are missing, which is attributed to late Cretaceous foreland bulging and associated erosion (Mattern et al., 2022a). The western and southern parts of the Saih Hatat window host the lowest-grade metamorphic rocks with relatively old zircon-fission-track (ZFT) ages (Table 1) (Saddiqi et al., 2006). The main rock types of the Permian through mid-Cretaceous stratigraphic sequence are depicted in Fig. 5 (see also Fig.I-1 of Data Supplement Item I) and summarized in Scharf et al. (2021); a new, detailed geologic map of the entire Saih Hatat window is provided in the appendix of Hansman et al. (2021).

2.1.2. Non-high-P overriding plate

There is a major metamorphic break between the high-P nappes of the Saih Hatat window and the units above. The rocks of the non-high-P overriding plate start at the base with the Permian to Mesozoic deep-sea sediments of the Hawasina nappes. Intercalated in the Hawasina nappes are the Oman "Exotics": limestones, including reefal carbonate, of the Misfah Platform interpreted as a paleogeographic high dividing the Hawasina Basin into the Hamrat Duru and Umar subbasins (e.g., Glennie et al., 1974; Searle and Graham, 1982; Béchennec et al., 1990) (Fig. 5). The mid-Cretaceous, suprasubduction-zone Samail Ophiolite is at the top of the sequence. At the interface between the ophiolite and the most distal Hawasina rocks of the Umar Subbasin is a metamorphic sole (i.e., metamorphic rocks welded to the base of suprasubduction-zone ophiolites) of the Samail Ophiolite (Searle and Malpas, 1980; Guilmette et al., 2018; Garber et al., 2020; Ambrose et al., 2021).

Our review of the pre-subduction architecture of the Arabian rifted margin outlines the structure of the non-high-P overriding plate (Fig. 5). It mainly follows the work of Béchennec et al. (1986, 1990, 1992), which is based on the detailed BGRM mapping, but also Blechschmidt et al. (2004) and Searle (2007, 2019). A potential shortcoming of the palinspastic restorations is that standard cross sections have not been balanced, and simple in-sequence thrusting has been assumed.

Two rifting phases in the mid-Permian and the mid/late Triassic structured the Arabian margin in Oman. The mid-Permian rifting phase affected the Arabian Platform and inner margin forming the intracontinental Hamrat Duru Subbasin bordered by the Arabian and the Misfah platforms (Blechschmidt et al., 2004). The mid/late Triassic rifting event affected the outermost Hamrat Duru Subbasin separating the Baid Horst from the Misfah Platform by forming the Al Aridh Trough. This rifting event eventually caused drowning of the Baid Horst (Blechschmidt et al., 2004). It also created the distal Umar Subbasin, which transitioned into Neo-Tethyan oceanic lithosphere (Fig. 5). Searle et al. (1980) referred to the distal Umar Subbasin as the "Haybi complex" (Fig. 5). The latter is a series of imbricated rocks that include amphibolite- and greenschist-facies metamorphic rocks of the sole, relatively unmetamorphosed alkalic and tholeiitic volcanic rocks, serpentinite, chert, late Permian and late Triassic Oman exotic limestone blocks (Searle and Graham, 1982), a late Cretaceous sedimentary mélange and various other sedimentary and tectonic mélanges (Searle and Cox, 2002). The Haybi complex overlies marine sediments of the Exotics and underlies the Samail Ophiolite with its metamorphic sole (Searle and Malpas, 1980). The structure of the Arabian rifted margin established by the mid/late Triassic was retained until the onset of mid-Cretaceous subduction.

Apart from the mainly Triassic through Cretaceous Al Aridh Trough and Umar Subbasin, all other parts of the Hawasina Basin have Permo-

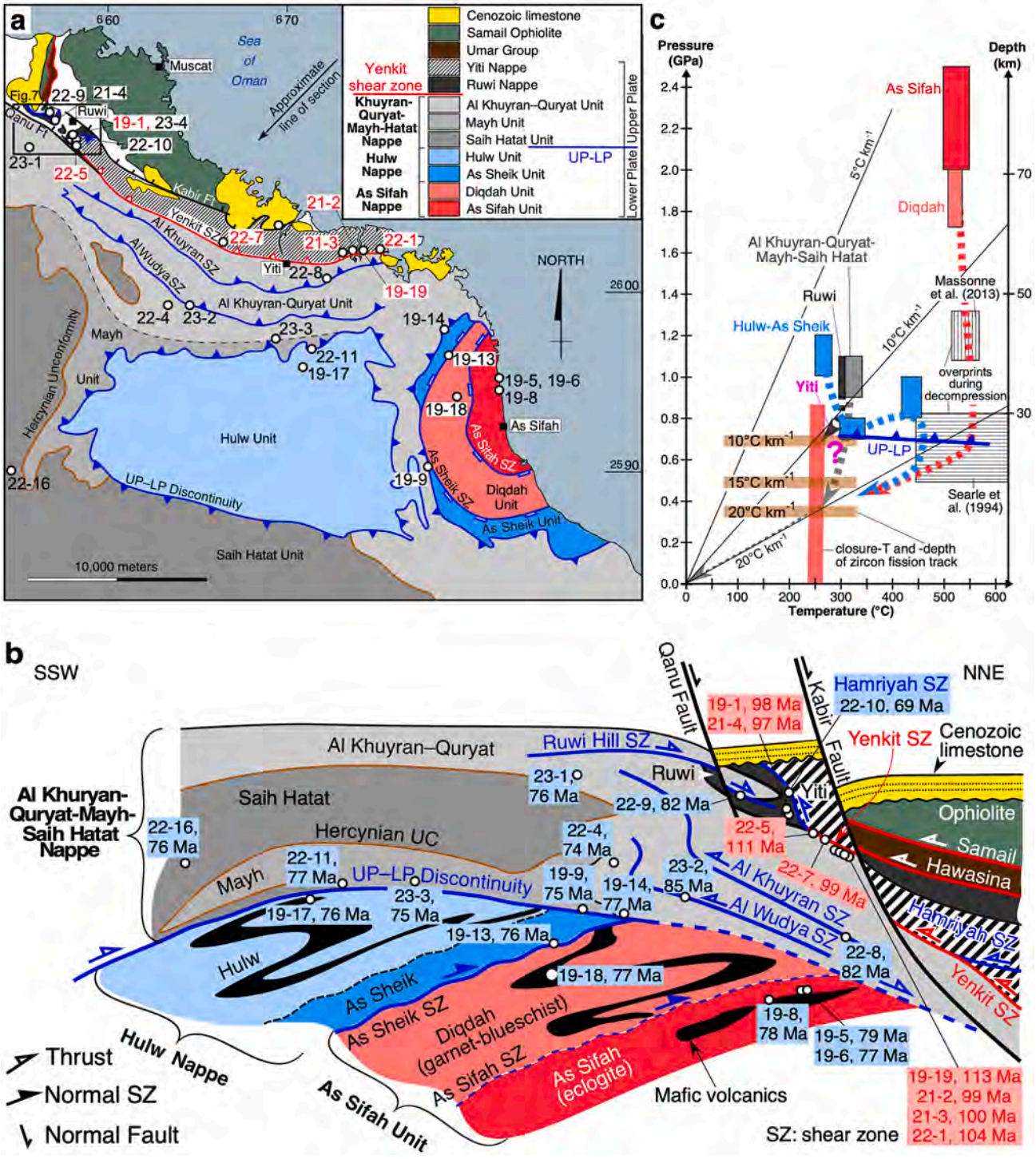

Fig. 3. Simplified structural and metamorphic map of NE Saih Hatat window (a) and schematic cross section (b) (modified from Hansman et al., 2021) with Rb—Sr sample localities in map and projected into cross section, and schematic P-T paths (c); colour code as in Fig. 1. (a) Map of metamorphic units at Saih Hatat window (modified from Yamato et al., 2007); based on P-T estimates and new age data, nine subunits categorized into five major nappes: Ruwi, Yiti, Al Khuryan-Quryat-Mayh-Saih Hatat (KQMS), Hulw, and As Sifah nappes. Note Al Khuyran-Quryat, Mayh, and Saih Hatat units not separated by continuous nappe boundaries, just shear zones of limited lateral extent, and unconformity; position of map in Fig. 7a indicated. (b) Cross section showing interpreted structural relationships and tectonic context of Rb—Sr ages (sample numbers with ages, mid-Cretaceous in red, late Cretaceous in blue); mafic rocks shown schematically in lower plate. (c) P-T data for major nappes based on Searle et al. (1994, 2004), Warren and Waters (2006), Yamato et al. (2007), Agard et al. (2010) and Massonne et al. (2013); note no P-T data available for Yiti Nappe; potential P-T paths dashed as shape not well constrained; thin dashed path for KQMS Nappe extending to origin of P-T diagram marks exhumation of Amdeh quartzite in latest Cretaceous. Note major P gap (~0.7–0.9 GPa) between As Sifah and Hulw nappes; no major P break across UP–LP Discontinuity but T data differ markedly with Hulw Nappe suggested to show major increase in T (and slight increase in P) (Yamato et al., 2007). Closure T for ZFT (Tagami et al., 1996) in red, projected depths of ZFT closure for thermal gradients of 10°, 15° and 20 °C km^{-1} in brown. (For interpretation of the references to colour in this figure legend, the reader is referred to the web version of this article.)

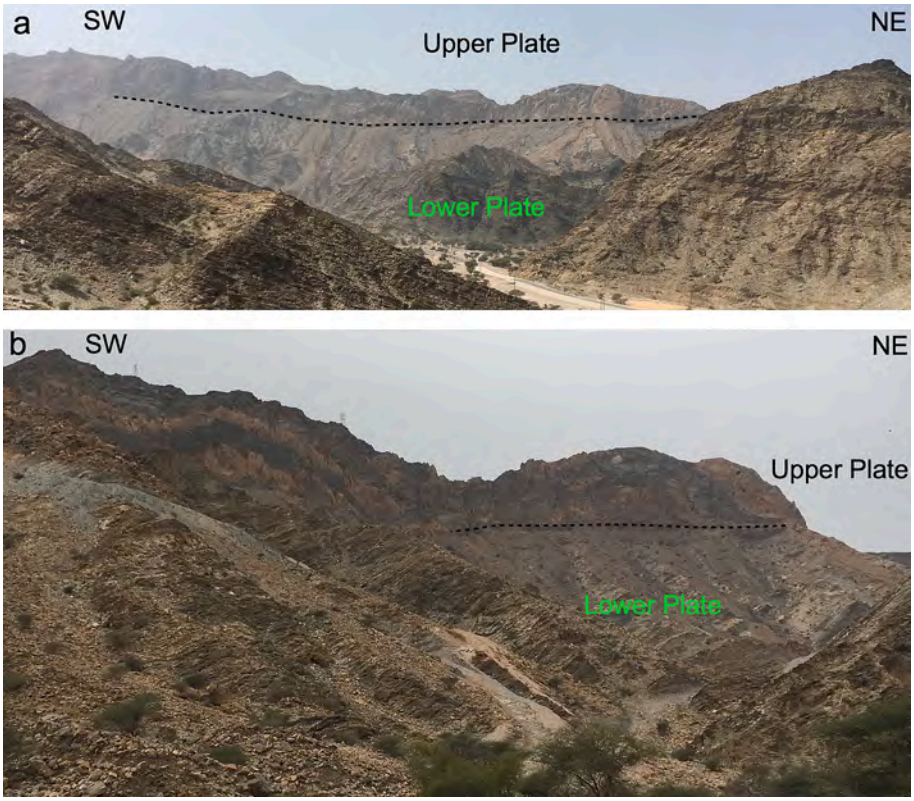

Fig. 4. (a) UP-LP Discontinuity looking N at 23°29′19″N, 58°44′29″E. (b) UP-LP Discontinuity in Wadi Al Zakt at 23°25′02″N, 58°45′20″E looking NW. Note sharp contrast in deformational style across discontinuity.

Table 1
P-T and isotopic data.

High-P Saih Hatat window							Non-high-P overriding plate				
	P	T	Thermal gradient	Age	ZFT, ZHe ages	AFT, AHe ages		P	T	Thermal gradient	Age
	(GPa)	(°C)	°C km^{-1}	(Ma)	(Ma)	(Ma)		(GPa)	(°C)	°C km^{-1}	(Ma)
As Sifah Nappe							Rifted-margin				
As Sifah Unit					76–58, 63–55 [10,11]	65–49, 26–20[10,11]	sequence[12–14]	0.2–0.4	>200–250 °C	<13–34	?
peak[1–3]	2.0–2.5	500–550	5.5–7.5	80–76[7,8]							
decompression[3]	1.1–1.3	510–565	10.5–14				High-grade				
decompression[1]	0.5–0.8	450–550	15–30				sole				
Diqdah Unit[2]	1.7–2.0	510–530	6.9–8.4	?	?	82–64, 22–10[10,11]	*prograde*[15]	c. 0.8	c. 550	c. 20	105.2-
Hulw Nappe[4,5]	0.7–0.9	450–500	13.5–19	?	79–59,?[10,11]	92–24, 31–8[10,11]	*peak*[15–16]	1.0–1.3	730–850	18.5–22	101.9
peak-P[5]	1.0–1.2	250–280	5.5–7.5				*decompression*[15–16]	0.5–0.7	880–950	36–54	100.4–92.4
decompression[5]	0.7–0.8	300–350	9.5–11								
heating[5]	0.8–1.0	c. 450	12–15.1				Low-grade	0.7–1.0	450–550	13–22.5	84.5–95.9
KQMS Nappe[6]	≤1.1	c. 340	c. 8.3	?	119–55, 85–57[10,11]	110–24,?[10,11]	sole[17]				
Yiti Nappe	?	?		?	77–61[10]	?					
Ruwi Nappe[6]	0.9–1.1	<330	c. 10	99–96[9]	?	?					

Data from: [1]Searle et al., 1994; [2]Warren and Waters, 2006; [3]Massonne et al., 2013; [4]Goffé et al., 1988, [5]Yamato et al., 2007; [6]Agard et al., 2010; [7]El-Shazly et al., 2001; [8]Warren et al., 2003, 2005; [9]Ring et al., 2023; [10]Saddiqi et al., 2006; [11]Hansman et al., 2017; [12]Breton et al., 2004; [13]Aldega et al., 2017, 2021; [14]Grobe et al., 2019; [15]Guilmette et al., 2018; [16]Goscombe et al., 2020; [17]Kotowski et al., 2021.
Age range includes maximum 2σ uncertainties.

Triassic carbonates above a pre-Permian basement. At the slopes of the intervening Misfah Platform, mass flows produced megabreccia deposits and turbidites into the adjacent basins (Fig. 5). Both rifting events were accompanied by extensive alkaline magmatism (and the Hamrat Duru Subbasin affected by both events). Mid/late Triassic mid-ocean-ridge-type basalts occur near the continent-ocean transition (Searle et al., 1980) in the outermost Umar Subbasin. Shear-wave velocity data of the rifted-margin crust show abundant mafic intrusions in the lower crust and potentially large mafic to ultramafic bodies at the base of the crust and the lithospheric mantle (Weidle et al., 2022, 2023).

Large parts of the Hamrat Duru Subbasin consist of silicic breccia, turbiditic carbonate and radiolarite (Blechschmidt et al., 2004). The

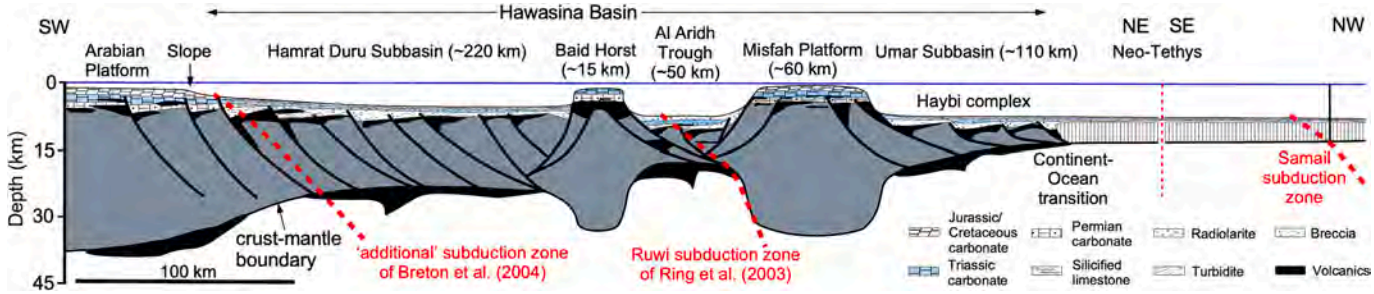

Fig. 5. Mid-Cretaceous paleogeographic restoration of NE Arabian margin before onset of subduction following Béchennec et al. (1986, 1990, 1992), Minoux and Janjou (1986), Breton et al. (2004) and Mattern et al. (2022a); margin structured during two rifting phases during late Permian and middle/late Triassic resulting in Hamrat Duru, Al Aridh and Umar subbasins, latter two basins separated by Baid Horst and Misfah Platform. Note that Baid Horst subsided after mid-Triassic extensional phase and was not bathymetric feature during convergence history. Searle (2007) and Weidle et al. (2022, 2023) envisage vast amounts of Permian/Triassic mafic rocks at distal platform and rifted margin. Note changing direction of rifted-margin section (compare to Fig. 1b). See Data Supplement Item I for different paleogeographic sketch with detailed stratigraphic columns.

latter constitute two distinct depositional phases, the first one from the late Anisian to early Norian (~240–225 Ma), the younger one started in the late Pliensbachian or early Toarcian (~185–180 Ma) and lasted, with some interruptions, until the Coniacian (90–86 Ma) (Blechschmidt et al., 2004). Deep-water facies of Permian age are rare (Blechschmidt et al., 2004). This suggests that, in general, the rifted continental crust was ≥12–15-km-thick, translating into a stretching factor of <2.3–2.9 (assuming plane strain, isochoric extension), i.e., the 220-km-wide Hamrat Duru Subbasin does not represent a hyperextended margin. This would be in line with the presence of widespread mafic rocks, which are uncommon at hyperextended margins (cf. Doré and Lundin, 2015). The narrow Al Aridh Trough contains distinctly more radiolarite suggesting deep-water conditions and, thus, thinner crust and a greater stretching factor than the Hamrat Duru Subbasin.

2.2. Metamorphism

2.2.1. Saih Hatat high-P window

Reviews by Goscombe et al. (2020) and Hansman et al. (2021) summarized and discussed P-T data (Table 1) from the Saih-Hatat window in detail. Metamorphic P-T is highest in the As Sifah Nappe (peak P-T of 2.0–2.5 GPa and 500–550 °C in the As Sifah Unit; 1.7–2.0 GPa at 510–530 °C in the Diqdah Unit) (Searle et al., 1994; Warren and Waters, 2006; Massonne et al., 2013). This was followed by re-equilibration during decompression (Table 1; Fig. 3c).

For the Hulw Nappe, chloritoid-bearing schist and glaucophane-bearing metabasite provided peak P-T of 0.7–0.9 GPa at 450–500 °C (Goffé et al., 1988). Yamato et al. (2007) suggested a P-T path showing many segments (Fig. 3c), which is strikingly different to the P-T paths of the other high-P nappes. The nappes above the UP-LP Discontinuity record similar P and T of 1.0–1.2 GPa and 320–340 °C (Goffé et al., 1988; Agard et al., 2010) (Fig. 3c).

2.2.2. Non-high-P overriding plate

The rocks of the rifted-margin succession are hardly metamorphosed. P-T conditions are 0.2–0.4 GPa and <200–250 °C (e.g., Breton et al., 2004; Aldega et al., 2017, 2021; Grobe et al., 2019). The metamorphic sole of the Samail Ophiolite is the only distinctly metamorphosed unit. It consists of high-grade granulite/upper-amphibolite-facies rocks tectonically above low-grade greenschist/lower amphibolite-facies rocks (e.g., Searle and Cox, 2002; Cowan et al., 2014). After prograde to peak P-T, the high-grade sole heated up during decompression and locally attained temperatures of up to ~850–900 °C at ~20 km depth. The low-grade sole has distinctly lower P-T conditions (Kotowski et al., 2021) (Table 1).

2.3. Age data for metamorphism and crystallization of Samail Ophiolite

2.3.1. Saih Hatat high-P window – peak metamorphism

Rb—Sr white-mica analyses by El-Shazly et al. (2001) constrained the age of peak high-P metamorphism of the As Sifah Unit at 78 ± 2 Ma (all ages reported with 2σ uncertainties) (Table 2). This age is confirmed by U—Pb zircon and rutile dating (79 ± 1 Ma; Warren et al., 2003, 2005) and Sm/Nd whole rock-garnet(−glaucophane) ages of 80.9 ± 1.3 to 77.5 ± 2.2 Ma (Garber et al., 2021).

There are some indications that high-P metamorphism in the Ruwi Nappe already occurred at 95 ± 8 Ma (K—Ar white-mica age of Montigny et al., 1988). Recent Rb—Sr multimineral isotopic data by Ring et al. (2023) provided ages of 98.03 ± 0.88 and 97.04 ± 0.76 Ma for waning high-P metamorphism of the Ruwi Nappe. The Rb—Sr ages corroborate the suggestion of Searle et al. (2022), (their Fig. 6a) that the Ruwi Nappe was accreted already during the mid-Cretaceous. In contrast, El-Shazly and Lanphere (1992) reported a $^{40}Ar/^{39}Ar$ white-

Table 2
Age data (in Ma) for metamorphism of metamorphic sole and high-P nappes of Saih Hatat window.

Non-high-P overriding	*Prograde/Peak-high-T*
High-grade metamorphic sole	105.2–101.9 (Lu/Hf grt)[1] 102.0–93.9 (U—Pb ttn, Th—Pb mnz)[2] 100.4–92.5 (U—Pb zrn)[3]
Low-grade metamorphic sole	95.9–84.5 (U—Pb ttn)[4]

Saih Hatat high-P nappes (structurally from top to bottom)	*Peak high-P*	*Decompression*
Ruwi Nappe	98.9–96.3 (Rb—Sr wm)[5] 95 ± 8 (K—Ar wm)[7]	79.1 ± 2.0 (Rb—Sr wm)[6] 80.2 ± 1.6 (Ar/Ar wm)[8]
Yiti Nappe	?	
KQMS Nappe	75.5 ± 4.4 (Rb—Sr wm)[6]	
Hulw Nappe	76.4 ± 1.9 (Rb—Sr wm)[6]	
As Sifah Nappe	80–76 (Rb—Sr wm)[9] 80–78 (U—Pb zrn, rt)[10] 81.2–75.3 (Sm/Nd grt)[11] 79.8–75.4 (Rb—Sr wm)[6]	78.7 ± 2.0 (Rb—Sr wm)[6] 77.0 ± 1.3 (Rb—Sr wm)[6]

Age span given includes maximum 2σ uncertainties of analyses, for single ages 2σ errors provided.
[1]Guilmette et al. (2018), [2]Soret et al. (2022), [3]Garber et al. (2020), [4]Kotowski et al. (2021), [5]Ring et al. (2023), [6]this study, [7]Montigny et al. (1988), [8]El-Shazly and Lanphere (1992), [9]El-Shazly et al. (2001), [10]Warren et al. (2003, 2005), [11]Garber et al. (2021) – age range represents average between prograde, peak and early decompression stages.
Grt = garnet, ttn = titanite, mnz = monazite, zrn = zircon, wm = white mica, rt = rutile.

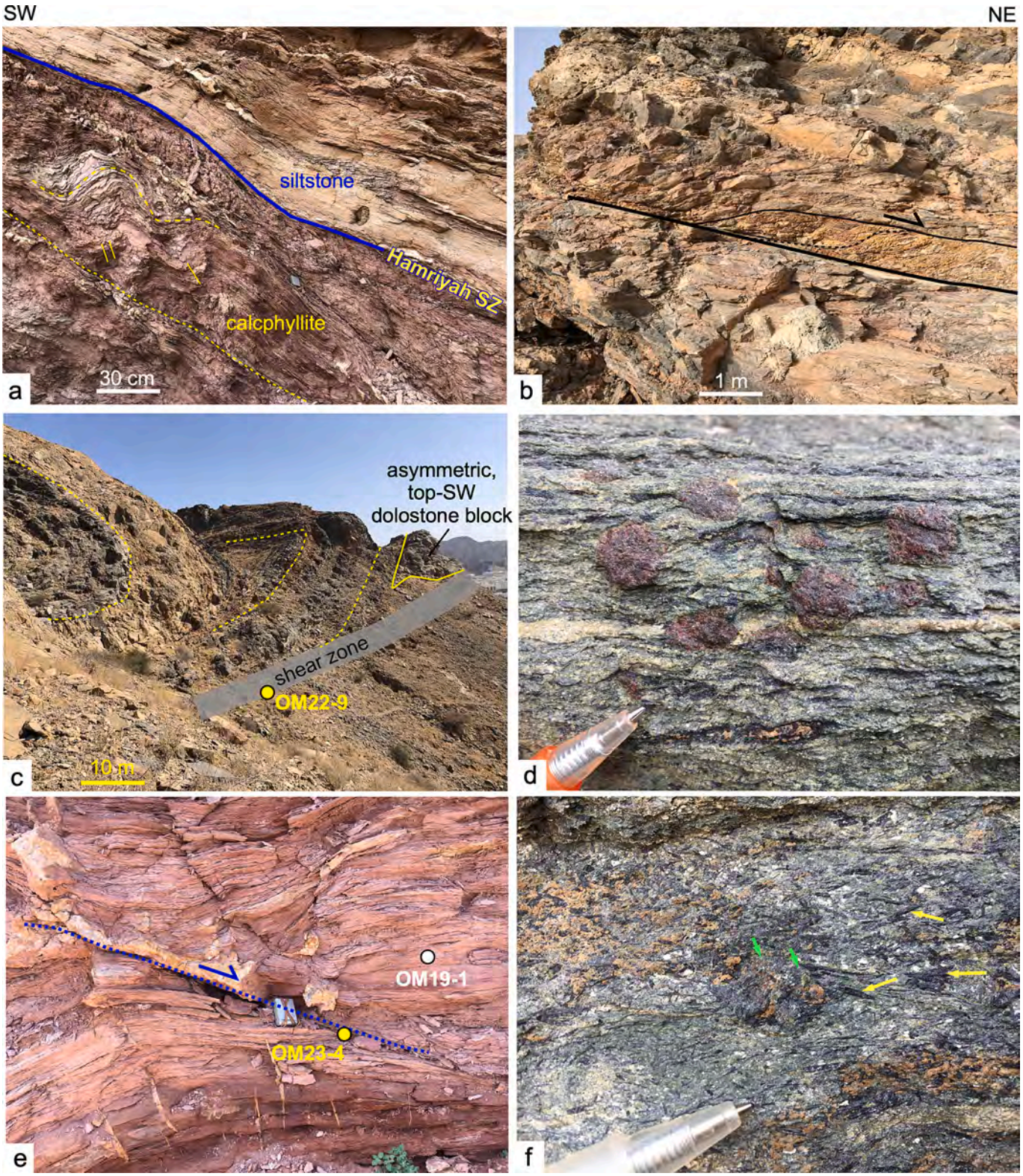

Fig. 6. (a) Hamyriah shear zone at top of Ruwi Nappe, SW-verging folds, NE-dipping crenulation cleavage in calcareous phyllite (sample OM22–10) (23°34′33”N, 58°33′01″E). (b) Top-NE S-C-type structures in localized shear zone at contact between Mahil dolostone of Yiti Nappe and overlying Sahtan Group rocks (23°31′44”N, 58°39′56″E). (c) Ruwi Hill shear zone and overlying recumbent N-closing fold made up of Sahtan Group rocks (OM22–9) (23°35′29”N, 58°32′22″E). (d) Pristine eclogite with cm-sized garnet; omphacite, glaucophane and epidote define foliation, As Sifah Nappe (23°27′19”N, 58°46′47″E). (e) Red carpholite-bearing phyllite of Ruwi Nappe at Yiti Street SE of Al Hamriyah (23°34′32”N, 58°32′59″E, sample OM19–1); top-NE shear bands at ~20° to main foliation (sample OM23–4). (f) Outcrop showing stable glaucophane (yellow arrows) while garnet and omphacite show rinds of epidote and quartz formed during initial decompression (green arrows), As Sifah Nappe (23°28′08”N, 58°42′22″E). SW and NE indicated at top provide orientation for all samples. (g) Hematite-rich calcareous schist with top-NE shear bands, sample OM19–6, As Sifah Nappe (23°27′33”N 58°46′49″E). (h) Carbonate mylonite in Yenkit shear zone with S-vergent asymmetric folds (23°31′07”N, 58°42′20″E) (sample OM19–19). (i) Top-SW SC structure in calcareous phyllite of Al Khuryan shear zone (sample OM22–8, 23°30′47”N 58°41′53″E). (j) Carbonate mylonite in As

Sheik shear zone showing top-NE shear sense, sample OM19–13 (23°28′52”N, 58°45′10″E). (k) Top-NE shear sense in mylonitic calcschist of UP-LP Discontinuity shear zone, sample OM19–14 (23°29′19”N, 58°44′30″E). (l) Top-NE shear sense in fine-grained silvery-green mylonitic rock, sample OM19–9 (23°23′35”N, 58°45′09″E). SW and NE indicated at top provides orientation for all samples. (For interpretation of the references to colour in this figure legend, the reader is referred to the web version of this article.)

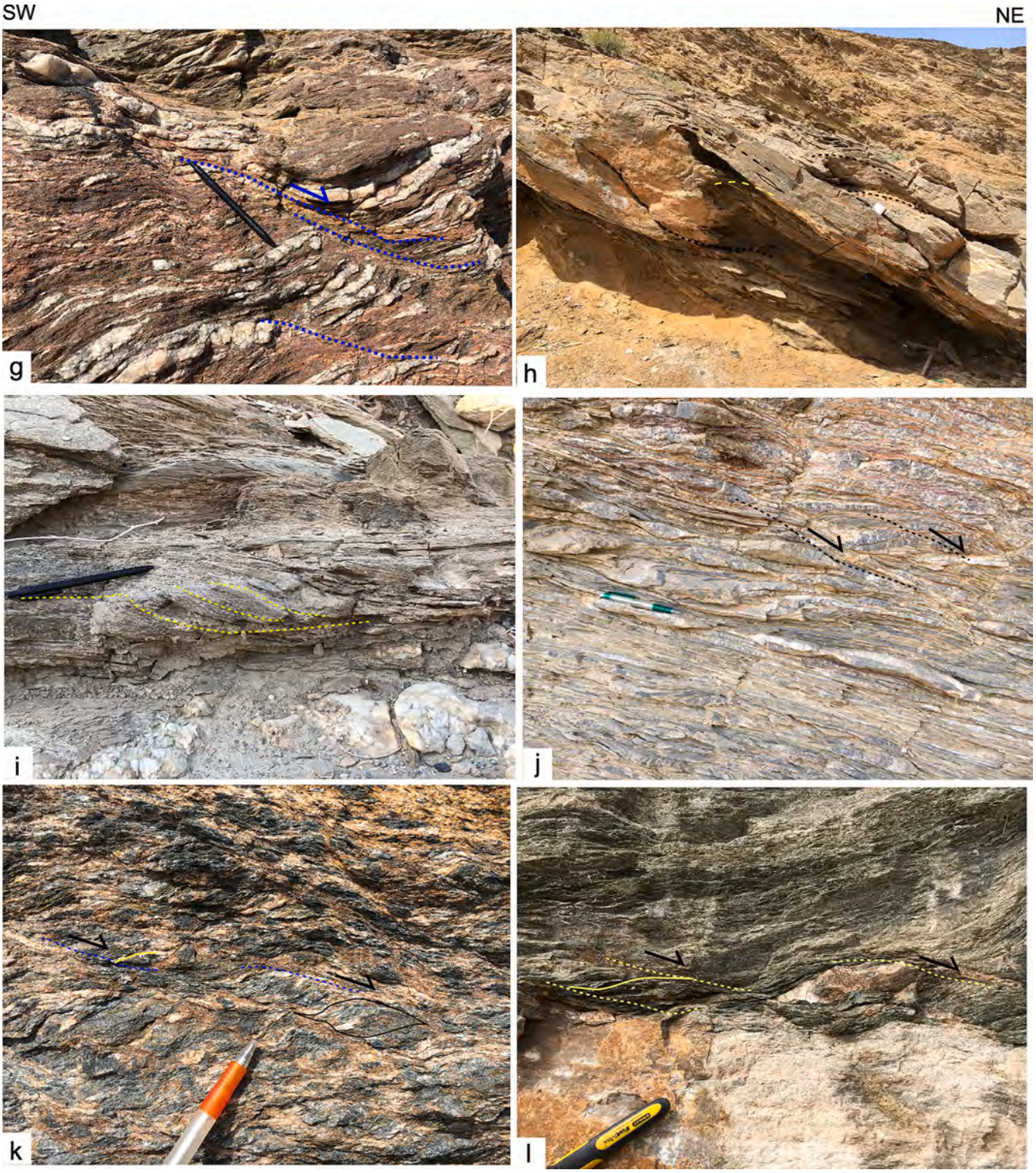

Fig. 6. (*continued*).

mica age of 80.2 ± 1.6 Ma from a lawsonite schist of the Ruwi Nappe.

2.3.2. Saih Hatat high-P window – cooling ages

The fission-track and (U—Th)/He cooling ages are summarized in Fig. 2 and Table 1. Despite the relatively large uncertainties, the age data

are consistent and show cooling below ~250 °C and 110 °C (closure T for ZFT and apatite fission tracks (AFT), respectively; Tagami et al., 1996; Gallagher, 1995) after ~70 Ma. In general, low-T thermochronologic ages for rocks above the UP-LP Discontinuity are older than those below the discontinuity.

2.3.3. Crystallization of Samail Ophiolite

A plethora of detailed studies showed that the Samail Ophiolite formed at 96.2 to 95.0 Ma, with plagiogranite crystallizing between 95.9 and 94.0 Ma (Tilton et al., 1981; Rioux et al., 2021, and references therein). Hacker (1991) and Hacker et al. (1996) proposed that the Samail Ophiolite was initially rapidly emplaced at rates of ~15 cm a^{-1}, first by intraoceanic thrusting over young and hot suprasubduction-zone lithosphere followed by equally fast thrusting over cold Triassic/Jurassic oceanic lithosphere. Thrust propagation rates of ~15 cm a^{-1} at a 30°-dipping thrust are greater than the plate-convergence rates, but are of the same order as the full-spreading rates reported by Rioux et al. (2013).

2.3.4. Metamorphic sole

Three identical Lu—Hf garnet-whole rock isochron ages of 105.2 to 101.9 Ma (age range includes 2σ uncertainties; the weighted mean of the garnet ages is 103.7 ± 0.7 Ma) (Guilmette et al., 2018) constrain the timing of late prograde to peak high-T metamorphism of the sole. Soret et al. (2022) reported U—Pb titanite and Th—Pb monazite ages ranging from 100 ± 2 to 94.7 ± 0.8 Ma (with most ages in the 99–97 Ma range) and interpreted the ages to reflect prograde to peak metamorphism (Table 2).

Overall, the prograde to peak metamorphic ages for the sole would allow up to 10 Ma between initiation of subduction, partial melting and formation of new suprasubduction-zone oceanic lithosphere at 96–94 Ma. Partial melting during decompression of the exhuming sole has been constrained by the mean of five U—Pb zircon ages of 96.19 ± 0.14 Ma which reflect crystallization of late, highly fractionated melts at a time the rocks cooled to ~700 °C, and a titanite U—Pb age of 95.60 ± 0.27 Ma interpreted to date cooling through 650 to 600 °C (Guilmette et al., 2018).

Others (e.g., Hacker et al., 1996; Garber et al., 2020; Rioux et al., 2021) suggested that coinciding $^{40}Ar/^{39}Ar$ and U—Pb ages from the metamorphic sole and the suprasubduction-zone oceanic lithosphere imply that sole metamorphism and upper-plate spreading were synchronous. U—Pb zircon-rim ages of 98.7 ± 1.7 to 94.1 ± 1.6 Ma (i.e., 100.4 to 92.5 Ma) (Garber et al., 2020) were interpreted to date metamorphism and, thus, indirectly as a minimum age for the initiation of subduction. In addition, Garber et al. (2020) reported a modelled Lu—Hf garnet-whole rock isochron age of 93.0 ± 0.5 Ma for prograde to peak metamorphism of the sole (growth from ~550 °C/0.4 GPa to 630–700 °C/0.63–0.87 GPa). Hacker et al. (1996, 1997) proposed that amphibolite-facies metamorphism and deformation was completed by ~93 Ma. In line with this, Garber et al. (2020) reported a U—Pb titanite age of 92.2 ± 1.8 Ma for the juxtaposition of high- and low-grade rocks of the sole. The latter ages agree, within uncertainties, with two U—Pb titanite ages of 90.2 ± 5.7 and 90.8 ± 2.5 Ma for the tectonically underlying low-grade sole (Kotowski et al., 2021).

Garber et al. (2020) also reported a U—Pb age of 106.9 ± 2.3 Ma for a zircon core from the metamorphic sole and interpreted the core to be detrital. If so, this age would be a maximum age for the onset of subduction.

2.4. Thickness of Samail Ophiolite

Béchennec et al. (1992), Scharf et al. (2021) and Weidle et al. (2022) estimated the current thickness of the Samail Ophiolite at ~10 to 5 km. Aldega et al. (2017, 2021) used paleothermal indicators to calculate a 4.1–5.5 km thick, southward tapering ophiolite wedge.

The original thickness of the ophiolite is unknown. Hacker and Gnos (1997) discussed various models assuming that the metamorphic sole formed at ~40 km depth. They considered three options: (1) A 15–20 km thick thrust sheet lay on top of the ophiolite (Nicolas, 1989), (2) the ophiolite was a single thrust sheet 30–40 km thick and the sole rocks were exhumed by normal faulting to their present position beneath a thinner section of the ophiolite, or (3) the ophiolite was a single thrust sheet 30–40 km thick and has subsequently been thinned during extension, a view also advocated by van Hinsbergen et al. (2015). Hacker and Gnos (1997) admitted that all three options have shortcomings. van Hinsbergen et al. (2015) suggested that the ophiolite's spreading, which is an extensional process, caused the shallowing of the nascent plate contact.

2.5. Sedimentary response to subduction of high-P nappes and obduction of Samail Ophiolite

The Arabian Platform is considered stable until ~92 Ma, as inferred from the sediments of the latest Aptian to mid-Turonian (~114-~92 Ma) Wasia Group (Searle et al., 2003; Forbes et al., 2010). The latter occurs over large parts of Oman, thins towards the southwest and mainly consists of limestone with some shale reflecting a subtidal platform environment (Rabu et al., 1986; Forbes et al., 2010). Prior to obduction of the overriding plate onto the Arabian Platform, a flexure of the latter is recorded by the erosion of the platform deposits above the forebulge, the "Wasia-Aruma break" (Glennie et al., 1974).

The formation and fill of the foreland basin are reflected by the Aruma Group. The latter consists of the Muti Formation (~92–84 Ma) in the Oman Mountains, and the subsurface Fiqa Formation (~88–72 Ma) southwest of the mountain chain (Warburton et al., 1990). Correlative with the upper Fiqa Formation are the Campanian (~83–72 Ma) deep-marine mudstones of the Juwaiza Formation exposed in the northern Oman Mountains. The Juwaiza Formation reflects rapid subsidence starting at ~83 Ma (Abdelmaksoud et al., 2022).

The conglomerates and turbidites of the Muti Formation contain fossil-bearing clasts derived from all members of the Hajar Supergroup eroded off the forebulge of the Arabian Platform (Glennie, 2005). Notably, there is no detritus from the advancing Samail Ophiolite thrust wedge in the Muti Formation (Robertson, 1987). Only the younger Juwaiza Formation contains ophiolite detritus (Rabu et al., 1993; Abdelmaksoud et al., 2022).

Different opinions about forebulge migration exist. Robertson (1987) proposed that the forebulge migrated to the southwest. Warburton et al. (1990) critically discussed the lateral significance of the Wasia-Aruma Break with respect to potential forebulge migration. They compared the magnitude of the hiatus on the forebulge and on the foredeep flexure, and concluded that the forebulge remained in situ while the basin narrowed during top-to-the-SW thrusting of the overriding plate. Based on burial curves, Warburton et al. (1990) also proposed that the forebulge grew coevally in its present location with flexing of the foreland panel to the northeast. Mattern et al. (2022a) argued that the lack of evidence for forebulge migration, such as lithoclasts from underlying Jurassic and early Cretaceous formations of the Hajar Supergroup, reflects a stationary forebulge and suggested that lateral forebulge migration was largely prevented by the increasing thickness of the Arabian lithosphere to the southwest.

The Aruma Group sediments are supposed to reflect thrusting of the overriding plate onto the foreland basin and the underlying Arabian Platform (e.g., Robertson, 1987). If so, the obduction of the non-high-P overriding plate onto the Arabian Platform preceded (by ≥10 Ma) the second stage of high-P metamorphism at 80–76 Ma.

The high- and non-high-P tectonic divisions in the Oman Mountains are blanketed by late/postorogenic sediments. At the bottom is the Maastrichtian (~72–66 Ma) Al-Khod (or Qahlah) Formation, which was deposited after the obduction of the Samail Ophiolite (Scharf et al., 2021, and references therein). The Al-Khod Formation displays a classic unroofing sequence with ophiolite clasts at the bottom, carbonate

pebbles derived from the Hajar Supergroup above, and quartzite of the pre-Permian Amdeh Formation at the top (Mann and Hanna, 1990; Nolan et al., 1990). The Al-Khod Formation indicates the resurrection of a stable Arabian Platform (Glennie et al., 1974; Abbasi et al., 2014) and, thus, the end of the Cretaceous Samail orogeny (Mattern et al., 2020).

2.6. One or two subduction zones?

The Samail subduction zone is commonly regarded as the only subduction zone at the Arabian margin (e.g., Agard et al., 2010; Searle, 2007; Rioux et al., 2021). Thermal gradients in this subduction zone were ~20–25 °C km^{-1} during prograde-to-peak metamorphism and increased to >30 °C km^{-1} during subsequent decompression, partial melting and suprasubduction-zone crystallization of the Samail Ophiolite (Searle and Cox, 2002; Ambrose et al., 2021; Garber et al., 2020) (Table 1). Most workers explain sole metamorphism, ophiolite obduction, and the distinctly younger (~20 Ma) formation of the high-P nappes and their exhumation by tectonic processes in this single subduction zone. However, Searle et al. (2022), (their Fig. 6a) envisaged a mid-Cretaceous age of 96–94 Ma for high-P metamorphism of the Ruwi Nappe, coeval with crystallization of the Samail Ophiolite.

Some researchers discussed the existence of two subduction zones. Hacker and Gnos (1997) considered that the Ruwi Nappe may be an old high-P unit forming before or coeval with the crystallization of the ophiolite. For this possibility, they suggested that the metamorphic sole formed in an intraoceanic subduction zone and the high-P rocks in a second subduction zone closer to the Arabian margin (their Fig. 3) (see also El-Shazly et al., 2001). Hacker and Gnos (1997) maintained that either a one- or two-subduction-zone proposition would be compatible with the geologic record.

Breton et al. (2004), (their Fig. 8) proposed a tectonic model involving two NE-dipping subduction zones. In line with all others, the authors invoked an outer, intraoceanic Samail subduction zone, but they were quite specific about the inner, intracontinental subduction zone near the Arabian Platform (Fig. 5). Breton et al. (2004) defined the 'North Muscat microplate' in between these two subduction zones and suggested that the Samail subduction zone formed first, followed by intracontinental subduction at 95–90 Ma.

New geochronologic data by Ring et al. (2023) demonstrated that a second, mature (Ruwi) subduction zone must have existed inboard of the Samail subduction zone (Fig. 5) and that the final stages of high-P metamorphism at thermal gradients of ~8–10 °C km^{-1} of the Ruwi Nappe occurred at 99–96 Ma in the Ruwi subduction zone. Ring et al. (2023) further suggested that the Ruwi subduction zone was the first to form at the Arabian margin at ≥110 Ma as a result of the increased Arabia-Eurasia convergence rate.

Restoring the orientation of the Samail subduction zone using paleomagnetic data of the gabbro sequences (Morris et al., 2016) and the sheeted dykes (van Hinsbergen et al., 2019) revealed that the ophiolite has rotated 90° in the south and 150° in the southwest from an original NE-SW orientation (Fig. 1b). Because the dykes formed in that orientation, spreading was perpendicular to the trench. Such a subduction zone is parallel to the West Oman/UAE Arabian margin in a paleomagnetic reference frame (van Hinsbergen et al., 2019). Subduction zones are plate boundaries that must connect to other plate boundaries, or end in triple junctions. There is no evidence that the NE-SW striking subduction segment continued into the Arabian continent. Thus, it must have connected to a plate boundary that was parallel to the northeast Oman margin. van Hinsbergen et al. (2021) tentatively inferred such a subduction segment. Their kinematic reconstruction predicted that a NW-SE-striking plate boundary along the northeastern Oman margin must have accommodated oblique convergence and was overthrust by the Samail Ophiolite, but they did not provide geological evidence for the existence of this subduction segment.

3. Discussion of reviewed data: controversies and open questions

This discussion emphasizes problems in the understanding of aspects of Oman geology and provides the motivation for the Rb—Sr data presented in section 4. It will also set the scene for the general discussion in section 5.

3.1. Architecture of convergent margin

3.1.1. Yenkit shear zone and Yiti Nappe

We showed that the Yenkit shear zone is the oldest major Cretaceous shear zone in the Saih Hatat window and underlies the Yiti Nappe. Important questions are: (1) Does the Yenkit shear zone continue above or below the Ruwi Nappe (which is the oldest high-P nappe), and (2) whether or not the Yiti Nappe is a high-P nappe?

Agard et al. (2010), (their Fig. 3) suggested that the Yenkit shear zone occurs above the Ruwi Nappe and is associated with top-to-the-NE kinematic indicators. Hansman et al. (2021) and Ring et al. (2023) agreed with widespread top-to-the-NE kinematics of the upper Ruwi Nappe. However, Hansman et al. (2021, their Fig. 18) also showed that the upper contact of the Ruwi Nappe directly underneath the Yiti Nappe is characterized by a structurally late crenulation cleavage associated with top-to-the-SW kinematic indicators (Fig. 6a). This observation makes it feasible that the small segment of the Yenkit shear zone above the Ruwi Nappe represents a late, re-imbricating out-of-sequence thrust that reactivated a segment of the Yenkit shear zone, which we name the "Hamriyah shear zone" (Fig. 7).

For better understanding the geometry of the upper parts of the Saih Hatat window, we mapped the contacts of the Ruwi Nappe and produced geometrically feasible cross sections (Fig. 7). The cross sections (Fig. 7b, c) match the surface geology and faulting/shearing is restorable (see Fig. II-1 in Data Supplement Item II, which shows evolutionary steps that duplicate the geometry and match the age data, forming the basis for the cross sections in Fig. 7b, c). Nevertheless, folding is less constrained (not balanced) as folds are tight and overturned, and plane strain cannot be assumed. The overall architecture of the area is obscured by the postorogenic Qanu Fault, which is a N-dipping normal fault (Mattern and Scharf, 2018; Scharf et al., 2020) (Fig. 7). Southeast of Al Hamriyah township, the Qanu Fault splays and its displacement diminishes. Top-to-the-N normal displacement appears to have been transferred by a structural relay-ramp to the Kabir Fault in the northeast. About 50 m above the Qanu Fault southeast of Al Hamriyah, we mapped a top-to-the-SW ductile shear zone at the base of the Ruwi Nappe (arrow in Fig. 7a, c). This shear zone appears to be the western continuation of the Yenkit shear zone. Above the Ruwi Nappe is the new Hamriyah shear zone (that has partly reactivated the Yenkit shear zone).

Our mapping indicates that the Yenkit shear zone occurs below the Ruwi Nappe. If so, the latter with its >99–96 Ma high-P metamorphism would be the topmost high-P nappe in the Saih Hatat window. Further, the newly mapped segment of the Yenkit shear zone below the Ruwi Nappe should be >~100 Ma in age and the Hamriyah shear zone at the upper contact of the Ruwi Nappe should be younger. Both are testable hypotheses, and our Rb—Sr study will shed light on these questions. Note that because of the new mapping, our structural interpretation of the Yenkit and Hamriyah shear zones, as well as the juxtaposition of the Yiti and Ruwi nappes have changed from Ring et al. (2023) (Figs. 1, 2) compared to this new paper (Figs. 1, 2).

(2) The Yiti Nappe above the Yenkit shear zone is considered a high-P nappe. Agard et al. (2010) described carpholite from Sahtan Group rocks at the coast north of Yiti (Fig. 3) but could not quantify P-T conditions. Le Métour et al. (1986a) noted that the contact between the Sahtan Group and the underlying Mahil Formation of the Yiti Nappe is highly sheared, suggesting a tectonic contact (Fig. 6b). Our field work at the contact between the Ruwi Nappe and the Sahtan Group west of Ruwi (Fig. 7) shows an isoclinal recumbent fold largely made up by Sahtan

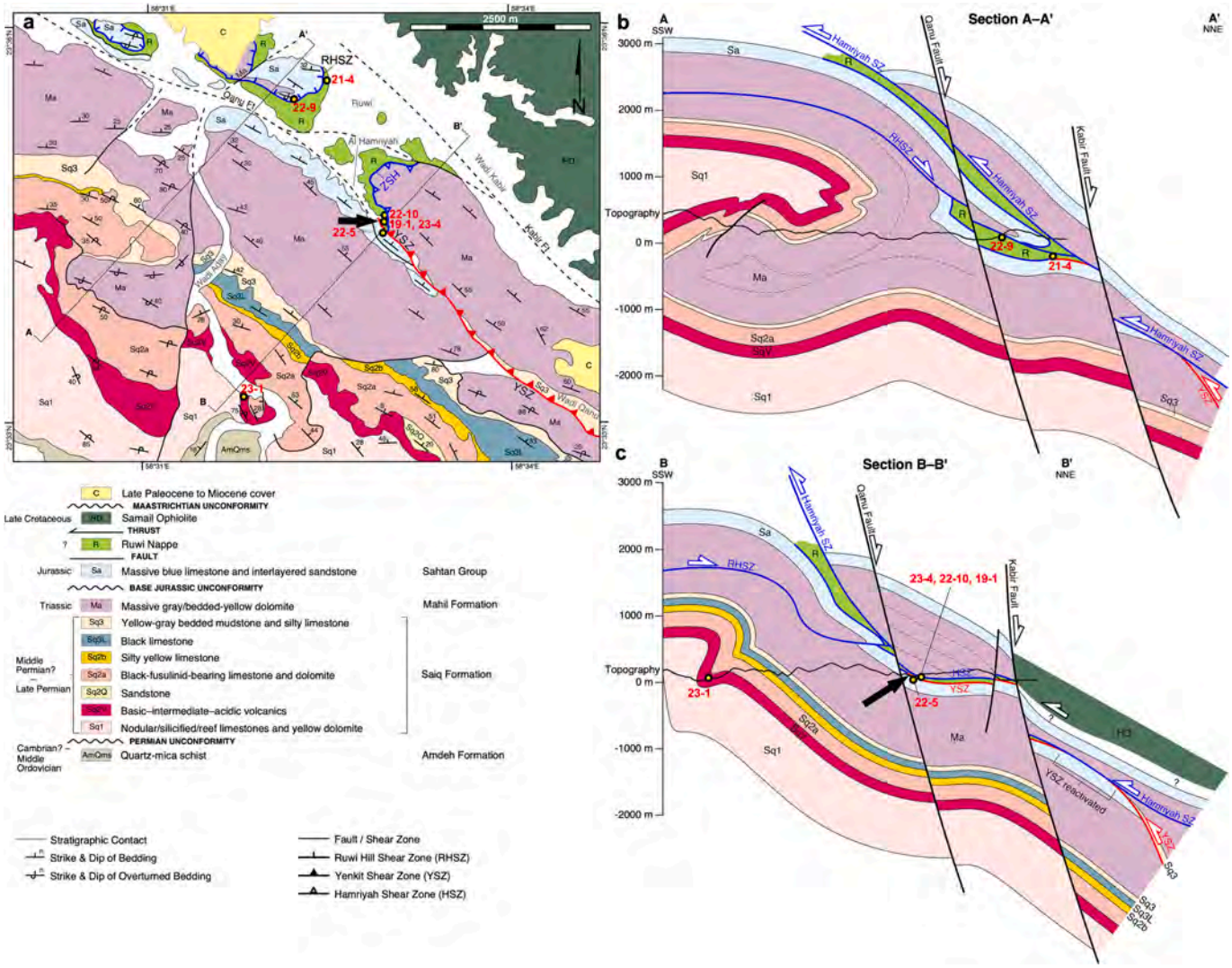

Fig. 7. (a) Detailed map of Wadi Kabir – Wadi Aday area based on Le Métour et al. (1986b), Miller et al. (2002) and own mapping. Ruwi Nappe sandwiched between Yiti and Al Khuryan-Quryat-Mayh-Saih Hatat (KQMS) nappes; Yenkit shear zone at base of Ruwi Nappe, splay of Yenkit shear zone (Hamriyah shear zone) separates Ruwi Nappe from overlying Yiti Nappe; Ruwi Hill shear zone associated with NE-closing recumbent fold cored by Mahil Formation, strongly deformed lower limb of fold stretched out in top-NE shear zone; shear sense in Ruwi Nappe top-NE at top and top-SW at base and of nappe. Postorogenic Qanu Fault tapers out near Al Hamriyah and displacement transferred to Kabir fault in Ruwi area forming relay-ramp structure. Rb-Sr sample localities of OM19–1, 21–4, 22–5, 22–8, 22–10 and 23–1 shown in map and cross sections; see Fig. 3 for location of map. (b, c) Geometrically permissible NW-SE cross sections outlining general architecture and geometry and sequence of faulting. Yenkit shear zone already active *before* Ruwi Nappe emplaced, therefore Yenkit shear zone cannot be structure that puts Mahil Formation of Yiti Nappe on top of Ruwi Nappe. Colour code as in Fig. 1. See also Fig. II-1 in Data Supplement Item II.

Group and cored by Mahil Formation. The recumbent fold has a strongly sheared lower limb that is associated with a 20–40-m-thick mylonite zone (Fig. 6c) (see also Miller et al., 2002). Therefore, we concur with Le Métour et al. (1986a) that the contacts of the Sahtan Group rocks above the Ruwi and Yiti nappes are shear zones. Consequently, the Sahtan Group rocks might have been tectonically emplaced above the Ruwi and Yiti nappes. Searle et al. (1994) had already suggested that these Sahtan Group rocks belong to the KQMS Nappe (carpholite-bearing Wadi Aday unit). If so, the Sahtan Group would not necessarily belong to the Yiti Nappe and consequently there would be no evidence for high-P metamorphism of the Yiti Nappe.

3.1.2. *Upper/lower-plate discontinuity*

A major controversy of Saih Hatat tectonics is whether the top-to-the-NE UP-LP Discontinuity is a backthrust or a normal fault. This issue has relevance for reconstructing the high-P nappe stack, its exhumation history, and for explaining the peculiar P-T path of the Hulw Nappe (Yamato et al., 2007) (Fig. 3c).

Gregory et al. (1998), Miller et al. (1998), and Gray et al. (2005) regarded the UP-LP Discontinuity as a top-to-the-NE backthrust that formed the NE-closing Saih Hatat fold nappe in its hanging wall. These authors drew the analogy to the Helvetic fold nappes (e.g., Durney and Ramsay, 1973; Dietrich and Casey, 1989), which are characterized by a similar strain gradient towards their basal shear zones.

Searle et al. (2004) and Agard et al. (2010) considered the UP-LP Discontinuity an exhumation-related normal fault (i.e., assuming that it was originally a N-dipping fault). Semi-restorable cross sections by Hansman et al. (2021) suggest that the UP-LP Discontinuity was initially a subhorizontal structure. A $^{40}Ar/^{39}Ar$ muscovite age of 75.6 ± 1.2 Ma (Miller et al., 1999) constrains the age of the mid-crustal UP-LP Discontinuity (Fig. 2b). Above the UP-LP Discontinuity are the KQMS, Yiti and Ruwi nappes. Especially the KQMS nappe is intensively folded by the Saih Hatat fold and associated folds (Figs. 2, 3). Muscovite from an axial-plane cleavage of one of these folds provided a $^{40}Ar/^{39}Ar$ age of 70.7 ± 1.4 Ma (Miller et al., 1999). The Hulw and As Sifah nappes are below the UP–LP Discontinuity (Fig. 3).

We concur with Gregory et al. (1998), Miller et al. (1998), and Gray et al. (2005) and consider the large-scale nature, the pronounced strain gradient and the analogy with the Helvetic fold nappes convincing evidence for a backthrust. To the best of our knowledge, there is no analogy for such features occurring in the hanging wall of low-angle normal faults, which have no ≤1-km-thick high-strain zones in both hanging- and footwall. The exhumed footwall of large-scale normal faults is commonly distinctly more strongly ductilely deformed than the hanging wall. There is usually also a pronounced break in metamorphic P-T conditions across exhumation-related normal faults.

3.2. Metamorphism

Most of the metamorphic data are straightforward and, in general, show a discontinuous downward increase in P-T conditions. There are two distinct clusters: (1) The As Sifah Nappe at the bottom has P_{max} >2 GPa, (2) the Hulw, KQMS and Ruwi nappes have distinctly lower P_{max} of ~1 GPa. We debate the peculiar P-T path of the Hulw Nappe (Yamato et al., 2007).

The convoluted P-T path of the Hulw Nappe is tectonically poorly understood. Yamato et al. (2007, their Fig. 13) and Agard et al. (2010), (their Fig. 6) proposed that the As Sifah Nappe underwent pronounced extensional deformation and boudinage during subduction at depths of ~40 km and that this extension controlled upward advection of heat explaining the localized thermal excursion of the Hulw Nappe. Layer-parallel boudinage as sketched by these authors demands stretching factors >3, which, if plane strain, isochoric deformation was assumed, converts into layer-perpendicular shortening of >65%. These figures appear unlikely for downgoing slabs at shallow levels (Jarrard, 1986; Pacheco and Sykes, 1992; Hyndman et al., 1997). The Hulw Nappe was probably part of the Arabian Platform. However, stretching factors >3 suggest that the platform was a hyperextended margin (cf. Doré and Lundin, 2015), which is unlikely. We note that the heating and potentially slight thickening (increase in P) of the Hulw Nappe occurred directly beneath the UP-LP Discontinuity (Fig. 3).

3.3. Age data

3.3.1. Saih Hatat window

There is no controversy about the Rb—Sr and U—Pb ages for peak high-P metamorphism of the As Sifah Unit at 78 ± 2 and 79 ± 1 Ma (El-Shazly et al., 2001; Warren et al., 2003, 2005). The Garber et al. (2021) Sm/Nd garnet ages show a greater scatter. The garnet chemical zoning patterns suggest that garnet cores formed during late prograde stages of metamorphism, whereas garnet rims were formed at peak P-T and early decompression. The Sm/Nd ages thus reflect average garnet growth ages. Hence, peak metamorphic conditions are considered to have occurred between 80 and 76 Ma.

The K—Ar age of 95 ± 8 Ma (Montigny et al., 1988) and the $^{40}Ar/^{39}Ar$ age of 80.2 ± 1.6 Ma (El-Shazly and Lanphere, 1992) from the top of the Ruwi Nappe are considered geologically meaningful, at least as maximum ages for the end of white-mica recrystallization (Table 2).

3.3.2. Metamorphic sole

Our interpretation of the reviewed P-T and isotopic data shows that metamorphism of the sole was a two-stage process: (1) subduction initiation and accretion at ~40 km depth (depth estimates are calculated from the reviewed P estimates assuming a rock density of 3000 kg m^{-3}) by 105–102 Ma (Guilmette et al., 2018). Even if one ignores the whole-rock data, the spread in the Lu—Hf garnet data results in very similar ages, indicating a sound and robust dataset. (2) Decompression and partial melting at ~20 km depth between 100 and 94 Ma. Partial melting was associated with crystallization of oceanic lithosphere in the overriding plate and formation of the Samail Ophiolite at 96–94 Ma. The modelled Lu—Hf age of 93.0 ± 0.5 Ma for garnet growth between ~550 and 630–700 °C is suggested to be associated with crystallization and fluid escape from the melts of the sole. At about the time the high-grade sole melted, the low-grade sole was underthrust (Kotowski et al., 2021). The tectonic juxtaposition of high-grade onto low-grade sole would classically be interpreted as a thrust (e.g., Ampferer, 1906; Ring and Kassem, 2007) and juxtaposition occurred at ~93 Ma (Hacker et al., 1996, 1997).

The zircon data of Garber et al. (2020) are consistent with the zircon ages of Guilmette et al. (2018) and earlier zircon ages of the sole (e.g., Rioux et al., 2016). They are probably best interpreted to date decompression at high-T conditions. Nonetheless, the single Lu—Hf garnet-whole rock age of 93.0 ± 0.5 Ma (Garber et al., 2020) appears remarkably young. One would expect the Lu—Hf garnet age to be older than the zircon ages, because it should also include the onset of garnet growth and would, thus, be a prograde-to-peak metamorphic age. The P-T conditions over which the dated garnet grew were estimated between ~0.4 GPa and 550 °C and 0.63–0.87 GPa and 630–700 °C (Garber et al., 2020). These P-T estimates are significantly different from those reported by Guilmette et al. (2018), although both groups sampled at Wadi Tayin (Fig. 1c). Garber et al. (2020) internally reproduced the Lu—Hf garnet data, but not the whole-rock data, which is commonly the case when detrital zircon populations are present. They reported one single Lu—Hf isochron age, and this age is from a metasediment in which garnet is an accessory phase. Metamorphism does not have to be isochemical, which Garber et al. (2020) assumed in their thermodynamic modelling. Searle and Malpas (1980), Ghent and Stout (1981) and Cowan et al. (2014) suggested that the rocks of the sole were hydrated during metamorphism. If garnet growth in the metasediment was driven by a fluid pulse (perhaps generated by the solidification of the last zircon-crystallizing melts), the fluids may have transported Fe, Mn, Mg (elements which are abundant in the mafic country rocks) from the mafic rocks into the sediment and minor garnet grew using the Si and Al in the metasediment late in the metamorphic history. The Lu—Hf garnet-whole rock age of Garber et al. (2020) could potentially date a local metamorphic fluid event, thus, reflecting metasomatism-driven garnet growth. Therefore, this single Lu—Hf age is problematic for inferring tectonic models. It would need to be reproduced and confirmed by ages from the surrounding mafic rocks. Apart from the single Lu—Hf age of 93.0 ± 0.5 Ma, the data sets of Guilmette et al. (2018) and Garber et al. (2020) are compatible. We conclude that the Guilmette et al. garnet ages of 105.2 to 101.9 Ma are firmly constraining the initiation of the Samail subduction zone.

The age of 106.9 ± 2.3 Ma for a zircon core interpreted to be detrital (Garber et al., 2020) is critical, as it would provide a maximum age for sole metamorphism and thus a maximum age for inception of Samail subduction. This age overlaps within uncertainties with the older Lu—Hf garnet ages of Guilmette et al. (2018). Given that the Samail subduction zone is an intraoceanic subduction zone, the question where the detrital zircons would come from arises. There is no mid-Cretaceous volcanism known from Arabia, and the ocean floor that subducted below the Samail Ophiolite was Permian in age. Erosion of the Arabia basement would produce distinctly older zircons. The nearest known Cretaceous zircon source would be the magmatic arc in Iran (Fig. 1b), which during the mid-Cretaceous was positioned >1500 km north of the Samail subduction zone (e.g., van Hinsbergen et al., 2019, 2021). How were zircons transported over such distances, even if they were part of an ash cloud?

3.4. Thickness of Samail Ophiolite

The very rapid displacement rates of ~15 cm a^{-1} (Hacker et al., 1996) dictate that the Samail Ophiolite was thrust onto the rocks of the Umar Subbasin and the Misfah Platform soon after it formed (Fig. 5). Therefore, the metamorphism, or the lack thereof, of the rocks of the Umar Subbasin and the Misfah Platform carbonates constrains the thickness of the ophiolite at the time it was thrust onto the platform. Breton et al. (2004) suggested that the Misfah Platform rocks southwest

of Jabal Akhdar are anchizonal (~0.2–0.4 GPa, <200 °C). Calcite starts to recrystallize below 150 °C (Bauer et al., 2018) and, as the fossil-bearing limestones of the Misfah Platform are well preserved, one can assume that T_{max} was <150–200 °C. The Samail Ophiolite (plus the rocks of the Umar Subbasin) overrode the Misfah Platform probably by 93 Ma when the various high- and low-T segments of the metamorphic sole were juxtaposed with each other (Hacker et al., 1996; Garber et al., 2020). These data suggest a maximum thickness of the overburden above the Misfah platform rocks of <8 km (i.e., 5–6 km of Samail oceanic crust, 2–3 km of Samail lithospheric mantle and a few 100 m of Umar Subbasin rocks). Such an overburden estimate would be in line with the P estimates of Breton et al. (2004).

If these calculations were accepted, then after partial melting of the sole and attaching it to the base of the Samail Ophiolite, severe thinning of the Samail oceanic lithosphere from ~20 km (partial melting of sole) to ~8 km (overriding of Misfah Platform) must have occurred (60% vertical thinning, which, if isochoric, plane-strain deformation was assumed, would translate into 150% of horizontal extension). As discussed in Hacker and Gnos (1997), Casey and Dewey (1984) suggested that the mantle section of an ophiolite may be thinned during intra-oceanic subduction if deeper-level underplating causes extension of the overlying ophiolite. Horizontal extension can be accommodated by normal faulting, which disrupts a sequence, or vertical ductile thinning, which attenuates it (Ring et al., 1999). We suggest that the attenuation of the Samail Ophiolite involved a pronounced component of vertical ductile thinning at temperatures between 550 and 950 °C (Guilmette et al., 2018; Garber et al., 2020; Goscombe et al., 2020) during the onset of intraoceanic thrusting of the Samail Ophiolite (cf. Ring and Kassem, 2007). The high displacement rates of ~15 cm a^{-1} (Hacker et al., 1996) would suggest high rates of vertical ductile thinning.

3.5. Obduction of Samail Ophiolite

Robertson (1987) explained the absence of ophiolite detritus in the Muti Formation by submarine thrusting. The advancing thrust wedge included the Samail Ophiolite at the top, as well as underlying rocks of the Umar Subbasin, Exotics, and sediments of the Hamrat Duru Subbasin. This thrust wedge must have been some 10 km thick (see calculations above, plus Misfah Platform and Hamrat Duru sediments). If one envisages that ~7–9 km of dense oceanic lithosphere exerted enough load on the lithosphere that the wedge was submarine, the Muti foreland basin should have had a water depth exceeding 10 km.

We consider it more likely that despite being tapering to the south, the advancing Samail thrust wedge was probably exposed above sea level. If so, the Muti Formation may reflect the early stages of the foreland basin development while the ophiolite was still too remotely positioned to shed material into the basin realm of the Muti Formation. A corollary of this proposition would be that the thrust wedge overrode the Aruma foreland basin, and, thus, the subjacent Arabian Platform, not much before ~83–80 Ma, consistent with the first occurrence of ophiolite detritus in the Juwaiza Formation and rapid subsidence of the Arabian Platform (Abdelmaksoud et al., 2022).

3.6. Two-subduction-zone models

The two-subduction-zone models have been criticized and it has been argued that the Ruwi subduction zone requires a suture zone, which appears to be missing (e.g., Agard et al., 2010). Hacker and Gnos (1997), Breton et al. (2004) and Ring et al. (2023) proposed that the 'second' intracontinental suture zone is at the interface between the Saih Hatat high-P rocks (As Sifah, Hulw, and KQMS nappes) and the overriding high-P Ruwi Nappe, i.e., subparallel to the Samail Thrust (suture) zone and underlying Hawasina Thrust. The contact between the Ruwi high-P rocks and the overlying non-high-P Hawasina nappes was overprinted by post-subduction/obduction tectonic events during the Cenozoic at the edges of the Saih Hatat window (i.e., Qanu and Kabir faults) and eroded away above the window. Therefore, the original contact zone is not preserved. A related question is how such an intracontinental suture would look like. Ophiolitic rocks are not to be expected; at best some serpentinized mantle rocks derived from the subcontinental mantle wedge above the subduction zone may occur. These serpentinites would be difficult to distinguish from serpentinite slivers derived from the Samail Ophiolite as both 'serpentinite zones' would be subparallel to each other and approximately project to similar structural levels. In short, the 'missing suture zone' of this second subduction zone does *not* appear to be a convincing argument against a two-subduction-zone scenario.

It has been argued that buoyant continental crust could not be subducted to depths of ~80 km without a significant amount of leading oceanic slab dragging it down. However, the development of a subduction zone reflects relative density contrasts and is triggered by gravitational instability (Turcotte and Schubert, 2002). Stüwe and Schuster (2010) showed that regions of thin continental crust and thick mantle lithosphere can be negatively buoyant. In general, continental lithosphere is older, colder, thus potentially may have a higher density than oceanic lithosphere (Jaupart and Mareschal, 2015). The formation of Mediterranean intracontinental subduction zones was controlled by the high-density lithosphere of the Adria microcontinent (Ring et al., 2010). Poupinet et al. (2002) suggested that subduction of the mantle part of the lithosphere in the interior of the Asian Plate formed the Tien Shan intracontinental mountain range. Faure et al. (2009) presented evidence from an early Paleozoic orogen of Southeast China showing that continental subduction occurred in the absence of a precursor oceanic slab.

The Arabian rifted margin was substantially thinned during two rifting events and is made up of attenuated crust underlain by thermally thickened and negatively buoyant mantle lithosphere. The subducted lithosphere was intruded and/or underplated by dense mafic rocks (Weidle et al., 2022, 2023), which substantially increased its overall density. Subsequently, extension was partitioned into the oceanic domain of Neo-Tethys, and the continental lithosphere of the rifted margin started to cool. Passive thermal equilibration (Holt et al., 2010) of high-density lithospheric mantle causes subsidence. We suggest that the transition from negative to positive vertical buoyancy occurred on the Arabian Platform. The distal platform, which is now the Saih Hatat window, contains abundant mafic rocks (Le Métour et al., 1986a, 1986b; Weidle et al., 2022, 2023) (Fig. 3). Further southwest in the Jabal Akhdar window, hardly any mafic rocks occur and the crust was not significantly extended, hence, had normal crustal thickness. We consider it mechanically plausible that the onset of subduction at the Arabian rifted margin was aided by a gravitational instability caused by prolonged cooling after pervasive magmatism during Permo-Triassic rifting.

3.7. Protolith issues and subduction localization

Lithospheric strength contrasts play an important role in localizing and forming an intracontinental subduction zone. Therefore, Ring et al. (2023) suggested that Ruwi subduction commenced at a locus of pronounced strength contrast between the Al Aridh Trough and the Misfah Platform, the latter being hardly affected by Permo-Triassic extension and, therefore, had normal lithospheric thickness. In contrast, Breton et al. (2004) considered that the second, inboard subduction zone localized close to the Arabian Platform where gravitational instabilities might be less likely. A possibility to distinguish between subduction under the Misfah Platform and subduction initiation close to the Arabian Platform would be a close inspection of potential protoliths of the Ruwi and Yiti nappes. The Ruwi Nappe is the oldest high-P nappe in the Saih Hatat window and its origin would help to pinpoint where subduction initiated. The Yiti Nappe is also critical as it occurs above the oldest (Yenkit) shear zone. In the model proposed by Ring et al. (2023), the Yiti Nappe should be derived from the Misfah Platform.

We have studied the literature for finding a possible protolith candidate for the Ruwi Nappe (see Data Supplement III). Most of the paleogeographic zones of the Arabian rifted margin (Fig. 5) do not expose potential units that may serve as a protolith of the Ruwi Nappe rock types. Only on the Arabian Platform and the Hamrat Duru Subbasin are three potential formations.

Béchennec et al. (1992) reported turbiditic oolitic calcarenite, calcirudites, marly limestone and carbonate breccia from the Jurassic Guwayza Formation of the Hamrat Duru Subbasin. Volumetrically these rock types are small. Problematic for correlations with the Ruwi Nappe is that there are only a few beds in three cycles that are 40, 30 and 15 m thick, and that these beds are alternating with other lithologies that do not match any Ruwi Nappe rocks.

During the early Cretaceous widespread clastic deposits accumulated on the Arabian Platform with carbonates along the platform margin (Forbes et al., 2010). The Albian (~113–100 Ma) Nahr Umr Formation of the Wasia Group consists of varyingly calcareous shales, marls and some argillaceous limestones (Béchennec et al., 1992). The Al Hassanat Formation in the Saih Hatat area is a platform-margin carbonate succession that has been interpreted as correlative with the Nahr Umr Formation (Immenhauser et al., 2001). A potential problem is the Albian age of the Nahr Umr Formation.

The Salil Formation of the Kahmah Group (Arabian Platform) appears to have some lithologies that match those of the rocks of the Ruwi Nappe. It is a sequence of alternating thin limestone, argillaceous limestone, conglomerate and marl of Valanginian to Barremian age (~145–120 Ma) (Le Métour et al., 1986a, 1986b; Rabu et al., 1993; Forbes et al., 2010).

Our summary suggests that the lithologies of the Nahr Umr and Salil formations could be a possible protolith of the Ruwi Nappe. Both formations would indicate that the Ruwi Nappe originated near the platform margin. By contrast, sediments of the Hamrat Duru Basin may contain suitable lithologies but not in needed amounts to form the Ruwi calcareous phyllite and suitable lithologies are absent in the rocks of the Misfah Platform.

Another potential problem are the platform carbonates of the Yiti Nappe and whether they can be derived from the Arabian or Misfah platforms (Fig. 5). If derived from the Misfah Platform, the carbonates of the Mahil Formation should hardly be dolomitic. Spot check analyses at 68 localities in the field using dilute HCl reveals that 94% of the Mahil Formation is dolostone, making it likely that they did not originate from the Misfah Platform.

A comparison of the Permian to Jurassic sedimentary rocks of the Arabian Platform (Hajar Supergroup of the Jabal Akhdar and Saih Hatat windows) with time-equivalent rocks of the Misfah Platform (Kawr Group; Misfah Formation) based on Searle and Graham (1982), Béchennec et al. (1986, 1990, 1992), Beurrier et al. (1986), Le Métour et al. (1986c), Breton et al. (2004), Rousseau et al. (2005, 2006), Bernecker (2007), Koehrer et al. (2010) and Forke et al. (2012) reveals: (1) differences in their primary lithology and facies, most notably expressed by the presence of late Triassic coral reefs in the Misfah Formation which are absent in the Triassic Mahil Formation of the Hajar Supergroup; (2) that the rocks of the Hajar Supergroup have been metamorphosed while the rocks of the Misfah Formation remained unmetamorphosed; and (3) that extensive dolomitization affected the Permo-Triassic carbonates of the Hajar Supergroup (Saiq and Mahil formations), whereas dolomitization of late Triassic inter- to supratidal limestones of the Misfah Formation is minor by comparison. Dolomitization in the Jabal Akhdar window took place at different times from the late Paleozoic to the late Cretaceous (estimates by Vandeginste et al., 2013, 2015) and in the Saih Hatat window during the late Paleozoic and the mid Cretaceous (estimates by Mattern et al., 2022b). The various Cretaceous dolomitization events largely coincide with subduction and associated metamorphic processes.

The far lesser dolomitization of the late Triassic carbonates of the Misfah Formation may be explained by the limited areal extent of the Misfah Platform (Béchennec et al., 1990), which may have impacted late/deep burial dolomitization (no Mg^{2+} source in the limited area and/or rapid fluid loss at the nearby flanks of the platform). Substantial late/deep burial dolomitization may not have taken place in the Misfah Formation. Dolomitization may have been limited to early dolomitization, likely reflux dolomitization in an inter- to supratidal setting. In contrast to the Misfah Platform, both the Saiq and Mahil formations represent an epeiric facies realm of the Arabian Platform (Forke et al., 2012).

Most workers derive the Mahil Formation dolostones from the proper Arabian Platform and not from the Misfah Platform (e.g., Béchennec et al., 1992; Blechschmidt et al., 2004; Breton et al., 2004; Searle, 2019). Bedding in the Yiti Nappe dolostone has the same dip (~50° to the NE) as bedding in the dolostones of the Arabian Platform of the KQMS nappe to the south.

The work of Mattern et al. (2022b) suggested two dolomitization/precipitation phases in the Saih Hatat window during the late Paleozoic and mid Cretaceous. The Paleozoic event is too early for the Triassic Mahil dolostones. Hence, we assume that their dolomitization occurred during the mid-Cretaceous about coevally with high-P metamorphism of the Ruwi Nappe. P-T conditions for the Yiti Nappe are not known but it is possible that it was shallowly subducted (Agard et al., 2010). Potential subduction and associated (high-P) metamorphism would distinguish the Yiti Nappe from the rest of the non-metamorphosed remnants of the Misfah Platform, and these processes may have caused mid-Cretaceous dolomitization of the Permo-Triassic carbonates of the Yiti Nappe. We envisage deformation/metamorphism-controlled fluid flow in the subduction channel providing Mg^{2+} to the carbonates. According to Mattern et al. (2022b), the suggested mid-Cretaceous dolomitization, which affected the low-grade Hijam Formation of the western Saih Hatat window, only caused minor dolomite precipitation in open fractures. Nevertheless, it also shows that Mg^{2+} fluids existed. The Hijam Formation occurs in the lower parts of the KQMS Nappe and was potentially largely shielded from the fluid-inundated subduction interface. The Yiti Nappe as envisaged by Ring et al. (2023) was much closer to the subduction interface and, therefore, Mg^{2+} fluids had easy access to the Yiti dolostones.

The depositional environments of the Triassic of the Arabian and Misfah platforms are different, which causes a potential problem for deriving the Triassic dolomite of the Yiti Nappe from the Misfah Platform. The Triassic of the Misfah Platform is shallow marine (intertidal to supratidal) with abundant coral reefs (Bernecker, 2007; Koehrer et al., 2010). In contrast, the Mahil Formation of the Arabian Platform displays no reefs but sabkha facies (supratidal). Even if there were no coral reefs in a 'Yiti sector' of the Mahil Platform, it might be expected that reef detritus would be preserved in the well-layered Yiti dolostone. The volume of reef debris could be distinctly larger than the actual reef cores (Wright and Burchette, 1996; Kiessling and Flügel, 2002) and tidal, rip, storm and longshore currents should have spread this debris across most of the platform. Debris from small coral colonies might also be expected. Even if the aragonite of corals was converted to calcite, or the reefs were later dolomitized and/or weakly metamorphosed, remnants of corals should still be visible, but Le Métour and Villey (1986) noted that "the Mahil Formation as a whole is practically azoic in the Muscat area, with only rare debris of gastropods, pelecypods and echinoderms". In other words, no corals are reported.

A final potential problem of the sedimentary record is the extent of the sediments of the Wasia Group, which are considered to reflect a stable Arabian Platform from 114 to 92 Ma. The Wasia Group is not exposed in the Saih Hatat window and the nearest deposits are the Natih Formation (upper member of the Wasia Group) at the southwest flank of Jabal Akhdar (~70 km away from Ruwi). This raises the question whether the Wasia Group was never deposited at Saih Hatat, which would mean that a stable Arabian Platform is only confirmed southwest of the Saih Hatat window in the Jabal Akhdar region.

4. Rb—Sr geochronology

4.1. Rationale

Because previous geochronologic work of the Saih Hatat high-P rocks focused on the tectonically lowest As Sifah Nappe, our main goal was to collect samples from the overlying high-P nappes (Fig. 2). We also sampled the As Sheik shear zone, the UP-LP Discontinuity, as well as the Al Wudya, Al Khuryan, Yenkit, Ruwi Hill and Hamriyah shear zones. Further, we use the recently published Rb—Sr ages from the Ruwi Nappe (two ages) and the Yenkit shear zone (two ages) of Ring et al. (2023). Because of the widespread problem with excess ^{40}Ar, particularly in high-P rocks (e.g., Hacker and Gnos, 1997; Warren et al., 2011, 2012), we employ the Rb—Sr multimineral isochron method. The latter has the advantage that age data can be readily related to the formation of a metamorphic mineral paragenesis or to the waning stages of recrystallization (e.g., Inger and Cliff, 1994; Freeman et al., 1997; Glodny et al., 2005; Halama et al., 2018; Glodny and Ring, 2022).

Rb—Sr multimineral isochron dating mainly relies on muscovitic to phengitic white mica as a high-Rb/Sr phase. In the absence of ductile deformation or free fluids, the Rb—Sr system of white mica is thermally stable against diffusional reset at temperatures up to >600 °C (Glodny et al., 2008; Ribeiro et al., 2023) Grain-size reduction during progressive synkinematic recrystallization may lead to open-system behaviour, Sr-isotopic exchange with simultaneously recrystallizing phases or with fluids, and age resetting at temperatures as low as ~300 °C (Müller et al., 2000). In strongly sheared low- to medium-grade rocks, as in the here analyzed schists and mylonites, the Rb/Sr age signal will, thus, date the waning stages of ductile deformation, when both, the syndeformational metamorphic P-T conditions were frozen in, and synkinematic recrystallization of white mica and its paragenetic phases came to an end. The grain-size sensitivity of mineral shear strengths (Platt and Behr, 2011) provides a means to test for both the presence of pre- or early-deformational Sr-isotopic relics and for protracted non-penetrative deformation. In our approach, white mica is, whenever feasible, analyzed in different grain-size fractions. Identical ages for all grain-size fractions testify to recrystallization and age reset due to penetrative deformation, whereas a positive correlation between white-mica grain size and apparent age may indicate prolonged shearing, with the apparent age for the smallest grain-size fraction being a maximum age for the end of deformation (e.g., Halama et al., 2018).

The specific advantage of using the Rb—Sr system is its capability to directly date fabric formation, combined with its stability against thermal overprints, and its link to mica phases (typically muscovite and/or phengite) that directly co-define the fabric of a rock. Even strain partitioning between small domains can be detected and directly dated (Halama et al., 2018; Ribeiro et al., 2023). Geochronologic information on processes at low metamorphic grade, down to the ductile- to brittle transition, is otherwise notoriously difficult to obtain because minerals datable by U—Pb, Sm—Nd or Lu—Hf methods typically do not form or recrystallize at such conditions. Age information equivalent to the Rb—Sr record might be obtained using ^{40}Ar/^{39}Ar dating of mica (but see above for problems with excess ^{40}Ar in high-P rocks). A more detailed outline on the methodology is provided in Data Supplement Item IV.

4.2. Age data for high-pressure metamorphism

Mineralogical and textural descriptions of the analyzed samples and further specifics of the analyses are in Data Supplement IV, the Rb—Sr analytical data in Data Supplement V. Sample locations are shown in Figs. 2, 3 and 7, as well as examples of the analyzed rocks in Fig. 6 and Fig. IV-1 of Data Supplement Item IV. The relation between metamorphic grade, texture and the interpretation of the Rb—Sr ages is in most cases straightforward and discussed in the following sections.

4.2.1. As Sifah Nappe

The As Sifah Unit is at the bottom of the Saih Hatat nappe stack. Sample OM19–8 is a strongly foliated felsic schist associated with the As Sifah eclogite body. The sample contains blue amphibole and rutile together with cm-sized, elongated aggregates of white mica. Regression of Rb—Sr mineral data for three grain-size fractions of white mica together with apatite and calcite results in a five-point isochron age of 78.4 ± 1.4 Ma (MSWD = 97, Fig. 8a). The high MSWD value is mainly due to slight Sr-isotopic disequilibrium between calcite and apatite. The age information is insensitive to the selection of either calcite or apatite data for age calculation (calcite + three white mica fractions: 78.5 ± 2.1 Ma; apatite + three white mica fractions: 78.6 ± 1.9 Ma) and, therefore, reliably dates a late stage of ductile deformation at high-P conditions.

Sample OM19–18 from Diqdah Unit yields an age of 77.2 ± 1.8 Ma (n = 6, MSWD = 42, Fig. 8b). There are slight isotopic disequilibria between the low Rb—Sr phases epidote, apatite and blue amphibole. Omission of the data for blue amphibole results in an age of 77.2 ± 2.6 Ma, with a lower MSWD of 3.2. One may speculate that the slight Sr-isotopic disequilibria may be related to post-deformational partial alteration of blue amphibole. Given the insensitivity of the age information on the low-Rb/Sr phases selected for age calculation we consider the age of 77.2 ± 1.8 Ma to date the waning stages of ductile deformation at high-P metamorphic conditions.

4.2.2. Hulw Nappe

There is a distinct decrease in peak high-P conditions between the As Sifah and Hulw nappes across the top-to-the-NE displacing As Sheik shear zone (Searle et al., 2004) (Fig. 3c). The Hulw Nappe experienced mild high-P metamorphism (Agard et al., 2010). Sample OM19–17 is a deformed blueschist from the Hulw Unit. A six-point regression line provides an age of 76.2 ± 1.6 Ma (MSWD = 106, Fig. 8c). The elevated MSWD is due to slight but significant disequilibria among the low-Rb/Sr phases blue amphibole, apatite and epidote. Omission of the data for blue amphibole results in an age of 76.4 ± 1.9 Ma, with a lower MSWD of 3.3. Therefore, we consider the ages to reliably date blueschist-facies metamorphism.

4.2.3. Al Khuryan-Quryat-Mayh-Saih Hatat (KQMS) Nappe

Sample OM23–1 is an extremely fine-grained, moderately deformed blueschist from the Al-Khuryan-Quryat Unit of the KQMS Nappe. A four-point regression line provides an age of 75.5 ± 4.4 Ma (MSWD = 30, Fig. 8d). Given the fine-grained nature of the rock and the related difficulty to detect potential textural relics or minor post-blueschist facies alteration in thin section, the reasons for the elevated MSWD remain largely unclear. However, the most abundant phase in the rock is micron-sized, needle-shaped blue amphibole that is intimately intergrown with the age-defining white mica in the two <27 μm fractions (Fig. 8d). This indicates that the age information from this sample robustly dates blueschist-facies metamorphism of the KQMS Nappe.

4.2.4. Ruwi Nappe

Ring et al. (2023) reported ages of 98.03 ± 0.88 Ma and 97.04 ± 0.76 Ma for samples OM19–1 and OM21–4 (Fig. 3). Both ages are from deformed carpholite-bearing phyllite (Fig. 6e) and constrain the age of late increments of deformation during ceasing high-P metamorphism in the Ruwi Nappe.

4.3. Age data for decompression and greenschist-facies metamorphism

For better understanding exhumation rates of the well-studied high-P rocks of the As Sifah Nappe, we studied an eclogite sample that shows partial conversion to blueschist-facies assemblages and thus records initial decompression at blueschist-facies conditions. We also analyzed a former eclogite that was thoroughly reworked under greenschist-facies metamorphism.

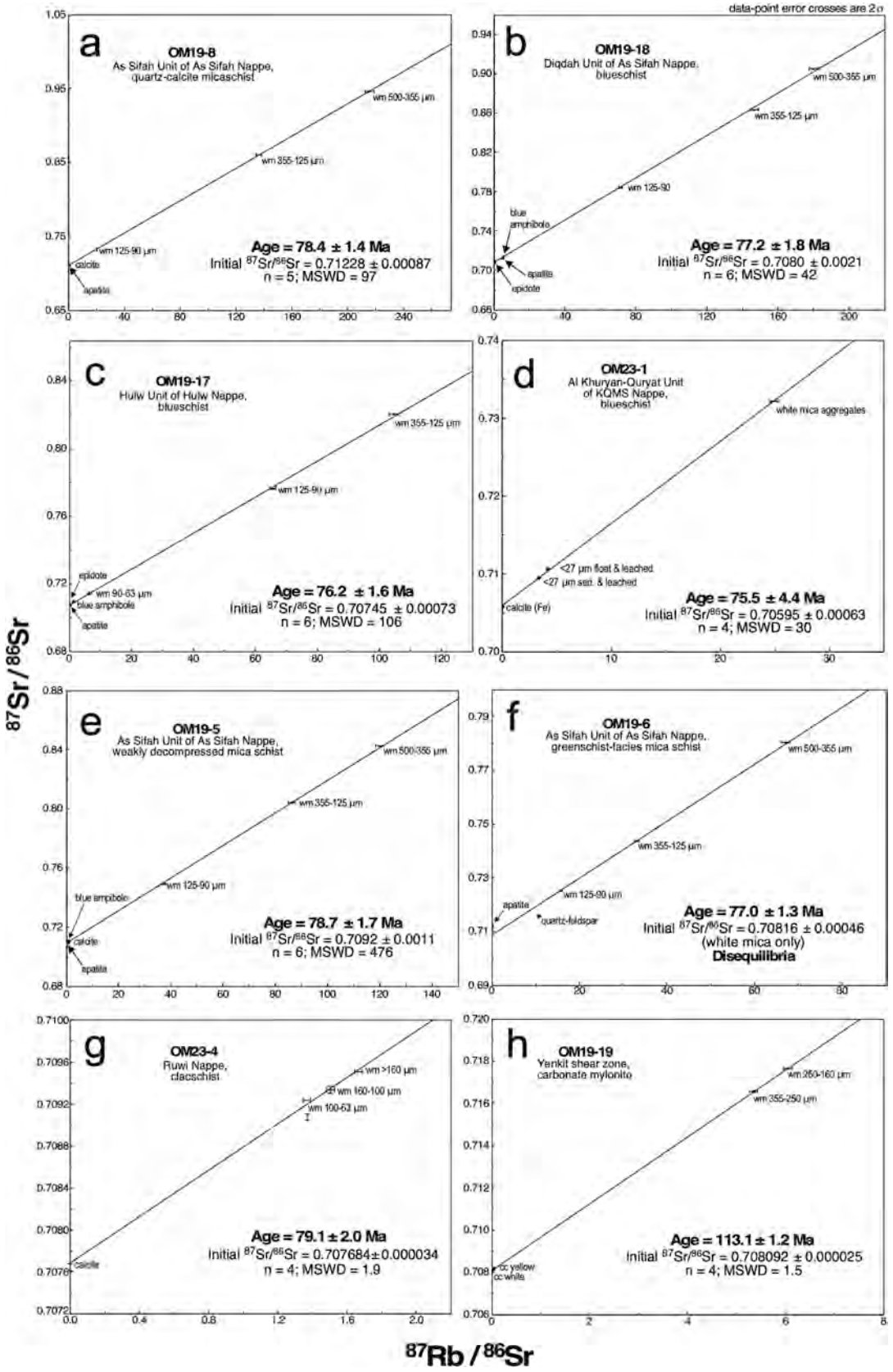

Fig. 8. Rb—Sr data, see also Data Supplement Items IV and V.

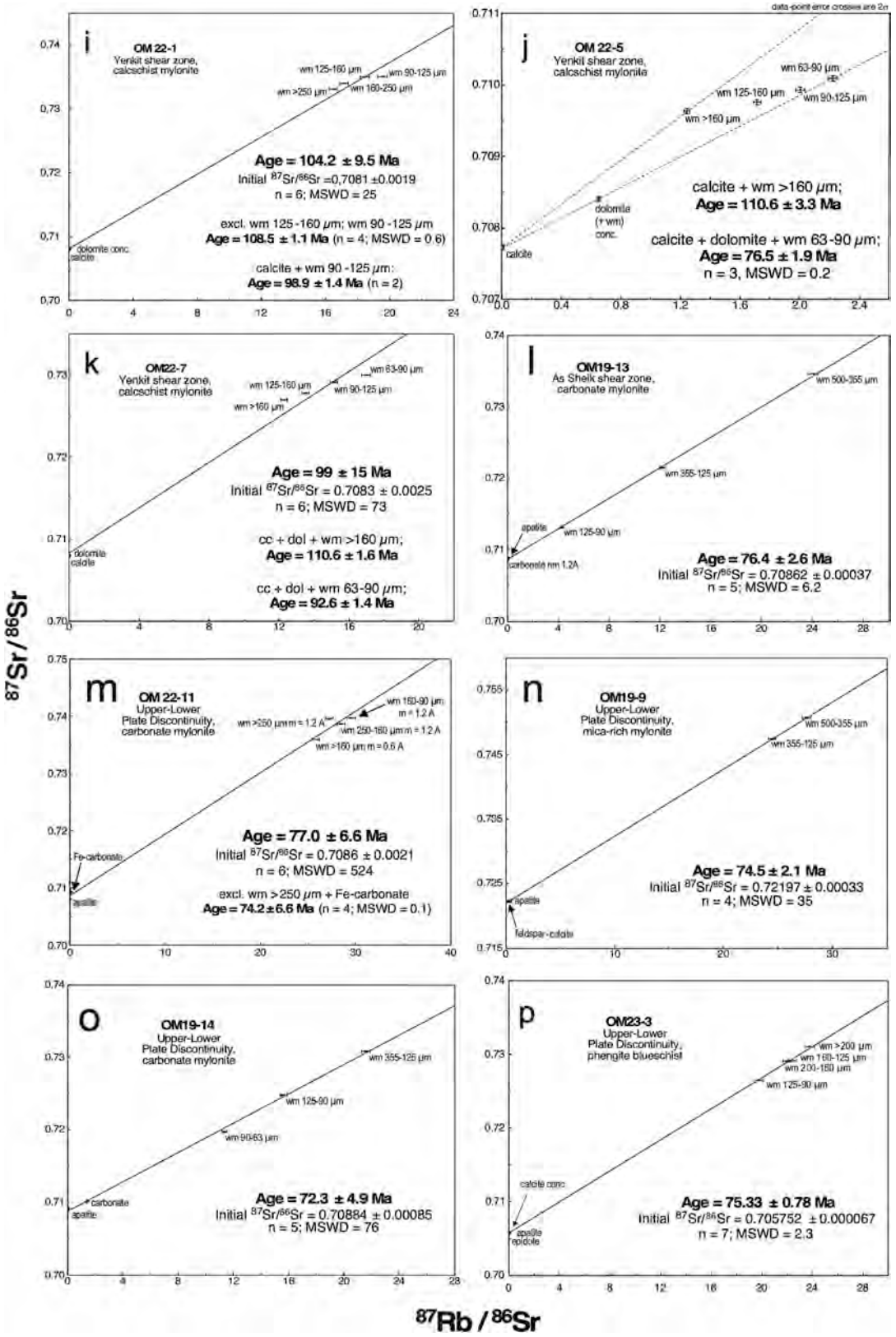

Fig. 8. (*continued*).

4.3.1. Initial decompression of As Sifah Nappe

Sample OM19–5 is a strongly sheared eclogite from the As Sifah Unit with a penetrative foliation and stretching lineation. The outcrop shows abundant top-to-the-NE shear-sense indicators. Both garnet and omphacite are altered, whereas blue amphibole and chlorite are stable in mm-thick layers in the eclogite (Fig. 6f). Rb—Sr mineral data for three grain-size fractions of white mica, apatite, calcite and blue amphibole provide an age of 78.7 ± 1.7 Ma (n = 6, MSWD = 476, Fig. 8e). There are marked Sr-isotopic disequilibria between the three low-Rb/Sr phases (apatite, calcite, blue amphibole), possibly related to the partial

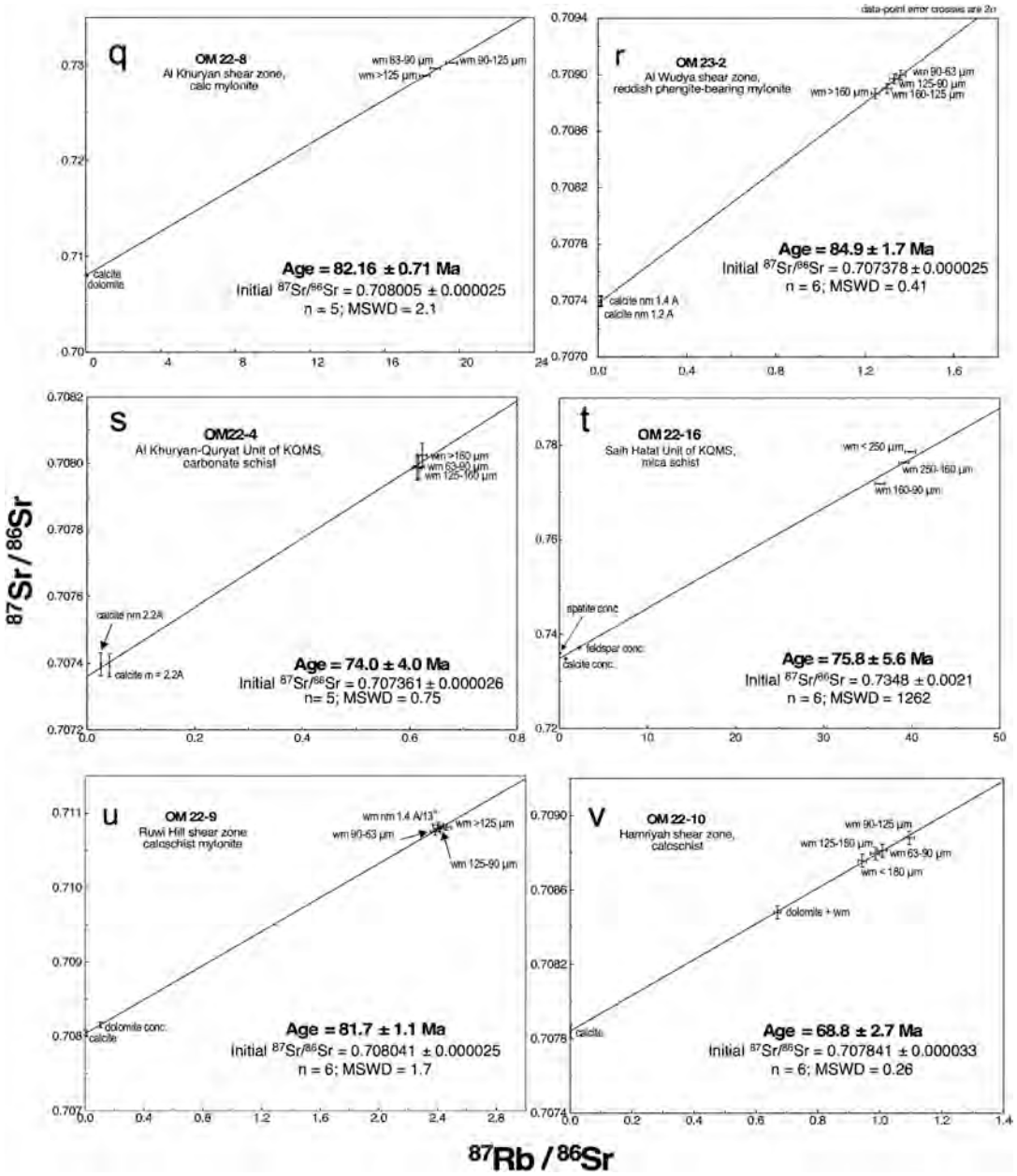

Fig. 8. (*continued*).

blueschist-facies reworking evident in the sample. Nevertheless, partial preservation of the eclogitic high-P phases omphacite and garnet indicates that retrogression was far from being penetrative. We interpret the age of 78.7 ± 1.7 Ma as dating top-to-the-NE shearing during initial decompression from peak high-P conditions, as blue amphibole is still a stable mineral in the rock.

4.3.2. *Greenschist-facies metamorphism of As Sifah Nappe*

Sample OM19–6 is from the same outcrop as OM19–5 but the distinctly rusty-brown coloured rock (Fig. 6g) shows intense greenschist-facies overprinting of an inferred earlier eclogite-facies assemblage. There is no garnet, omphacite or blue amphibole in this sample, which instead contains abundant white mica, chlorite and hematite. The Rb—Sr mineral data show pronounced Sr-isotopic disequilibria. If only the three white-mica fractions are used, an age of 77.0 ± 1.3 Ma (Fig. 8f) results, which is interpreted to date a greenschist-facies overprint.

4.3.3. *Top-NE shearing in Ruwi Nappe*

There is a set of conspicuous top-to-the-NE shear bands associated with carbonate veins in the upper Ruwi Nappe (Fig. 6e). Three white mica grain-size fractions of sample OM23–4 from one of these shear bands combine with calcite to an age of 79.1 ± 2.0 Ma (Fig. 8g). This age reflects the final increments of top-to-the-NE shearing and is distinctly younger than the age of 98.03 ± 0.88 Ma of sample OM19–1, which has been collected only ~30 cm above sample OM23–4 (Fig. 6g). The initial $^{87}Sr/^{86}Sr$ ratios of both samples are distinctly different (0.7077 for OM23–4 vs 0.7094 for OM19–1). We explain this difference with pronounced fluid infiltration and carbonate precipitation during top-to-the-NE shearing.

4.4. *Major shear zones*

The age data for high-P metamorphism fall into two groups: (1) Waning high-P metamorphism in the Ruwi Nappe at 99–96 Ma. (2) Waning high-P metamorphism in the high-P units below the Ruwi Nappe

at 80–76 Ma. The two age clusters are separated by about 20 Ma and classify the Yenkit shear zone as a first-order tectonic boundary. Therefore, we focussed on sampling this shear zone, but also sampled shear zones below the Yenkit shear zone. We first provide an outline on the various shear zones we sampled.

The Yenkit shear zone is a ≥104 Ma (Ring et al., 2023), top-to-the-SW mylonite zone (Michard et al., 1994; Le Métour et al., 1986b; Miller et al., 2002; Searle et al., 2004) (Fig. 6h). For most of its extent, the Yenkit shear zone separates the Yiti and KQMS nappes. Only at its western end, the Ruwi Nappe crops out between the Yiti and KQMS nappes (Le Métour et al., 1986b; Agard et al., 2010; Searle et al., 2022). As mentioned in section 3.1.1., it is possible that this small segment of the Yenkit shear zone above the Ruwi Nappe represents a late top-to-the-SW out-of-sequence re-imbricate structure (see Hansman et al., 2021, their Fig. 18), the Hamriyah shear zone (Fig. 7). If the Hamriyah shear zone above the Ruwi Nappe is indeed a late structure (Searle and Cox, 2002), then the Ruwi Nappe would represent the topmost nappe of the exposed Saih Hatat nappe stack (Data Supplement Item II).

In section 3.1.1., we outlined some problems with the occurrence of Jurassic Sahtan Group rocks above the Ruwi Nappe at the top of Ruwi Hill in the west, and above the Triassic Mahil Formation of the Yiti Nappe northeast of Yiti (Fig. 7). Le Métour et al. (1986a, 1986b, 1986c) suggested that the latter contact is sheared. At Ruwi Hill, our field work identified a tectonic contact (the Ruwi Hill shear zone) between the Ruwi Nappe and the Sahtan Group rocks (Fig. 6c, 7). The Ruwi Hill shear zone could be equivalent to the late top-to-the-SW out-of-sequence re-imbricate structure at the Hamriyah shear zone described in the last paragraph. However, the shear sense at the Ruwi Hills shear zone is top-to-the-NE.

The Al Khuryan and Al Wudya shear zones are below the Yenkit shear zone within the Al Khuryan-Quryat Unit. In places, the structural distance between these three shear zones is <100 m (Fig. 3), making it likely that the Al Khuryan and Yenkit shear zones have, at least in part, a common deformation history. All three shear zones have an early top-to-the-SW shear sense (Le Métour et al., 1986b; Searle et al., 2004) (Fig. 6i).

The top-to-the-NE As Sheik shear zone (Fig. 6j) and the UP-LP Discontinuity (Fig. 4, 6k, l) are described and discussed in sections 2.1.1. and 3.1.2. The data below will address the geochronology of the mylonites in the discussed shear zones.

4.4.1. Yenkit shear zone

Samples OM21–2 and OM21–3 are calcschists from the Yenkit shear zone and belong to the lowermost Yiti Nappe. The samples are mylonitic and provide a consistent top-to-the-SW shear sense. The Rb—Sr ages of these samples were reported in Ring et al. (2023): OM21–2 98.5 ± 7.4 Ma, OM21–3 99.6 ± 3.7 Ma. In addition to these formal ages, there is a slight but significant positive correlation between white-mica apparent ages and grain size in the data pattern for OM21–2. Apparent ages range between 102.7 ± 1.5 Ma (for white-mica grain size >200 μm) and 94.5 ± 1.4 Ma (for white-mica grain size of 90–63 μm). Ring et al. (2023) interpreted this pattern to reflect either a prolonged episode of non-penetrative deformation during top-to-the-SW shearing or, alternatively, partial reworking of an assemblage with an age >102.7 Ma during a deformation event at or after 94.5 Ma.

Here, we provide new Rb—Sr data for samples OM19–19, 22–1, 22–5 and 22–7 (Fig. 7, 8h-k). Sample OM19–19 shows two distinct lithological domains, a medium-grained calcschist and a fine-grained calcareous phyllite (see Data Supplement Item IV). We analyzed both domains separately. The medium-grained calcschist provided mineral data defining a four-point isochron age of 113.1 ± 1.2 Ma (MSWD = 1.5, Fig. 8h). This well-defined age is interpreted to date mylonitic shearing. In contrast, minerals from the calcareous phyllite show Sr-isotopic disequilibrium, formally providing an age of 109 ± 15 Ma. Combining all data of sample OM19–19 results in an age value of 108.2 ± 5.3 Ma (Fig. 8h). It appears that ductile deformation in this sample was heterogeneously distributed through time, and that the age of 108.2 ± 5.3 Ma is best interpreted as delineating a prolonged episode of mylonitization. We admit that the results obtained from sample OM19–19 are not robust in a strict sense. Nevertheless, the results are interpretable in terms of age information.

The white-mica populations of the remaining three calcschist samples show Sr isotopic disequilibrium. OM22–1 depicts a slight but significant positive correlation between white-mica apparent ages and grain size (Fig. 8i). Formally, all data provide a six-point regression line corresponding to an age of 104.2 ± 9.5 Ma (MSWD = 25). Exclusion of the two fine-grained white-mica fractions results in an apparent age of 108.5 ± 1.1 Ma with an MSWD of 0.6, while the most fine-grained white-mica size fraction of 90–63 μm combines with calcite to an apparent age of 98.9 ± 1.4 Ma (Fig. 8i). Sample OM22–5 shows a similar pattern. The coarse-grained white-mica fraction (>160 μm) together with calcite provides an apparent age of 110.6 ± 3.3 Ma, while the finest fraction (63–90 μm) combined with calcite and dolomite yields an age of 76.5 ± 1.9 Ma (MSWD = 0.2, Fig. 8j). Finally, OM22–7 shows again an analogous covariation of white-mica grain sizes and Rb—Sr isotopic characteristics. The largest size fraction gives an apparent age of 110.6 ± 1.6 Ma and the smallest analyzed grain-size fraction one of 92.6 ± 1.4 Ma (Fig. 8k).

In summary, despite isotopic disequilibria, the six Rb—Sr data sets from top-to-the-SW mylonites of the Yenkit shear zone yield consistent and reliable age information (Fig. 9, Fig.III-11 in Data Supplement Item III). Apparent ages of coarse-grained white mica are between 114 and 101 Ma. They are interpreted as minimum ages for metamorphic white-mica growth and initial shearing in the Yenkit shear zone. Apparent ages of fine-grained white mica are considered as maximum ages for the end of ductile shearing and recrystallization of white mica. Hence, the six samples provide evidence for a long-lasting episode (or consecutive increments) of ductile shearing starting at ~114 Ma (113.1 ± 1.2) and lasting until ~93 Ma or, alternatively, for two distinct episodes of shearing, one at ≥114 Ma and one at ≤93 Ma. Sample OM22–5 from the westernmost segment of the Yenkit shear zone provides evidence for reactivation at ≤76.5 Ma.

With the current data we cannot rule out that late increments of non-penetrative shearing occurred even later. Results from sample OM22–5 may either be interpreted as indicating low-intensity, non-penetrative deformation lasting locally until at least 76.5 Ma, or as indicating a more local distinct reactivation of the Yenkit shear zone at or after 76.5 Ma.

4.4.2. As Sheik shear zone and UP-LP discontinuity

We collected four mylonite samples from the UP-LP Discontinuity and the As Sheik shear zone. Sample OM19–13 is a fine- to medium-grained mylonitic calcschist from the As Sheik shear zone (Fig. 6j). The sample is characterized by pervasive top-to-the-NE shear bands. A five-point regression line provides an age of 76.4 ± 2.6 Ma (MSWD = 6.2, Fig. 8l). The largest white-mica grain-size fraction (500–355 μm) plots slightly above the regression line, while the smallest fraction (125–90 μm) slightly below. We interpret this pattern to reflect progressive recrystallization during mylonitization and that the age of 76.4 ± 2.6 Ma dates the final stage of this process.

Sample OM22–11 is from the uppermost Hulw Nappe within the UP-LP Discontinuity (Fig. 3). Mylonitic deformation is associated with a top-to-the-NE shear sense. A six-point regression line supplies an age of 77.0 ± 6.6 Ma (MSWD = 524, Fig. 8m). The largest white-mica grain-size fraction (>250 μm) plots above the regression line, while the three grain-size fractions <250 μm provide consistent data just below the regression line. Formally, the data for these more fine-grained mica fractions combine with the Fe-rich carbonate (the main carrier of Sr in the rock) to an isochron age of 74.2 ± 0.6 Ma (MSWD = 0.1). We argue that this isochron age may be the best estimate for the age of late-stage mylonitization, whereas the data for apatite and white mica >250 μm may point to partial inheritance of these mineral populations from the preceding high-P stage.

Sample OM19–9 is a fine-grained, mylonitic rock with a silvery,

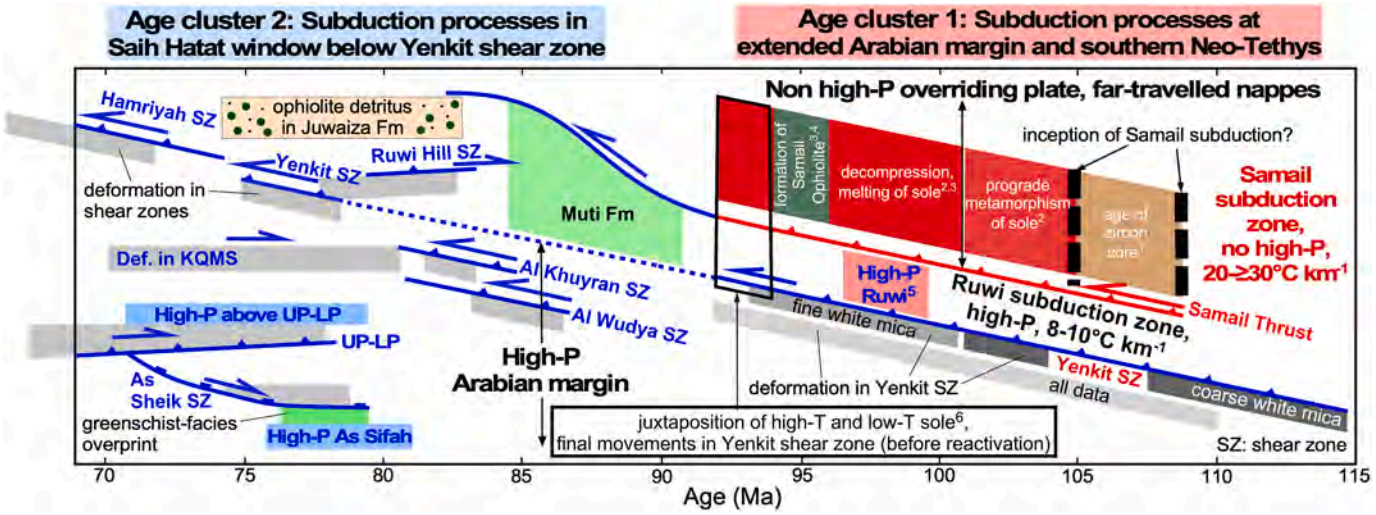

Fig. 9. Synoptic summary showing age clusters 1 and 2 separated by deposition of syntectonic sediments of Muti Formation as part of Aruma Group; note that younger Juwaiza Formation containing ophiolite detritus also part of Aruma Group. Age cluster 1 highlights two-fold evolution of 'hot' (thermal gradients 20->30 °C km^{-1}) Samail subduction zone and 'cold' (thermal gradients 8–10 °C km^{-1}) Ruwi subduction zone; final juxtaposition of contrasting settings after 93 Ma. Potential start of underthrusting of platform margin (possibly associated with formation of forebulge and sedimentation of Muti Formation) by 92 Ma. Age cluster 2 emphasizes subduction of high-P nappes of Saih Hatat window in Ruwi subduction zone. Note that Ruwi Hill shear zone not necessarily structurally above Hamriyah shear zone, but laterally west of it. Explanation: [1]Garber et al. (2020), [2]Guilmette et al. (2018), [3]Rioux et al. (2021), [4]Tilton et al. (1981), [5]Ring et al. (2023), [6]Hacker et al. (1997). Red colours highlight processes in Samail subduction zone, blue colours related to underthrusting of Arabian Platform, gray boxes show range of our Rb—Sr deformation ages (for Yenkit shear zone; Rb—Sr ages subdivided into coarse- and fine-grained white-mica fractions), pink box Rb—Sr ages for high-P in Ruwi Nappe, blue boxes Rb—Sr ages for high-P in nappes below Ruwi Nappe, green box highlights Rb—Sr age for greenschist-facies overprint of As Sifah Nappe; widths of boxes reflect maximum 2σ uncertainties of age data. See text for interpretation and Fig. III-11 in Data Supplement Item IV. (For interpretation of the references to colour in this figure legend, the reader is referred to the web version of this article.)

phyllitic appearance from the UP-LP Discontinuity and shows abundant top-to-the-NE shear-sense indicators (Fig. 6k). A four-point regression line defines an age of 74.5 ± 2.1 Ma (MSWD = 35, Fig. 8n), which is interpreted to date the final stages of mylonitic shearing in this sample.

Sample OM19–14 is a fine to medium-grained, glaucophane-bearing, mylonitic calcschist (Fig. 6l) from the uppermost As Sheik Unit of the Hulw Nappe at the base of the UP-LP Discontinuity with top-to-the-NE shear-sense indicators. It provides a five-point regression line corresponding to an age of 72.3 ± 4.9 Ma (MSWD = 76, Fig. 8o). The white-mica grain-size fractions show the same grain size vs apparent age pattern as sample OM19–13. Accordingly, we interpret the age to date the waning stages of mylonitic shearing, probably still at blueschist-facies conditions.

Finally, sample OM23–3 is a fine-grained, strongly deformed, greyish phengite-bearing micaschist with a well-defined stretching lineation on foliation planes, from the KQMS Nappe directly below the UP-LP Discontinuity (Figs. 2, 3). Besides phengite, the assemblage is comprised of chlorite, carbonates, quartz, epidote, tourmaline and ilmenite. The Rb—Sr data points define a well-constrained seven-point isochron corresponding to an age of 75.33 ± 0.78 Ma (MSWD = 2.3, Fig. 8p). We interpret this age to reflect the waning stage of shearing at greenschist-facies metamorphic conditions, similar to sample QM19–14.

4.4.3. Al Khuryan and Al Wudya shear zones, and deformation of Al Khuyran-Quryat-Mayh-Saih Hatat Nappe

Sample OM22–8 from the Al Khuryan shear zone is another calcschist mylonite with top-to-the-SW kinematic indicators. Three white-mica grain-size fractions, calcite and dolomite combine to a robust five-point isochron with an age of 82.2 ± 0.7 Ma (MSWD = 2.1, Fig. 8q). This age is interpreted to reflect the waning stages of top-to-the-SW mylonitic shearing in the Al Khuryan shear zone.

Sample OM23–2 is a very fine grained, strongly foliated, reddish, phengite-bearing phyllite from the top-to-the-SW Al Wudya shear zone, with calcite and Fe-bearing carbonate, phengite and hematite as the dominant phases. The Rb—Sr isotopic data define a well-constrained six-point isochron with an age of 84.9 ± 1.7 Ma (MSWD = 0.41, Fig. 8r). This age nearly coincides with the age of sample OM22–8 from the Al Khuryan shear zone.

Sample OM22–4 from the Al Khuryan-Quryat Unit of the KQMS Nappe (Fig. 3) is a strongly deformed carbonate schist containing blue-green amphibole. The shear sense in the outcrop is top-to-the-NE. Three white-mica grain-size and two calcite fractions (contrasted by their magnetic susceptibility and thus by their Fe concentration) provide an isochron age of 74.0 ± 4.0 Ma (n = 5, MSWD = 0.75, Fig. 8s).

Sample OM22–16 is a micaschist from the Proterozoic Hatat Formation of the Saih Hatat Unit of the KQMS Nappe. The Rb—Sr data from three fractions of white mica, calcite, apatite and feldspar define a regression line corresponding to an age of 75.8 ± 5.6 Ma (n = 6, MSWD = 1262, Fig. 8t). There is a distinct positive correlation between white-mica grain size and apparent age, which together with disequilibria among the low-Rb/Sr phases apatite, calcite and feldspar explains the high MSWD. We interpret the age of 75.8 ± 5.6 Ma as reflecting protracted non-penetrative top-to-the-NE deformation. An apparent age for the smallest white-mica grain-size fraction of 160–90 μm is difficult to define, given the Sr-isotopic disequilibria between the low-Rb/Sr phases. Calculation of an apatite-based isochron results in an apparent age of 70.5 ± 1.0 Ma, whereas calculation of a calcite-based isochron points to an age of 74.3 ± 1.1 Ma. The time bracketed by these two apparent ages is regarded as a maximum age for the end of deformation.

4.4.4. Ruwi Hill and Hamriyah shear zones

Sample OM22–9 is a carbonate mylonite with top-to-the-NE shear sense indicators from the Ruwi Hill shear zone. Three white-mica grain-size, plus a magnetically separated white-mica fraction show a tight cluster of Rb—Sr isotopic data yielding, when combined with the data for calcite and dolomite, a robust six-point isochron with an age of 81.7 ± 1.1 Ma (MSWD = 1.7, Fig. 8u). Again, this well-defined age is best interpreted as constraining the waning stage of mylonitization in the Ruwi Hill shear zone.

Sample OM22–10 is from the Hamriyah shear zone above the Ruwi

Nappe (Fig. 6a, 7) and characterized by an intense crenulation cleavage associated with top-to-the-SW shear-sense indicators (Hansman et al., 2021, their Fig. 18c, d). Rb—Sr data for the Sr-rich white-mica, calcite and a mixed dolomite-white mica fraction provide a robust six-point isochron defining an age of 68.8 ± 2.7 Ma (MSWD = 0.26, Fig. 8v), which is distinctly younger than the age for OM22–9.

4.5. Summary and interpretation of Rb—Sr age data

4.5.1. History of high-P metamorphism

Our ages for high-P metamorphism indicate two distinct age clusters: (1) 99–96 Ma and, (2) 80–76 Ma (Fig. 9). Ages of 99–96 Ma for waning high-P metamorphism in the Ruwi Nappe. Our mapping indicates that these ages are associated with top-to-the-NE shear-sense indicators in the upper Ruwi Nappe (Fig. 6a) and top-to-the-SW kinematic indicators in the lower parts of the nappe. We suggest that this pattern defines an extrusion wedge aiding early exhumation, and also the subsequent emplacement along the Ruwi out-of-sequence thrust (ROOST in Fig. II-1 in Data Supplement Item II) of the Ruwi Nappe.

The tectonic significance of age cluster (1) for the subduction history and geometry at the Arabian margin has been discussed in Ring et al. (2023). Ages of about 80–76 Ma for high-P metamorphism of the As Sifah Unit are not new. Our Rb—Sr ages from the two high-P units below the As Sheik shear zone date the waning stages of high-P metamorphism at 78.7 ± 1.7 Ma (OM19–5 from As Sifah Unit) and 77.2 ± 1.8 Ma (OM19–18 from the Diqdah Unit). New is that we constrained initial decompression from eclogite- to blueschist-facies metamorphism at 78.7 ± 1.7 Ma (OM19–5), which together with the age of 77.0 ± 1.3 Ma for a greenschist-facies overprint from the same outcrop (OM19–6) indicates rapid exhumation at rates ≥1 cm a^{-1}. Also new is that the second age cluster is recognized in the overlying Hulw (below the UP-LP Discontinuity; 76.2 ± 1.6 Ma, OM19–17) and KQMS nappes (above the UP-LP Discontinuity at 75.5 ± 4.4 Ma, OM23–1), as well as in the UP-LP Discontinuity shear zone (72.3 ± 4.9 Ma, OM19–14).

4.5.2. History of shear-zone activity

The age ranges for the various shear zones are summarized in Table 3 and schematically illustrated in Fig. 9 and Figure Fig. III-11. The isotopic data of six samples from the Yenkit shear zone consistently indicate protracted (or multi-episodic) top-to-the-SW shearing between 114 and ≤76.5 Ma (sample OM22–5). The latter age may also be interpreted as being related to a distinct reactivation event. The age data for the coarse and fine white-mica grain-size fractions in Fig. 9 may be best explained to reflect long-lasting deformation between ~114 and ~93 Ma. The data show that the Yenkit shear zone is the most long-lasting structure at the Cretaceous Arabian margin being active during age clusters 1 and 2 (Fig. 9). An important and unresolved issue is whether there was slow, continuous, non-penetrative shearing over almost 40 Ma, or punctuated events of shearing at ~114–104,~94.5 and ≤76.5 Ma? The permissible ages of ≤~94.5 and ≤76.5 Ma and ≤76.5 Ma overlap with ages for thrusting along the base of the Samail Ophiolite, as well as backthrusting and the development of the Saih Hatat fold nappe (Fig. 9).

Table 3
Age data for shear zone activity in Saih Hatat window (structurally from top to bottom).

Shear zone (sample)	Age (Ma)	Shear sense
Hamriyah shear zone (22–10)	71.5–66.1	Top-SW
Ruwi Hill shear zone (22–9, 23–4)	82.8–77.1	Top-NE
Yenkit shear zone (22–7, 22–5, 22–1, 19–19 21–3, 21–2)	114.3 Ma – ≤74.6	Top-SW
Al Wudya shear zone (23–2)	86.6–83.2	Top-SW
Al Khuryan shear zone (22–8)	82.9–81.5	Top-SW
Upper-Lower Plate (UP-LP) Discontinuity (23–3, 22–11, 19–14, 19–9)	(83.6) 77.1–67.4	Top-NE
As Sheik shear zone (19–13)	79.0–73.9	Top-NE

Note that maximum age of 83.6 Ma from Upper-Lower Plate Discontinuity reflects large uncertainties of age of sample OM22–11 and that age of 74.2 ± 0.6 Ma from OM22-11 probably better estimate for movement at Upper-Lower Plate Discontinuity, in which case age range would be 77.1–67.4 Ma.

Important is the age of 111 Ma of sample OM22–5 from the westernmost Yenkit shear zone as it strongly suggests that the Yenkit shear zone originated below the Ruwi Nappe. The age of 68.8 ± 2.7 Ma (OM22–10) shows that the Hamriyah shear zone above the Ruwi Nappe is a late re-imbrication locally emplacing the Yiti Nappe above the Ruwi Nappe (Searle et al., 1994, 2004, and Data Supplement Item II). This age for re-imbrication coincides with the timing of the final stages of formation of the Saih Hatat fold nappe (Gregory et al., 1998), suggesting that the two structures are related.

The Al Khuryan and Al Wudja shear zones provide similar ages of 82.2 ± 0.7 Ma and 84.9 ± 1.7 Ma for top-to-the-SW thrusting with no indication for earlier increments of deformation. Again, important are the isotopic data of OM22–5 with an apparent age of 76.5 ± 1.9 Ma for the most fine-grained white-mica grain-size fraction, interpreted to provide a maximum age for a final stage of reactivation at the Yenkit shear zone. This would be the only indication so far for reworking of the Yenkit shear during the second cycle of high-P metamorphism in the Saih Hatat window. After movement on the Al Khuryan and Al Wudja shear zones during underthrusting causing the 80–76 Ma high-P event, segments of the Yenkit shear zone were reactivated during exhumation of the high-P rocks.

The Ruwi Hill shear zone yields a similar mylonitization age of 81.7 ± 1.1 Ma as the Al Khuryan and Al Wudja shear zones. However, the Ruwi Hill shear zone has an opposite (top-to-the-NE) shear sense and is structurally above the Al Khuryan and Al Wudja shear zones. The age of 79.1 ± 2.0 Ma (OM22–9) for top-to-the-NE shearing in the Ruwi Nappe overlaps in age with the directly overlying Ruwi Hill shear zone. It is likely that all these shear zones are related to each other (see Data Supplement II).

Exhumation of the highest-P As Sifah Nappe was mainly accomplished by the top-to-the-NE As Sheik normal shear zone (Searle et al., 2004; Agard et al., 2010). The final stages of normal shearing were dated at 76.4 ± 2.6 Ma (OM19–13) and corroborate rapid exhumation rates >1 cm a^{-1} of the As Sifah Nappe. The As Sheik normal shear zone is being crosscut by the UP-LP Discontinuity, which is in line with ages of 74.5 ± 2.1 and 72.3 ± 4.9 Ma (samples OM19–9 and OM19–14). These ages are similar to the ages of 75.6 ± 1.2 Ma for the UP-LP Discontinuity and 70.7 ± 1.4 Ma from the Saih Hatat fold nappe by Miller et al. (1999). As indicated above, the latter age coincides with our age for the Hamriyah shear zone.

In summary, the age data from the shear zones (Table 3) show no simple progradation of shear-zone activity structurally downward. After initial movement at the Yenkit shear zone it appears that the Al Khuryan and Al Wudya shear zone are related to underthrusting of the Saih Hatat high-P nappes (except the Ruwi Nappe). The As Sheik shear zone is the only major exhumation structure in the Saih Hatat window. After considerable exhumation of the As Sheik footwall the UP-LP Discontinuity cuts the As Sheik shear zone. The Hamriyah shear zone reflects a late shortening stage, possibly associated with the final stages of emplacement of the Saih Hatat fold nappe.

5. Discussion

We discuss the tectonic significance of the two age clusters for waning high-P metamorphism at (1) 99–96 Ma (mid-Cretaceous) and (2) 80–76 Ma (late Cretaceous) (Fig. 9; Fig. III-11). For (1), we consider the position and geometry of the two subduction zones needed to explain

the P-T data. For (2), we focus on the potential subduction of a wide part of the rifted margin and which segment of the rifted margin and/or Arabian Platform might be preserved as high-P nappes in the Saih Hatat window. We also speculate on the initiation of the two mid-Cretaceous subduction zones, how the exhumation of the late Cretaceous high-P rocks was accomplished, and why and when subduction was fully transferred to the Eurasian side of Neo-Tethys.

5.1. Coeval mid-Cretaceous high-P and high-T metamorphism: Need for two subduction zones

Ring et al. (2023) showed that the Rb—Sr ages from the Ruwi Nappe indicate that high-P metamorphism and deformation occurred before and during the formation of the Samail Ophiolite and its metamorphic sole. They discussed a two-subduction-zone scenario for the Arabian margin. Here we expand on this work by discussing an alternative model of how subduction may have been partitioned at the Arabian margin.

The ages of 99–96 Ma for the closing stages of high-P metamorphism in the Ruwi Nappe have at least two important tectonic implications. Following our interpretation of metamorphism and partial melting processes in the sole (section 3.3.2.), the ages for waning high-P metamorphism are: (1) About 3–9 Ma younger than prograde to peak metamorphism (~800–850 °C at 105–102 Ma) of the sole (Guilmette et al., 2018) (note that the onset of the Ruwi high-P overprint was potentially as old, or even older, than sole metamorphism). (2) Our ages for ceasing high-P metamorphism of the Ruwi Nappe are largely coeval with partial melting of the sole during decompression and increasing temperature (T up to ~850–900 °C) between 100.4 and 92.4 Ma (Guilmette et al., 2018; Garber et al., 2020; Goscombe et al., 2020) and subsequent thrusting of the ophiolite and sole over the Misfah Platform.

Key for discussing the Cretaceous subduction-zone geometry at the Arabian margin in Oman is to reconcile the early processes after the initiation of the Samail subduction zone by 105–102 Ma (or slightly earlier, see box for zircon core in Fig. 9) with waning high-P metamorphism of the Ruwi Nappe and deformation in the Yenkit shear zone starting at ~114 Ma. One might speculate that the final stages of high-P metamorphism (at thermal gradients of ~8–10 °C km^{-1}) of the Ruwi Nappe at 99–96 Ma and prograde to peak metamorphism of the sole (at thermal gradients of ~20–25 °C km^{-1}) could have occurred in the same subduction zone (Searle et al., 2022; their Fig. 6).

In general, a subducting plate has initially a transient 'hot' thermal structure before approaching the final 'cold' steady-state configuration. A recent compilation of thermal data from 70 Cenozoic subduction zones by Lallemand and Arcay (2021) shows that it takes ~5–15 Ma between hot subduction-zone initiation and self-sustained, steady-state subduction under a stable thermal gradient of ~8–10 °C km^{-1}. This timeframe is in line with inferences from numerical models (e.g., Peacock, 1990; Gerya et al., 2002) suggesting that steady-state conditions are approached within 10–15 Ma. In accordance with that are geochronologic studies from many subduction complexes worldwide revealing that ages for cold high-P metamorphism substantially postdate subduction initiation (Okamoto et al., 2004; Penniston-Dorland et al., 2015; Takeshita et al., 2023). For blueschists in the Zagros Mountains in Iran, Angiboust et al. (2016) showed that it took ~30 Ma for the thermal gradient at the subduction interface to adjust from ~17 to ~7 °C km^{-1}.

It follows that if prograde 'hot' sole (105–102 Ma) and ceasing 'cold' Ruwi high-P metamorphism (99–96 Ma) occurred in the same subduction zone, the shortest time intervals for subduction-zone thermal equilibration of Lallemand and Arcay (2021) have to be assumed, as one would be forced to argue that the subduction zone fully thermally equilibrated within ~5 Ma after its initiation. This interpretation demands that high-P metamorphism in the Ruwi subduction zone was a short-lived process and that ages of 99–96 Ma mark the start and the end of high-P metamorphism. Such an inference would be in conflict with the general finding that high-P rocks usually develop substantially after the inception of subduction (Okamoto et al., 2004; Penniston-Dorland et al., 2015; Takeshita et al., 2023).

The ages for waning Ruwi high-P metamorphism are coeval with partial melting of the sole. Both processes *cannot* occur in one single subduction zone at the same time. Therefore, two mid-Cretaceous subduction zones at the Arabian margin in Oman must have existed: the Ruwi and Samail subduction zones. The above discussion on the timing of high-P metamorphism relative to subduction-zone initiation, and thermal arguments, make it likely that the Ruwi subduction zone developed first. The onset of Samail subduction could be as old as 105.2 Ma, or even 106.9 ± 2.3 Ma (if the 'detrital' zircon core of Garber et al. (2020) is considered metamorphic in origin). In contrast, the Ruwi subduction zone was fully equilibrated before 99 Ma and thermal considerations make it likely that subduction started at or before 110 Ma. The latter age estimate agrees with the data for initial deformation in the Yenkit shear zone at ~114 Ma.

Where would the Ruwi subduction zone have formed? The Ruwi Nappe is made up of continental rocks, which indicates that the Ruwi subduction zone should be closer to the Arabian margin than the intraoceanic Samail subduction zone.

5.2. Tectonic models

Tectonic models can be based on theoretical considerations, geologic constraints or, ideally, on both. Ring et al. (2023), (their Fig. 6) discussed a two-subduction-zone scenario that was motivated by theoretical/numerical predictions. Numerical simulations (e.g., Nikolaeva et al., 2010) show that favourable conditions for subduction initiation at rifted margins are where depleted continental lithosphere is thin. The Al Aridh Trough matches this prerequisite. Accordingly, Ring et al. envisaged that the thin, dense lithosphere of the Al Aridh Trough was underthrust beneath the thick lithosphere of the Misfah Platform (Fig. 5), an interface where gravitational instability triggered by density contrasts is pronounced.

The model of Ring et al. (2023) explains the ~20 Ma age gap between the two high-P age clusters, as the rocks producing the different ages are laterally distinctly separated from each other by the ~220 km wide Hamrat Duru Subbasin and the Baid Horst (Fig. 5). The occurrence of ~90–86 Ma old radiolarite in parts of the Hamrat Duru Subbasin also does not provide a problem, as long as one envisages relatively small subduction rates at the Ruwi subduction zone. However, our review on potential protoliths of the Ruwi calcareous phyllite and the tectonically underlying Yiti Nappe dolostones (section 3.7.) suggests that the rocks of the Ruwi and Yiti nappes originated at the Arabian Platform and platform margin, geologic constraints the Ring et al. (2023) model does not correspond to.

Searle et al. (2004) and Searle (2019) suggested that the Ruwi Nappe correlates with the Haybi complex of the distal Umar Subbasin (see above). In this case, the Ruwi subduction zone may have localized near the continent-ocean transition in the Umar Subbasin, and both (Ruwi and Samail) subduction zones would have formed close to each other during the mid-Cretaceous (Fig. 5). Again, such a scenario is not in line with the origin of the rocks of the Ruwi and Yiti nappes.

An even greater problem of placing the Ruwi subduction zone near the continent-ocean transition is that the Misfah Platform would need to have entered the Ruwi subduction zone soon after the latter formed (Fig. 5). Ring et al. (2023) discussed that Ruwi subduction commenced at ≥110 Ma and, thus, potentially before the inception of the Samail subduction zone. The 'docking' of the Misfah Platform at the Ruwi subduction zone could have initiated the Samail subduction zone (but both subduction zones were oriented ~90° to each other). However, the Ruwi subduction zone with the incoming Misfah Platform would have interfered with the Samail subduction zone at a stage when the Samail subduction zone rolled back, the metamorphic sole underwent peak metamorphism, and before partial melting of the sole and the formation of the Samail oceanic lithosphere occurred. Such a scenario appears geometrically impossible. For these reasons, we consider localization of

Ruwi subduction near the continent-ocean transition unreasonable. This conclusion would be in line with our proposition that the Haybi complex is an unlikely source for the Ruwi Nappe.

Below we present a new tectonic model that is based on the geologic constraints. It still highlights the problem of poorly constrained subduction rates. Adjusting subduction rates would either cause or eliminate problems of the discussed model.

5.2.1. Inboard subduction near Arabian platform margin - platform evolution model

We argued that the Saiq and Mahil formations represent a continuous facies realm of the Arabian Platform. We also favour an origin of the calcareous phyllite of the Ruwi Nappe on the platform slope. Consequently, it is likely that the Yiti and Ruwi nappes, and the Yenkit shear zone at its base, formed on the distal Arabian Platform and not within the rifted margin section. It is likely that the Yenkit shear zone reactivated a Permian normal fault.

The model illustrated in Fig. 10 is similar to the two-subduction zone interpretation of Breton et al. (2004). Most tectonic details are shown in the model directly and in the figure caption. The Ruwi subduction zone is close to the Arabian platform margin (continental slope) allowing deposition of the carbonate-rich precursor rocks of the Ruwi Nappe at water depth <~3000 m. The Yiti Nappe and the top-to-the-SW Yenkit shear zone formed on the Arabian Platform. If so, the Yiti Nappe and the Yenkit shear zone would be unrelated to high-P metamorphism and exhumation of the Ruwi Nappe (Fig. 10a).

The underthrusting and high-P metamorphism of the Ruwi, As Sifah, Hulw and KQMS, nappes occurred successively as the platform margin was subducted (Fig. 10b-f). However, the accretion and high-P overprint of the Ruwi Nappe took place distinctly earlier (~20 Ma) than that of the As Sifah, Hulw and KQMS nappes, even though they originated in relative proximity to each other (Fig. 10a). Deriving all high-P nappes from the Arabian Platform (As Sifah, Hulw and KQMS nappes) and slope (Ruwi Nappe) may be explained by high-P accretion of the Ruwi Nappe before the thicker (and more buoyant) continental crust of the leading edge of the Arabian Platform entered the subduction zone. This slowed down subduction considerably and lowered the subduction dip angle, reducing wedge taper (Davis et al., 1983). The latter caused exhumation of the Ruwi extrusion wedge (Fig. 10c-e). The Arabian Platform continued to be subducted to depths of ~80 km until ~80 Ma when the As Sifah Nappe formed. Deriving the high-P As Sifah, Hulw, and KQMS nappes from the leading edge of the Arabian Platform demands slow subduction rates of <0.7 cm a^{-1} (for average subduction angles of 30–45°). Such slow rates are considered possible (e.g., Abers, 2011). In contrast, subduction at the outboard Samail subduction zone would have consumed almost the entire width of the rifted-margin section and adjacent Neo-Tethys oceanic crust (>450 km) requiring minimum subduction rates of 2–3 cm a^{-1}, which are about 3–4 times greater than those at the continental Ruwi subduction zone (due to rotation subduction rates are variable along strike of the Samail subduction zone).

In the platform evolution model, the significant high of the Misfah Platform would have approached the Samail subduction zone at ~93 Ma (Fig. 10d). The arrival of the Misfah Platform at the Samail subduction zone would have caused a reduction in wedge taper and increased shortening across the Samail wedge (Davis et al., 1983). The subduction thrust of the Samail subduction zone (the Samail Thrust) would have been forced to step back and override the incoming bathymetric high of the Misfah Platform causing out-of-sequence thrusting. The additional shortening across the Samail subduction wedge may have triggered movement of the Samail Ophiolite and stacking of the metamorphic sole. This additional shortening might have been needed to explain, or would have strongly aided, the high displacement rates of ~15 cm a^{-1} proposed by Hacker et al. (1996). These processes in the Samail subduction zone were largely coeval with initial exhumation of the Ruwi Nappe.

The platform evolution model is compatible with several geologic constraints and allows the overriding-plate thrust wedge (Samail and Hawasina nappes) to be still relatively far outboard at ~90 Ma (Fig. 10e), readily explaining the lack of ophiolite detritus in the Aruma foredeep sediments of the Muti Formation. The ongoing deposition of radiolarite until ~90–86 Ma in the Hamrat Duru Subbasin (Blechschmidt et al., 2004) would also be explained by the model.

The Wasia-Aruma break reflecting a stable Arabian Platform until ~92 Ma would be hard to reconcile with movement at the Yenkit shear zone on the platform since ~114 Ma. However, as outlined above, the Wasia-Aruma break sensu stricto may apply only for the Jabal Akhdar region.

5.2.2. Role of Yenkit shear zone

The Yenkit shear zone with incipient deformation starting at ~114 Ma is the oldest known Cretaceous structure in the Saih Hatat window. We discuss the implications of (1) prolonged non-penetrative deformation from ~114 to ≤76.5 Ma, i.e., maximum age of reactivation of sample OM22–5, and (2) distinct periods of reactivation of the Yenkit shear zone at ≤94.5 Ma and ≤76.5 Ma.

(1) Prolonged non-penetrative deformation of the Yenkit shear zone could be related to reactivation of a former normal fault that evolved as a slowly moving thrust on the Arabian Platform. Formation of the shear zone would be a result of accelerated convergence after 118 Ma. Upper-crustal top-to-the-SW shearing of the Yiti Nappe has been shown by Searle (2019, his Fig. 12.13). Subduction of the Yenkit shear zone as part of a segment of the Arabian Platform occurred close to the later Al Khuryan shear zone at a time when the overriding plate wedge was thrust onto the Arabian Platform and the Samail Ophiolite shed material into the Juwaiza Formation (Fig. 9, 10f). Prolonged non-penetrative deformation of the Yenkit shear zone would involve its initiation at ~114 Ma with partial re-equilibration stages at ~100–93 Ma, ≤94.5 Ma and ≤76.5 Ma.

(2) A distinct phase of reactivation at ≤94.5 Ma might be related to initial underthrusting of the platform margin and/or a first phase of top-to-the-SW out-of-sequence re-imbrication related to accretion of the Ruwi Nappe to the base of the overriding plate thrust wedge after its exhumation (Fig. 10e, and ROOST in Fig. II-1 in Data Supplement II). Both interpretations might be related to each other. The second reactivation at ≤76.5 Ma might be due to the formation of the Saih Hatat fold nappe (section 4.5.2.).

If the Yenkit shear zone indeed reactivated a former normal fault at ~114 Ma as depicted in our model (Fig. 10a), the question arises why not at least some of the Permo-Triassic normal faults in the Hawasina Basin were reactivated at about that time as well. In this case, we consider it most likely that this reactivation actually happened, but detecting these 114 Ma thrusts in the Hawasina Basin would be hard and demand detailed mapping of a rather monotonous section. If those thrusts existed, then ongoing deposition of radiolarite until ~90–86 Ma would be harder to picture in the platform evolution model.

5.3. Late Cretaceous subduction history

The 80–76 Ma high-P rocks reflect continental subduction of the leading edge of the Arabian Platform (Breton et al., 2004). The As Sifah, Hulw and KQMS nappes all contain abundant rifting-related mafic rocks. According to our model, the ~20 Ma age gap between the high-P age clusters 1 and 2 demands that Ruwi subduction was slow. We envisage that subduction of the leading edge of the Arabian Platform was aided by abundant dense mafic rocks, which were, at least in part, progressively transformed into eclogite in the As Sifah Nappe (note that according to Christensen and Mooney (1995) eclogite is ~10% denser than mantle peridotite). Once the full thickness (35–40 km) Arabian continental crust, with hardly any mafic rocks (Jabal Akhdar window; Scharf et al., 2021; Weidle et al., 2022, 2023), entered the subduction zone, buoyancy caused subduction to cease and plate convergence between Arabia and Eurasia was eventually fully transferred to the Makran subduction

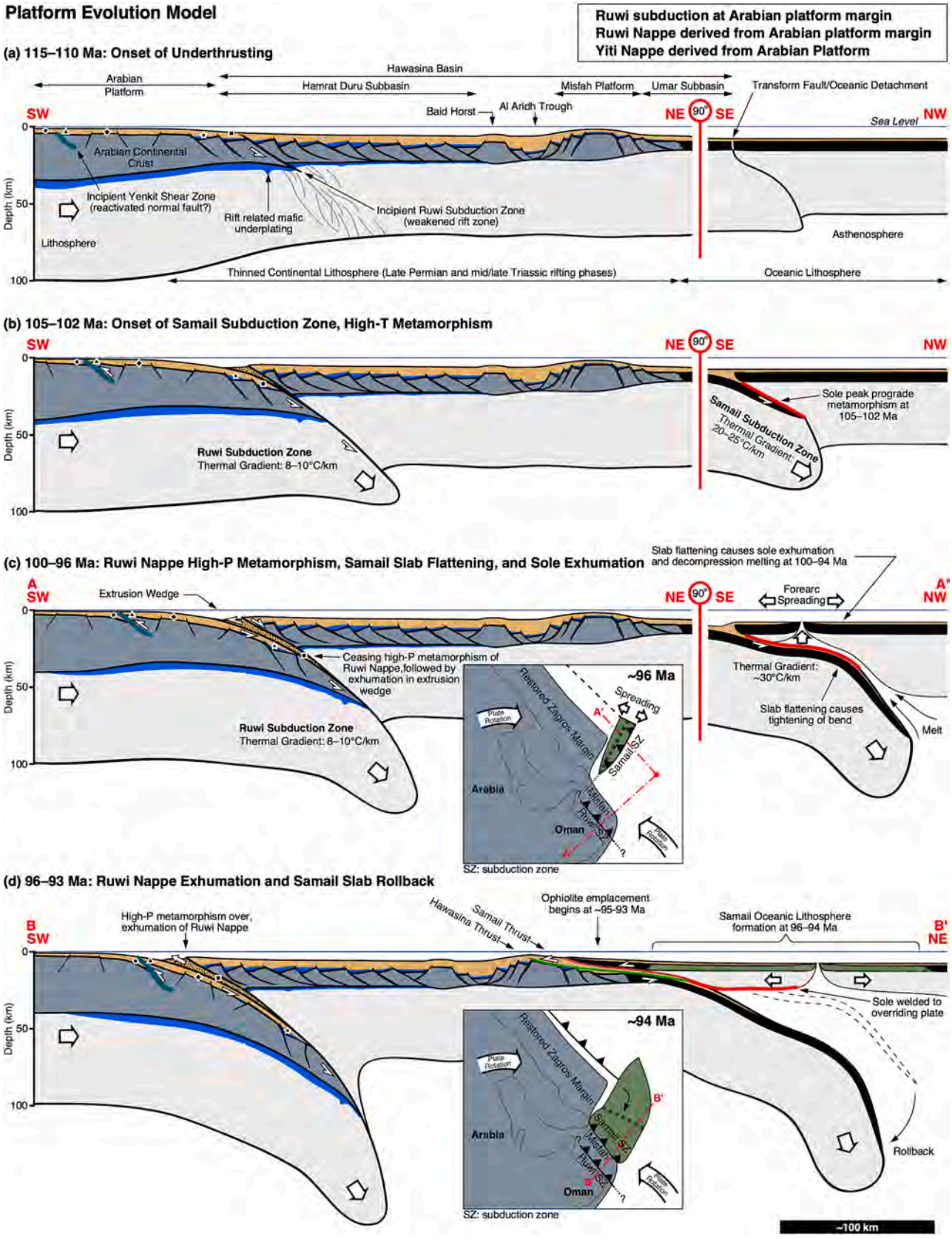

Fig. 10. Platform evolution model placing Ruwi subduction zone close to Arabian Platform in proximity to Hamrat Duru Subbasin (Breton et al., 2004). (a) Yenkit shear zone formed on platform followed by initiation of Ruwi subduction zone near platform slope, Ruwi calcareous phyllite protolith deposited at water depths <~3000 m; note that Ruwi, As Sifah, Hulw and KQMS nappes originated close to each other near mafic-rock-rich platform margin. (b) Incipient formation of Samail subduction zone and prograde to peak high-T metamorphism of metamorphic sole at 105–102 Ma (Guilmette et al., 2018), while Ruwi subduction zone started to thermally equilibrate; note different thermal gradients and that both subduction zones >90° apart from each other. (c) Advanced stage of Samail subduction,

decompressional partial melting of metamorphic sole under thermal gradient of ≥30 °C km^{-1} and incipient rollback-controlled forearc spreading; waning high-P metamorphism and incipient exhumation of Ruwi Nappe; note As Sifah Nappe already underthrusting in Ruwi subduction zone. Map view highlighting different orientations of subduction zones, convergence direction within Arabian Neo-Tethys and plume-induced rotation of Arabian Plate. (d) Exhumation of Ruwi Nappe while As Sifah Nappe underthrusts. Samail oceanic lithosphere crystallizing, exhuming metamorphic sole welded to base of ophiolite and both started to override sediments of Umar Subbasin; Misfah Platform envisaged to enter Samail subduction zone at end of this stage, reduced wedge taper due to underthrusting of bathymetric high of Misfah Platform caused increased shortening across Samail subduction zone aiding or triggering rapid movement of Samail Ophiolite at rates of 15 cm a^{-1} (Hacker, 1991) towards Arabian margin. Map view highlights rotation of Samail subduction zone. (e) At 92–88 Ma, Samail Ophiolite started to override Hamrat Duru Subbasin, Aruma foreland basin formed receiving sediments only from foreland bulge; radiolarite still depositing in parts of Hamrat Duru Subbasin (Blechschmidt et al., 2004). Note overriding-plate thrust wedge (composed in descending order of Samail Ophiolite with metamorphic sole, Umar section of Hawasina nappes, Exotics (i.e., carbonates of Misfah Platform), Al Aridh Trough and parts of Hamrat Duru section of Hawasina nappes) still far outboard explaining lack of ophiolite detritus in Aruma foredeep sediments and ongoing sedimentation in parts of Hamrat Duru Subbasin; i.e., forebulge potentially related to underthrusting of distal Arabian Platform. As Sifah Nappe still underthrusting in Ruwi subduction zone. (f) Al Khuryan and Ruwi Hill shear zones formed by 82 Ma before peak-high-P metamorphism of As Sifah, Hulw and KQMS nappes. Potential arc magmatism above Samail and Ruwi subduction zones. Close-up showing development of Al Khuryan (also Al Wudya, not shown) and Ruwi Hill thrusts. (g) At 79–76 Ma, As Sheik shear zone exhumed As Sifah Nappe; footwall of As Sheik shear zone rotated and domed, and cut by Upper/Lower Plate (UP-LP) Discontinuity causing heating of upper Hulw Nappe in footwall of UP-LP; doming considered to cause uplift potentially triggering ophiolite erosion and deposition in Juwaiza Formation. Note slab break-off shown as inferred process. Enlarged section shows UP-LP Discontinuity cutting As Sheik shear zone at mid-crustal depths (compare to Fig. 3c). Note unknown subduction rates leaving exact tempospatial aspects speculative; inferred minimum subduction rates of 2–3 cm a^{-1} for Samail (see text) and 0.5–0.7 cm a^{-1} for Ruwi subduction zones. (h) Development of Saih Hatat fold nappe above UP-LP Discontinuity. Enlarged section shows UP-LP Discontinuity cutting As Sheik shear zone at mid-crustal depths; Hamriyah shear zone forms, exploiting and reactivating segments of Yenkit shear zone.

system. The timing of this subduction transfer would roughly coincide with the slowdown of Arabia-Eurasia convergence from ~8 cm a^{-1} to 2–3 cm a^{-1} after 80 Ma (Gürer et al., 2022).

5.3.1. What happened between the two high-P stages?

Tectonometamorphic processes in the metamorphic sole terminated by ~93 Ma (Hacker et al., 1997; Garber et al., 2020 their Fig. 13) (Fig. 9). This age is similar to the permissible age of ≤94.5 Ma for potential reactivation of the Yenkit shear zone. It appears conceivable that both processes are related to each other. The potential reactivation of the Yenkit shear zone at ≤94.5 Ma might be due to the initial underthrusting and imbrication of the Arabian Platform at about the time the sediments of the Muti Formation started to accumulate.

What happened between ≤94.5/~93 and 80–76 Ma? We have argued, that the standard argument of a stable Arabian Platform until ~92 Ma does not necessarily apply to the present Saih Hatat window. The sediments of the Muti Formation of the Aruma Group are thought to reflect the development of a foredeep due to top-to-the-SW propagation of the overriding-plate thrust wedge towards the Arabian Platform between ~92–84 Ma (Robertson, 1987; Glennie, 2005) (Fig. 9). Gnos and Peters (1993) provided a K—Ar white-mica age of 81.3 ± 1.6 Ma for emplacement of the Samail Ophiolite (Fig. 2b), and Hansman et al. (2018) reported a U—Pb calcite age of 84 ± 5 Ma for top-to-the-SW thrusting in carbonate of the Arabian Platform below the overriding plate in the Jabal Akhdar window. The Fiqa Formation of the Aruma Group (~88–72 Ma) represents the non-exposed, southwestern portion of the marine foreland basin and its sedimentary fill is documented by seismic and borehole data (Boote et al., 1990; Warburton et al., 1990). The bottom sequence of the Fiqa Formation (FD-a Unit, ~88–86 Ma) was overridden by the Hawasina nappes. The overlying Fiqa FD-b Unit (~86–84 Ma) was deposited during the final stages of thrusting and slices of it were accreted to the overriding plate (Warburton et al., 1990). The upper two subunits (FD-c and FD-d, ~84–72 Ma) were deposited after the initial emplacement of the overriding-plate thrust wedge (Boote et al., 1990). This summary suggests emplacement of the thrust wedge onto the Arabian Platform between ~88 and ~84 Ma, consistent with the first occurrence of ophiolite detritus in the Juwaiza Formation at ~83–80 Ma (Abdelmaksoud et al., 2022) (Fig. 9).

The Samail Ophiolite with its metamorphic sole successively accreted slices of the Umar Subbasin and Misfah Platform (Exotics) at ~93 Ma. Subsequently, the underlying upper-crustal rocks of the Hamrat Duru Subbasin and the exhumed Ruwi Nappe were accreted, and all units approached the platform margin as part of the overriding-plate thrust wedge. If the Samail Ophiolite and its metamorphic sole were finally assembled by 93 Ma while being thrust onto the Umar Subbasin and Misfah Platform, even the extreme initial displacement rates of 15 cm a^{-1} proposed by Hacker et al. (1996) would have hardly allowed the ophiolite to arrive at the Arabian Platform by 92 Ma. The lack of any ophiolite detritus in the foredeep sediments may suggest that the rear part of the thrust wedge, which was probably subaerially exposed (section 2.4.), was finally thrust over the Arabian Platform at ~83–80 Ma. If so, the non-high-P overriding plate was thrust over the Arabian Platform just before the peak of late Cretaceous high-P metamorphism of the majority of the high-P nappes in the Saih Hatat window.

The middle and lower crust of the Hamrat Duru Subbasin was being underthrust in the Samail subduction zone while the upper-crustal rocks were accreted to the overriding plate and thrust towards the Arabian Platform. This was followed by underthrusting of the outermost Arabian Platform and slope, which subsequently received their high-P overprint in the Ruwi subduction zone. We envisage that the middle and lower crust of the Hamrat Duru Subbasin was fully subducted and never got exhumed. A consequence of this proposition would be that there was a décollement below the Hawasina sedimentary rocks that decoupled the overriding plate from the middle/lower crust (see also Agard et al., 2010). The complete subduction of the extended middle and lower crust was probably strongly aided by the extensive Permian/Triassic volcanics and potential mafic intrusions/underplates that were possibly largely converted to dense eclogite during subduction.

In our model, the age gap of ~20 Ma between the two high-P stages must be explained by slow subduction and distinctly differential accretion. The Arabian Platform and platform margin already started to subduct slowly before 99–96 Ma and, thus, >~10–15 Ma before the Samail Ophiolite overrode the Arabian Platform. One might assume that slow subduction was caused by underthrusting of the relatively thick Arabian continental crust. Segments of this crust, contaminated by abundant Permian mafic rocks that successively got eclogitized (e.g., As Sifah eclogite), were accreted and exhumed.

In the Ring et al. (2023) model, decoupling in the Hamrat Duru section would explain the ~20 Ma gap in ages of the preserved high-P rocks. If decoupling and complete subduction successfully occurred for ~20 Ma, why does the second, younger cluster of high-P metamorphism exist? Some change in the boundary conditions must have taken place. We envisage that the arrival of the Saih Hatat platform section of the Arabian Platform in the Ruwi subduction zone caused that change in subduction-zone dynamics. This platform section slowed down subduction but was deeply underthrust, high-P metamorphosed and parts of it, probably for a short period of time, accreted and exhumed. A short period would explain the tight cluster of high-P metamorphism of 80–76 Ma (high-P metamorphism in the KQMS nappe might be slightly younger) for the entire Saih Hatat nappe stack below the Ruwi Nappe. We further hypothesize that the subsequent arrival of the full thickness,

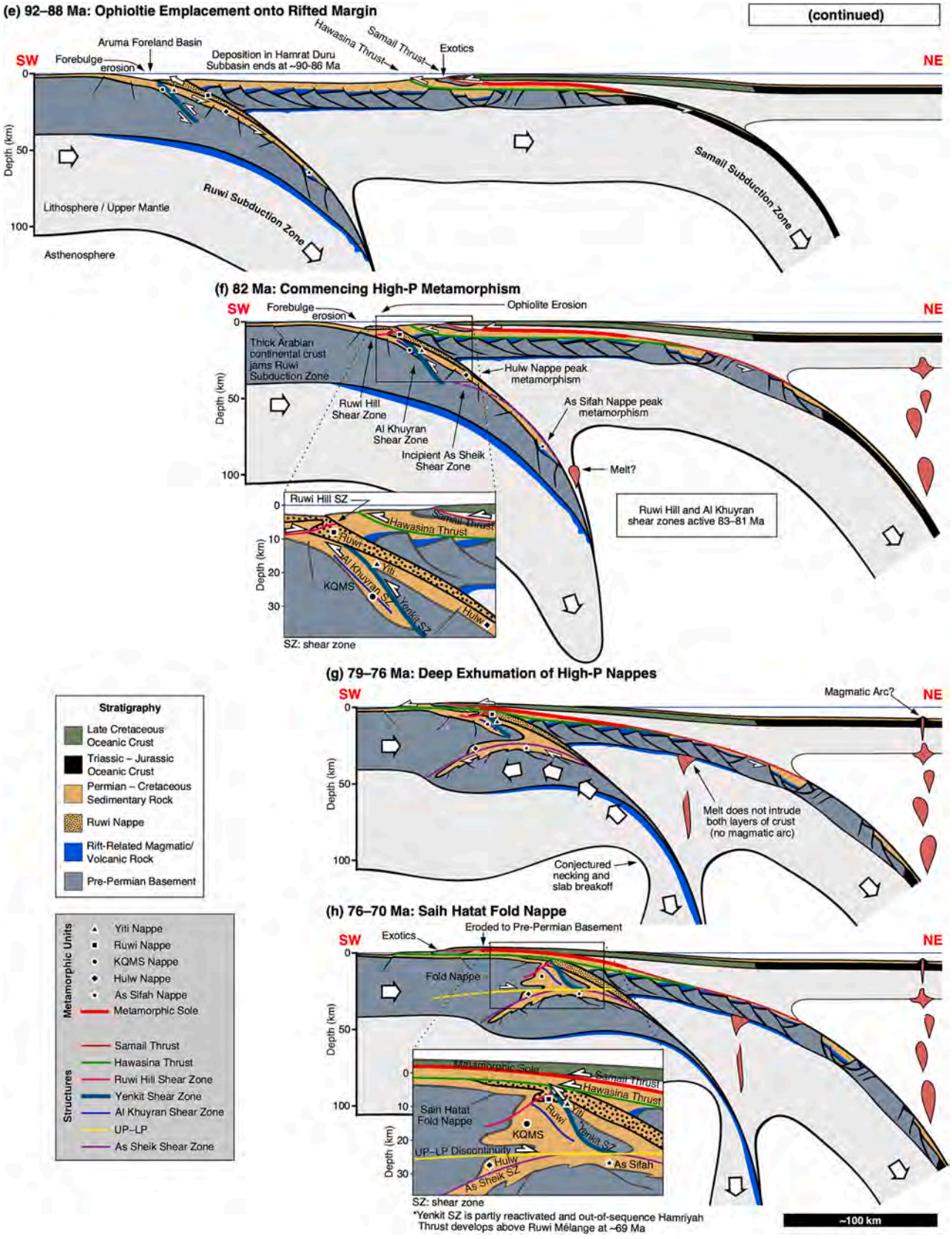

Fig. 10. (*continued*).

largely mafic-rock-free Jabal Akhdar section of the Arabian margin terminated subduction processes.

The two marked age clusters for the high-P overprint are different to the rather continuous downward propagation of high-P metamorphism in many orogens (see Introduction). Our discussion implies that the distinctly punctuated high-P age clusters are a consequence of the density structure of the Arabian Platform and rifted-margin sequence. Slow subduction of the leading edge of the Arabian Platform occurred for about 10–15 Ma before subduction choked due to the arrival of the full thickness Jabal Akhdar section of the Arabian lithosphere.

5.4. Exhumation of high-P rocks

The P-T data show two distinct clusters: (1) The Ruwi, KQMS and Hulw nappes have P_{max} of ~1 GPa, (2) the As Sifah Nappe P_{max} of ≥2 GPa. We start with the discussion of the exhumation of the mid-Cretaceous high-P rocks of the Ruwi Nappe. The top-to-the-NE shear-sense indicators at the top of the Ruwi Nappe are possibly associated with normal shearing (e.g., Agard et al., 2010) at 99–96 Ma. The maximum exhumation this event caused was modest, i.e., from ~1 GPa (~36 km, if an average rock density of 2800 kg m^{-3} is considered) and <330 °C to ~250 °C (ZFT closure, section 2.3.2.) which is from ~36 to 31–25 km for a thermal gradient of 8–10 °C km^{-1}, i.e., exhumation was 5–11 km before the Ruwi Nappe was accreted to the non-high-P overriding plate. Ongoing radiolarite deposition in the Hamrat Duru Subbasin (Blechschmidt et al., 2004) suggests accretion after 90–86 Ma (Fig. 10e), implying exhumation rates of <0.04–0.18 cm a^{-1}.

The main stage of deep exhumation of the Saih Hatat high-P rocks took place during the late Cretaceous. The majority of the exhumation of the As Sifah Nappe into the upper middle crust was accomplished by normal shearing at the As Sheik shear zone (Searle et al., 2004; Agard et al., 2010), with final stages of mylonitization at 76.4 ± 2.6 Ma. The P break across the As Sheik shear zone is 0.7–0.9 GPa, which correlates to crustal omission of ~25–32 km.

The UP-LP Discontinuity cuts the As Sheik shear zone (Figs. 3, 10h). Semi-balanced cross sections by Hansman et al. (2021) showed that the UP-LP Discontinuity is a neutral (i.e., originally subhorizontal), top-to-the-NE displacing fault that formed the N-closing Saih Hatat fold nappe above it (Miller et al., 1998; Gregory et al., 1998; Gray et al., 2005) (Fig. 2). Both structures developed at ~77–70 Ma (Miller et al., 1999; own data in Figs. 8i-k, 9). The P estimates for the greenschist/amphibolite-facies overprint of the As Sifah Unit (Searle et al., 1994) suggest a depth of 18–29 km for this metamorphic event. Because the UP-LP Discontinuity cuts the top of the Diqdah Unit above the As Sifah Unit (Fig. 3), we use ~22–25 km (~0.6–0.7 GPa, Fig. 3c) as a proxy for the deformation level of the subhorizontal UP-LP Discontinuity when it cut the As Sifah Nappe. Movement at the UP-LP Discontinuity and the formation of the overlying Saih Hatat fold nappe (Fig. 2) would have caused burial of the Hulw and As Sifah nappes. The P-T data of Yamato et al. (2007) for the Hulw Nappe suggest a modest increase in P of ~0.1–0.2 GPa (i.e., ~3.6–7.2 km), which is at best a crude hint of the degree of re-thickening. A thermal gradient of ~20 °C km^{-1} (Fig. 3c) and an increase in T of ~100 °C (Yamato et al., 2007) would suggest ~5 km of re-thickening. We argue that the near-isobaric heating of the Hulw Nappe is associated with the UP-LP Discontinuity. A subhorizontal fault resulting from subhorizontal shortening should have a low shear strength but still caused friction along the shear zone producing shear heating. Burg and Gerya (2005) and Mako and Caddick (2018) showed that the amount of shear heating could be up to ~200 °C. Given a weak fault, modest shear heating may help to explain the near-isobaric heating of ~100 °C of the Hulw Nappe.

The top of the Diqdah Unit was exhumed from ~60 km depth (Fig. 3c). As the UP-LP Discontinuity cuts the As Sheik shear zone at an inferred crustal depth of ~22–25 km (see above), the shear zone accomplished ~35 km of exhumation. Assuming a 30° dip of the normal shear zone would convert into a displacement of ~70 km. The Rb—Sr ages for high-P, decompression and the greenschist-facies metamorphism overlap. This indicates that the As Sheik shear zone was short-lived (≤2 Ma), exhumation rates were >1 cm a^{-1} and slip rates distinctly >2 cm a^{-1}. The As Sheik shear zone is the only significant exhumation agent in the Saih Hatat window.

How were the rocks above the As Sheik shear zone exhumed, especially the Hulw Nappe? Compared to the As Sifah Nappe, the age and depth of the high-P overprint of the Hulw Nappe suggests a distinctly slower late Cretaceous exhumation rate. The Hulw Nappe has peak metamorphic temperatures of 450–480 °C (after ~7 km (~0.2 GPa) of initial exhumation, Fig. 3c). If a thermal gradient of 20 °C km^{-1} was used (Fig. 3c), the T difference between peak-metamorphic-T and the closure-T for ZFT of ~250 °C would translate into ~10 km of crustal section. Evidence for a major top-to-the-NE normal shear zone aiding the exhumation of the Hulw and KQMS units is equivocal. Searle et al. (2004) and Agard et al. (2010) assumed normal reactivation at the Yenkit, Al Khuyran and Ruwi Hill shear zones.

Samples from below the UP-LP Discontinuity provide ZFT ages of 79 to 58 Ma (age range include 2σ uncertainties; Table 1) (Saddiqi et al., 2006; Hansman et al., 2017) indicating that these rocks remained near the brittle-ductile transition after the Samail Orogeny ceased by 70–68 Ma. Thus, the Oman Mountains are a rare example of an orogen that did not accomplish bringing its high-P rocks back to the surface during its orogenic cycle.

The exhumation of the units above the UP-LP Discontinuity is hard to interpret. The Ruwi Nappe was probably part of the overriding plate by the time the rock of the Muti Formation accumulated and was finally exhumed to the surface during early Cenozoic rifting (see below). The KQMS Nappe is most critical as the Al-Khod Formation includes carbonate clasts derived from the late Permian to mid-Cretaceous Hajar Supergroup in stratigraphically high conglomerates and metamorphic quartzite debris from the pre-Permian basement in the highest conglomerates (Mann et al., 1990; Nolan et al., 1990). Nolan et al. (1990) discussed that the Oman Mountains developed topographic relief at the end of the Campanian (~75–72 Ma) and that this relief and large annual rainfall inferred for the late Cretaceous Oman Mountains caused rapid erosion exhuming rocks from the core of the Saih Hatat fold during the deposition of the Maastrichtian Al-Khod Formation. Skelton et al. (1990) showed that most of the northern Oman Mountains subsided during the Maastrichtian and Mattern et al. (2023) concluded that the mountains were fully submerged by the mid-Eocene.

The work of Nolan et al. (1990), Mann et al. (1990), Skelton et al. (1990) and Mattern et al. (2023) shows that significant topography in the Oman Mountains existed only for a short period of time. This phenomenon is explained with the load of the dense Samail Ophiolite at the top of the nappe stack. Abundant dense eclogite at the base of the orogen also suppressed the build-up of topography. This summary again highlights the control of the lithospheric density structure for the Cretaceous orogenic development.

The three AFT ages from the core of the fold nappe (SO1, SO14, SO15) (Fig. 2) are between 52 ± 5 and 40 ± 7 Ma (Saddiqi et al., 2006) and younger than late Cretaceous erosion of the core of the fold nappe. Samples SO1, SO2, SO3 and SO28 from the westernmost Saih Hatat window (Fig. 2) provided ZFT ages up to 119 Na (Table 1) suggesting a detrital age component and thus limited burial of the basement there. We suggest that late Cretaceous erosion affected the southwestern Saih Hatat window above the closure depths of the AFT system (~4 km for a thermal gradient of 25 °C km^{-1}), i.e., late Cretaceous erosion caused ≤4 km of exhumation. This would be in line with the occurrence of quartzite pebbles from the Amdeh Formation in the Al-Khod conglomerates as the stratigraphic pile above the Amdeh Formation is ≤2.5 km (see section 2.1.1.).

Part of the exhumation of the KQMS could have been taken up by alleged top-to-the-NE normal reactivation of the Yenkit, Al Khuyran and Ruwi Hill shear zones (Searle et al., 2004; Agard et al., 2010). Fournier et al. (2006), Mattern and Scharf (2018) and Scharf et al. (2020)

suggested late Cretaceous normal faulting at the Front Range Fault, which would have also contributed to the exhumation of the Saih Hatat window. Saddiqi et al. (2006) and Hansman et al. (2017) showed a pronounced phase of cooling associated with early Cenozoic horizontal extension, which accomplished the final exhumation of the vast majority of the Saih Hatat high-P rocks to the surface.

5.5. Implications for Neo-Tethys subduction

We envisage that the increase in Arabia-Eurasia convergence rates at ~118 Ma initiated subduction at the southern (Arabian) margin of Neo-Tethys, i.e., at the Ruwi subduction zone, and also activation of the Yenkit shear zone at ~114 Ma. Starting at ~105 Ma, global changes in relative plate motions, including a directional change of the Africa-Eurasia convergence (DeMets et al., 2010; Torsvik et al., 2010), and potentially clockwise rotation of Africa/Arabia due to the Morondava Plume (van Hinsbergen et al., 2021), may have aided instigation of Samail subduction along a former transform ridge (Hacker et al., 1996; Morris et al., 2016; van Hinsbergen et al., 2019) (Fig. 1b). This proposition would consider Samail subduction to be a geometric effect of plate rotations moving a weak transform ridge into a suitable orientation.

Subduction and punctuated, late high-P metamorphism in the Ruwi subduction zone went on until about 80–76 Ma. Slab break-off to the north of Oman is a conjectured process envisaged to explain why subduction choked. Slab break-off is often considered to occur soon after light continental lithosphere follows dense oceanic lithosphere into the subduction zone (Davies and von Blanckenburg, 1995; von Blanckenburg and Davies, 1995). However, the Ruwi subduction zone did not have much of an oceanic precursor slab and subduction was proceeding for >30 Ma before it came to an end.

We argue that the arrival of the full-thickness and buoyant Arabian continent halted subduction (see also Agard et al., 2010) and suggest that stalling of subduction by 80–76 Ma caused the development of the UP-LP Discontinuity and the associated Saih Hatat fold nappe between 76 and 70 Ma (Fig. 10h). We envisage that the UP-LP Discontinuity took up the residual 'Arabian' fraction of plate convergence that was hitherto being accommodated at the Ruwi subduction zone. In other words, the UP-LP Discontinuity was transiently active between stalling of Ruwi subduction and complete transferal of convergence to the Eurasian side of Neo-Tethys during the latest Cretaceous.

The two-subduction-zone models with the inboard, intracontinental Ruwi subduction zone being the more prominent subduction zone is similar to the subduction-zone evolution in the Scandinavian Caledonides. Bender et al. (2018); (their Fig. 3) show two subduction zones for the late Ordovician and early Silurian: (1) Outboard oceanic subduction of Iapetus Ocean under Laurentia and (2) intracontinental subduction zone at the rifted, mafic-rock-bearing Baltica margin (Jakob et al., 2017). The Scandinavian Caledonides are known for their diamond-bearing ultrahigh-P rocks that formed in various nappes successively between 460 and 400 Ma (Hacker and Gans, 2005; Janák et al., 2013; Klonowska et al., 2014). These ultrahigh-P nappes formed when the rifted margin of Baltica was subducted along the inboard, intracontinental subduction zone. This example also demonstrates the importance of intracontinental subduction of a mafic-rock-rich rifted-margin architecture.

5.6. Suggested future work

In some respect, our work highlights problems with constraining and, thus, understanding the Cretaceous subduction-zone geometry at the Arabian convergent margin of Neo-Tethys. It appears self-evident to us that a one-subduction-zone scenario is not a sound option. We mentioned different geometries featuring two subduction zones and favour a platform evolution model similar to that proposed by Breton et al. (2004). We are convinced that a step forward for better constraining the subduction-zone dilemma would be detailed geochronologic studies as the timing of critical stages of the tectono-metamorphic evolution is not yet known well enough, which ultimately results in problems illustrating sound hypotheses/models.

We think that it does not help much to further constrain the timing of high-P metamorphism of the As Sifah eclogite, the age of metamorphic processes in the metamorphic sole or the crystallization of the magmatic rocks that eventually became the Samail Ophiolite. Instead, we suggest to focus geochronologic work on high-P metamorphism of the nappes above the As Sifah Nappe, and important ductile and brittle shear zones in the Saih Hatat window, as well as carbonate tectonites and gouge zones in the overriding plate. This may shed light on tempo-spatial aspects of metamorphism and deformation and may help to better define tectonic models for the subduction-zone history at the Arabian margin. This approach would also shed more light on displacement rates of the Samail Ophiolite. The 15 cm a^{-1} slip rate for initial movement of the Samail Ophiolite advocated by Hacker (1991) and Hacker et al. (1996, 1997) would need to be corroborated. Displacement rates for the overriding plate would more robustly constrain the timing of obduction of the Samail Ophiolite onto the Arabian continent.

The Yenkit shear zone is a long-lived shear zone in the upper Saih Hatat window. Its movement history needs to be better understood. Despite having six samples geochronologically analyzed, we are not yet able to decide whether the Yenkit shear zone moved continuously or was reactivated a number of times.

We infer deformation of the rocks of the Umar Subbasin and the Exotics at ~93 Ma. Although this view appears plausible, quantitative data, especially U—Pb dating of carbonate tectonites, are needed to corroborate this proposition.

The Hawasina nappes, especially those derived from the Hamrat Duru Subbasin, are understudied. Detailed tectonometamorphic and geochronologic work in these nappes would help to further elucidate the tempo-spatial deformation of the overriding-plate thrust wedge and whether or not there is evidence for early deformation in the Hawasina sediments associated with activity of the Yenkit shear zone. Such work may also help to improve constraining the position of the Ruwi subduction zone, i.e., was it inboard the Hamrat Duru Subbasin as sketched in Fig. 10?

6. Concluding remarks

Rb—Sr multimineral ages indicate two distinct clusters for waning high-P metamorphism in the mid (99–96 Ma) and late Cretaceous (80–76 Ma). Mid-Cretaceous metamorphism of the Ruwi Nappe and deformation in the Yenkit shear zone demand the existence of two subduction zones at the mid-Cretaceous Arabian margin. The Ruwi subduction zone likely formed as a result of an increase in Arabia-Eurasia convergence rates by 118 Ma. It was a long-lived, continental subduction zone, and the late Cretaceous high-P rocks formed within it. The Samail subduction zone produced the Samail Ophiolite and its metamorphic sole between 105 and 94 Ma, but no high-P rocks. Our work highlights the importance of continental subduction at the Ruwi subduction zone.

The exhumation of the Saih Hatat high-P rocks was a multistage process. The Ruwi Nappe was being accreted to the non-high-P overriding plate at a time when the underlying high-P rocks were underthrust. The highest-P rocks of the As Sifah Nappe were very rapidly exhumed in the footwall of the As Sheik normal shear zone, which was the only significant exhumation structure in the Saih Hatat window. Most of the Saih Hatat high-P rocks were only modestly exhumed during the Cretaceous orogeny, after which all high-P resided at depths of ~15–25 km and were exhumed to the Earth surface mainly by normal faulting during early Cenozoic rifting.

Declaration of competing interest

The authors declare that they have no known competing financial

interests or personal relationships that could have appeared to influence the work reported in this paper.

Data availability

additional data are located at https://doi.org/10.17045/sthlmuni.23735529

Acknowledgements

Funded by the Swedish Science Council (VR grant 2021-04075). We thank Sophia Harder for careful help with sample preparation. We acknowledge helpful comments by an anonymous reviewer and editor Yildirm Dilek. The supplementary data are located at https://doi.org/10.17045/sthlmuni.23735529.

Appendix A. Supplementary data

Supplementary data to this article can be found online at https://doi.org/10.1016/j.earscirev.2024.104711.

References

Abbasi, I.A., Hersi, O.S., Al-Harthy, A., 2014. Late Cretaceous Conglomerates of the Qahlah Formation, North Oman. In: Rollinson, H.R., Searle, M.P., Abbasi, I.A., Al-Lazki, A., Al Kindi, M.H. (Eds.), Tectonic Evolution of the Oman Mountains, Geol. Soc. London Spec. Publ, vol. 392, pp. 325–341.

Abdelmaksoud, A., Ali, M.Y., Searle, M.P., 2022. Tectono-stratigraphic evolution of the foreland fold-and- thrust belt of the United Arab Emirates. Tectonics 41. https://doi.org/10.1029/2022TC007470 e2022TC007470.

Abers, G.A., 2011. Subduction zones. In: Gupta, H.K. (Ed.), Encyclopedia of Solid Earth Geophysics. Encyclopedia of Earth Sciences Series. Springer, Dordrecht. https://doi.org/10.1007/978-90-481-8702-7_149.

Agard, P., Searle, M.P., Alsop, G.I., Dubacq, B., 2010. Crustal stacking and expulsion tectonics during continental subduction: P-T deformation constraints from Oman. Tectonics 29. https://doi.org/10.1029/2010TC002669. TC5018.

Aldega, L., Carminati, E., Scharf, A., Mattern, F., Al-Wardi, M., 2017. Estimating original thickness and extent of the Semail Ophiolite in the eastern Oman Mountains by paleothermal indicators. Mar. Pet. Geol. 84, 18–33.

Aldega, L., Carminati, E., Scharf, A., Mattern, F., 2021. Thermal maturity of the Hawasina units and origin of the Batinah Melange (Oman Mountains): insights from clay minerals. Mar. Pet. Geol. 133, 105316 https://doi.org/10.1016/j.marpetgeo.2021.105216.

Ambrose, T.K., et al., 2021. Burial, accretion, and exhumation of the metamorphic sole of the Oman-UAE ophiolite. Tectonics 40. https://doi.org/10.1029/2020TC006392 e2020TC006392.

Ampferer, O., 1906. Über das Bewegungsbild von Faltengebirgen. Jahrbuch K.K Geol. Reichsanstalt 56, 538–622.

Angiboust, S., Agard, P., Glodny, J., Omrani, J., Oncken, O., 2016. Zagros blueschists: Episodic underplating and long-lived cooling of a subduction zone. Earth Planet. Sci. Lett. 443, 48–58. https://doi.org/10.1016/j.epsl.2016. 03.017.

Bauer, H., Rogowitz, A., Grasemann, B., Decker, K., 2018. Intracrystalline deformation of calcite in the upper brittle crust. Geology 46, 375–378. https://doi.org/10.1130/G39990.1.

Béchennec, F., Beurrier, M., Hutin, O., Rabu, D., 1986. Explanatory notes to the geological map of Bahla, Sheet F 40-7A. Scale 1:100 000. Ministry of Petroleum and Minerals, Directorate of Minerals, Muscat.

Béchennec, F., Le Métour, J., Rabu, D., Bourdillon-de-Grissac, C., de Wever, P., Beurrier, M., Villey, M., 1990. The Hawasina Nappes; Stratigraphy, paleogeography and structural evolution of a fragment of the South-Tethyan passive continental margin. In: Robertson, A.H.F., Searle, M.P., Ries, A.C. (Eds.), The Geology and Tectonics of the Oman Region, 49, pp. 213–223. https://doi.org/10.1144/GSL.SP.1992.049.01.14.

Béchennec, F., Roger, J., Le Métour, J., Wyns, R., 1992. Geological Map of Seeb, Sheet NF40–03 1:250,000. Sultanat of Oman, Ministry of Petroleum and Minerals, Muscat.

Bender, H., Ring, U., Almqvist, B.S.G., Grasemann, B., Stephens, M.B., 2018. Metamorphic zonation by out- of-sequence thrusting at back-stepping subduction zones: Sequential accretion of the Caledonian internides, Central Sweden. Tectonics 37. https://doi.org/10.1029/2018TC005088.

Bernecker, M., 2007. Facies architecture of an isolated carbonate platform in the Hawasina Basin: the late Triassic Jebel Kawr of Oman. Palaeogeogr. Palaeoclimatol. Palaeoecol. 252, 270–280.

Beurrier, M., Béchennec, F., Rabu, D., Hutin, G., 1986. Geological map of Rustaq, Sheet NF40-3D, 1:100,000. Explanatory Notes. Sultanat of Oman, p. 69.

von Blanckenburg, F., Davies, J.H., 1995. Slab breakoff: a model for syncollisional magmatism and tectonics in the Alps. Tectonics 14, 120–131.

Blechschmidt, I., et al., 2004. Stratigraphic architecture of the northern Oman continental margin-Mesozoic Hamrat Duru Group, Hawasina complex, Oman. GeoArabia 9, 81–132.

Boote, D.R.D., Mou, D., Waite, R.I., 1990. Structural evolution of the Suneinah Foreland, Central Oman Mountains. In: Robertson, A.H.F., Searle, M.P., Poes, A.C. (Eds.), The Geology and Tectonics of the Oman Region, Geological Society Special Publication, vol. 49, pp. 397–418.

Breton, J.P., Béchennec, F., Le Métour, J., Moen-Maurel, L., Razin, P., 2004. Eoalpine (cretaceous) evolution of the Oman Tethyan continental margin: Insights from a structural field study in Jabal Akhdar (Oman Mountains). GeoArabia 9, 41–58.

Burg, J.-P., 2018. Geology of the onshore Makran accretionary wedge: Synthesis and tectonic interpretation. Earth Sci. Rev. 185, 1210–1231.

Burg, J.-P., Gerya, T.V., 2005. The role of viscous heating in Barrovian metamorphism of collisional orogens: thermomechanical models and application to the Lepontine Dome in the Central Alps. J. Metamorph. Geol. 23, 75–95.

Burke, K., 2011. Plate Tectonics, the Wilson Cycle, and Mantle Plumes: Geodynamics from the top. Annu. Rev. Earth Planet. Sci. 39, 1–29. https://doi.org/10.1146/annurev-earth-040809-152521.

Casey, J.F., Dewey, J.F., 1984. Initiation of subduction zones along transform and accreting plate boundaries, triple-junction evolution and fore-arc spreading centers implications for ophiolitic geology and obduction. Geol. Soc. Lond. Spec. Publ. 13, 269–290.

Chauvet, F., Dumont, T., Basile, C., 2009. Structures and timing of Permian rifting in the Central Oman Mountains (Saih Hatat). Tectonophysics 475, 563–574. https://doi.org/10.1016/j.tecto.2009.07.008.

Christensen, I., Mooney, W.D., 1995. Seismic velocity structure and composition of the continental crust: a global view. J. Geophys. Res. 100, 9761–9788.

Cowan, R.J., Searle, M.P., Waters, D.J., 2014. Structure of the metamorphic sole to the Oman ophiolite, Sumeini Window and Wadi Tayyin: implications for ophiolite obduction processes. Geol. Soc. 392, 155–175.

Davies, J.H., von Blanckenburg, F., 1995. Slab breakoff: a model of lithosphere detachment and its test in the magmatism and deformation of collisional orogens. Earth Planet. Sci. Lett. 129, 85–102.

Davis, D., Suppe, J., Dahlen, F.A., 1983. The Mechanics of Fold-and-Thrust Belts and Accretionary Wedges. J. Geophys. Res. 88, 1153–1172. https://doi.org/10.1029/JB088iB02p01153.

DeMets, C., Gordon, R.G., Argus, D.F., 2010. Geologically current plate motions. Geophys. J. Int. 181, 1–80.

Dewey, J.F., 1976a. Ophiolite obduction. Tectonophysics 31, 93–120.

Dewey, J.F., 1976b. Ancient plate margins: some observations. Tectonophysics 33, 379–385.

Dewey, J.F., Bird, J., 1971. Origin and Emplacement of the ophiolite suite: Appalachian ophiolites in Newfoundland. J. Geophys. Res. 76, 2120–2121. https://doi.org/10.1139/f70-24010.1029/jb076i014p03179.

Dietrich, D., Casey, M., 1989. A new tectonic model for the Helvetic nappes. In: Coward, M.P., Dietrich, D., Park, R.G. (Eds.), Alpine Tectonics Geological Society of London Special Publication, 45, pp. 47–63.

Dilek, Y., Furnes, H., 2011. Ophiolite genesis and global tectonics: Geochemical and tectonic fingerprinting of ancient oceanic lithosphere. Geol. Soc. Am. Bull. 123, 387–411.

Doré, T., Lundin, E., 2015. Hyperextended continental margins—Knowns and unkowns. Geology 43, 95–96. https://doi.org/10.1130/focus012015.1.

Duchène, S., Blichert-Toft, J., Luais, B., Télouk, P., Lardeaux, J.-M., Albarède, F., 1997. The Lu–Hf dating of garnets and the ages of the Alpine high-pressure metamorphism. Nature 387, 586–589.

Durney, D.W., Ramsay, J.G., 1973. Incremental strains measured by syntectonic crystal growth. In: Dejong, K., Scholten, R. (Eds.), Gravity and Tectonics. Wiley, New York.

El-Shazly, A.K., Coleman, R.G., 1990. Metamorphism in the Oman Mountains in relation to the Semail ophiolite emplacement. Geol. Soc. Spec. Publ. 49, 473–493. https://doi.org/10.1144/GSL.SP.1992.049.01.30.

El-Shazly, A.K., Lanphere, M.A., 1992. Two high pressure metamorphic events in NE Oman: Evi- dence from 40Ar/39Ar dating and petrological data. J. Geol. 100, 731–751. https://doi.org/10.1086/629625.

El-Shazly, A.K., Bröcker, M., Hacker, B., Calvert, A., 2001. Formation and exhumation of blueschists and eclogites from NE Oman: New perspectives from Rb–Sr and 40Ar/39Ar dating. J. Metamorph. Geol. 19, 233–248. https://doi.org/10.1046/j.1525-1314.2001.00309.x.

Faure, M., Shu, L., Wang, B., Charvet, J., Choulet, F., Monié, P., 2009. Intracontinental subduction: a possible mechanism for the early Palaeozoic Orogen of SE China. Terra Nova 21, 360–368.

Forbes, G.A., Jansen, H.S.M., Schreurs, J., Naft'Uman, S.T., 2010. Lexicon of Oman: Subsurface Stratigraphy: Reference Guide to the Stratigraphy of Oman's Hydrocarbon Basins. Gulf PetroLink.

Forke, H.C., Pöppelreiter, M., Aigner, T., Koehrer, B., Walz, L., Bendias, D., Haase, M., 2012. Integrated biostratigraphy of the Saiq Formation (Al Jabal al-Akhdar, Oman Mountains) and its implication for the regional correlation of Khuff time-equivalent deposits. GeoArabia 17, 230–234.

Fournier, M., Lepvrier, C., Razin, P., Jolivet, L., 2006. Late cretaceous to Paleogene post-obduction extension and subsequent Neogene compression in the Oman Mountains. GeoArabia 11, 17–40.

Freeman, S.R., Inger, S., Butler, R.W.H., Cliff, R.A., 1997. Dating deformation using Rb-Sr in white mica: Greenschist facies deformation ages from the Entrelor shear zone, Italian Alps. Tectonics 16, 57–76.

Gaina, C., van Hinsbergen, D.J.J., Spakman, W., 2015. Tectonic interactions between India and Arabia since the Jurassic reconstructed from marine geophysics, ophiolite geology, and seismic tomography. Tectonics 34. https://doi.org/10.1002/2014TC003780.

Gallagher, K., 1995. Evolving temperature histories from apatite fission-track data. Earth Planet. Sci. Lett. 136, 421–435.

Garber, J.M., et al., 2020. Petrochronology of Wadi Tayin metamorphic sole metasediment, with implications for the thermal and tectonic evolution of the Samail Ophiolite (Oman/ UAE). Tectonics 39. https://doi.org/10.1029/2020TC006135.

Garber, J.M., Rioux, M., Searle, M.P., Kylander-Clark, A.R.C., Hacker, B.R., Vervoort, J. D., et al., 2021. Dating continental subduction beneath the Samail Ophiolite: Garnet, zircon, and rutile petrochronology of the As Sifah eclogites, NE Oman. J. Geophys. Res. Solid Earth 126. https://doi.org/10.1029/2021JB022715 e2021JB022715.

Gerya, T.V., Stöckhert, B., Perchuk, A.L., 2002. Exhumation of high-pressure metamorphic rocks in a subduction channel: A numerical simulation. Tectonics 21, 6–1.

Ghent, E.D., Stout, M.Z., 1981. Metamorphism at the base of the Samail ophiolite, southeastern Oman Mountains. J. Geophys. Res. 86, 2557–2571.

Glennie, K.W., 2005. Geology of the Oman Mountains. Spriner, Berlin, Heidelberg, New York.

Glennie, K.W., Boeuf, M.G.A., Hughes-Clarke, M.W., Moody-Stuart, M., Pilaar, W.F.H., Reinhardt, B.M., 1974. Geology of the Oman Mountains, Verhandelingen Koninklijk Nederlands Geologisch Mijnbouwkundidg. Genootschap, Amsterdam.

Glodny, J., Ring, U., 2022. The Cycladic Blueschist Nappe of the Hellenic subduction orogen: Protracted high-pressure metamorphism, decompression and reimbrication of a diachronous nappe stack. Earth Sci. Rev. 224, 103883 https://doi.org/10.1016/j.earscirev.2021.103883.

Glodny, J., Ring, U., Kühn, A., Gleissner, P., Franz, G., 2005. Crystallization and very rapid exhumation of the youngest Alpine eclogites (Tauern Window, Eastern Alps) from Rb/Sr mineral assemblage analysis. Contrib. Mineral. Petrol. 149, 699–712.

Glodny, J., Kühn, A., Austrheim, H., 2008. Geochronology of fluid-induced eclogite and amphibolite facies metamorphic reactions in a subduction–collision system, Bergen Arcs, Norway. Contrib. Mineral. Petrol. 156 (1), 27–48.

Gnos, E., Peters, T., 1993. K-Ar ages of the metamorphic sole of the Semail ophiolite; implications for ophiolite cooling history. Contrib. Mineral. Petrol. 113, 325–332.

Goffé, B., Michard, A., Kienast, J.R., Le Mer, O., 1988. A case of obduction-related high-pressure, low-temperature metamorphism in upper crustal nappes, Arabian continental margin, Oman: P-T paths and kinematic interpretation. Tectonophysics 151, 363–386. https://doi.org/10.1016/0040-1951(88)90253-3.

Goscombe, B., Foster, D.A., Gray, D., Kelsey, D., Wade, B., 2020. Metamorphic response within different subduction–obduction settings preserved on the NE Arabian margin. Gondwana Res. 83, 298–371. https://doi.org/10.1016/j.gr.2020.02.002.

Gray, D.R., Miller, J.M.L., Gregory, R.T., 2005. Strain state and kinematic evolution of a fold-nappe beneath the Samail Ophiolite, Oman. J. Struct. Geol. 27, 1986–2007. https://doi.org/10.1016/j.jsg.2005.06.011.

Gregory, R.T., Gray, D.R., Miller, J.M., 1998. Tectonics of the Arabian margin associated with the formation and exhumation of high-pressure rocks, Sultanate of Oman. Tectonics 17, 657–670. https://doi.org/10.1029/98TC02206.

Grobe, A., von Hagke, C., Littke, R., et al., 2019. Tectono-thermal evoliution of Oman's passive contionental margin under the obducting Semail Ophiolite. A case study of Jebel Akhdar, Oman. Solid Earth 10, 149–175.

Guilmette, C., Smit, M.A., van Hinsbergen, D.J.J., et al., 2018. Forced subduction initiation recorded in the sole and crust of the Semail Ophiolite of Oman. Nat. Geosci. 11 https://doi.org/10.1038/s41561-018-0209-2.

Gürer, D., Granot, R., van Hinsbergen, D.J.J., 2022. Plate tectonic chain reaction revealed by noise in the Cretaceous Quiet Zone. Nat. Geosci. 15, 233–239.

Hacker, B.R., 1991. The role of deformation in the formation of metamorphic gradients: Ridge subduction beneath the Oman ophiolite. Tectonics 10, 455–473. https://doi.org/10.1029/90TC02779.

Hacker, B.R., Gans, P.B., 2005. Continental collisions and the creation of ultrahigh-pressure terranes: Petrology and thermochronology of nappes in the central Scandinavian Caledonides. Geol. Soc. Am. Bull. 117 (1), 117–134. https://doi.org/10.1130/B25549.1.

Hacker, B.R., Gnos, E., 1997. The conundrum of Samail: explaining the metamorphic history. Tectonophysics 279, 215–226. https://doi.org/10.1016/s0040-1951(97)00114-5.

Hacker, B.R., Mosenfelder, J.L., Gnos, E., 1996. Rapid emplacement of the Oman ophiolite: thermal and geochronologic constraints. Tectonics 15, 1230–1247. https://doi.org/10.1029/96TC01973.

Hacker, B.R., Mosenfelder, J.L., Gnos, E., 1997. Rapid ophiolite emplacement constrained by geochronology and thermal considerations. Tectonics 15, 1230–1247.

Halama, R., Glodny, J., Konrad-Schmolke, M., Sudo, M., 2018. Rb-Sr and in situ 40Ar/39Ar dating of exhumation-related shearing and fluid-induced recrystallization in the Sesia zone (Western Alps, Italy). Geosphere 14, 1425–1450.

Hansman, R.J., Ring, U., Thomson, S.N., Den Brok, B., 2017. Late Eocene uplift of the Al Hajar Mountains, Oman, supported by stratigraphy and low-temperature thermochronology. Tectonics 36, 3081–3109. https://doi.org/10.1002/2017TC004672.

Hansman, R.J., Albert, R., Gerdes, A., Ring, U., 2018. Absolute ages of multiple generations of brittle structures by U-Pb dating of calcite. Geology. https://doi.org/10.1130/G39822.1.

Hansman, R.J., et al., 2021. Structural architecture and late cretaceous exhumation history of the Saih Hatat Dome (Oman), a review based on existing data and semi-restorable cross-sections. Earth Sci. Rev. 217 https://doi.org/10.1016/j.earscirev.2021.103595.

Torsvik, T.H., Steinberger, B., Gurnis, M., Gaina, C., 2010. Plate tectonics and net lithosphere rotation over the past 150 My. Earth and Planetary Science Letters 291, 106–112.

Turcotte, D.L., Schubert, G., 2002. Geodynamics, second edition. Cambridge University Press, Cambridge, pp. 456–p.

van Hinsbergen, D.J., et al., 2015. Dynamics of intraoceanic subduction initiation: 2. Suprasubduction zone ophiolite formation and metamorphic sole exhumation in context of absolute plate motions. Geochem. Geophys. Geosyst. 16, 1771–1785.

van Hinsbergen, D.J.J., Maffione, M., Koornneef, L.M.T., Guilmette, C., 2019. Kinematic and paleomagnetic restoration of the Semail ophiolite (Oman) reveals subduction initiation along an ancient Neotethyan fracture zone. Earth Planet. Sci. Lett. 518, 183–196.

van Hinsbergen, D.J.J., Steinberger, B., Guilmette, C., Maffione, M., et al., 2021. A record of plume-induced plate rotation triggering subduction initiation. Nat. Geosci. 14, 626–630.

Holt, P.J., Allen, M.B., van Hunen, J., Bjørnseth, H.M., 2010. Lithospheric cooling and thickening as a basin forming mechanism. Tectonophysics. 495, 184–194.

Holtmann, R., et al., 2022. Cretaceous thermal evolution of the closing Neo-Tethyan realm revealed by multi-method petrochronology. Lithos 422-423, 106731.

Hyndman, R.D., Yamano, M., Oleskevich, D.A., 1997. The seismogenic zone of subduction thrust faults. Island Arc 6, 244–260.

Immenhauser, A., Van Der Kooij, B., Van Vliet, A., Schlager, W., Scott, R.W., 2001. An ocean-facing Aptian–Albian carbonate margin, Oman. Sedimentology 48, 1187–1207.

Inger, S., Cliff, R.A., 1994. Timing of metamorphism in the Tauern Window, Eastern Alps: Rb-Sr ages and fabric formation. J. Metamorph. Geol. 12, 695–707.

Jakob, J., Alsaif, M., Corfu, F., Andersen, T.B., 2017. Age and origin of thin discontinuous gneiss sheets in the distal domain of the magma-poor hyperextended pre-Caledonian margin of Baltica, southern Norway. J. Geol. Soc. Lond. 174, 557–571. https://doi.org/10.1144/jgs2016-049.

Janák, M., Van Roermund, H., Majka, J., Gee, D., 2013. UHP metamorphism recorded by kyanite-bearing eclogite in the Seve Nappe complex of northern Jämtland, Swedish Caledonides. Gondwana Res. 23, 865–879. https://doi.org/10.1016/j.gr.2012.06.012.

Jarrard, R.D., 1986. Relations among subduction parameters. Rev. Geophys. 24, 217–284.

Jaupart, C., Mareschal, J.-C., 2015. Heat flow and thermal structure of the lithosphere. Treat. Geophys. 6, 217–253.

Kelley, S., 2002. Excess argon in K–Ar and Ar–Ar geochronology. Chem. Geol. 188, 1–22. https://doi.org/10.1016/S0009-2541(02)00064-5.

Kiessling, W., Flügel, E., 2002. Paleoreefs—A database on Phanerozoic reefs. In: Kiessling, W., Flügel, E., Golomka, J. (Eds.), Phanerozoic Reef Patterns, SEPM Special Publication, vol. 72, pp. 77–92.

Klonowska, I., Majka, J., Janák, M., Gee, D.G., Ladenberger, A., 2014. Pressure–temperature evolution of a kyanite–garnet pelitic gneiss from Åreskutan: Evidence of ultra-high-pressure metamorphism of the Seve Nappe complex, west-central Jämtland, Swedish Caledonides. In: Corfu, F., Gasser, D., Chew, D.M. (Eds.), New Perspectives on the Caledonides of Scandinavia and Related Areas. Geological Society, London, pp. 321–336. Special Publication 390.

Koehrer, B., Zeller, M., Aigner, T., Pöppelreiter, M., Milroy, P., Forke, H., Al-Kindi, S., 2010. Facies and stratigraphic framework of a Khuff outcrop equivalent: Saiq and Mahil formations, Al Jabal al-Akhdar, Sultanate of Oman. GeoArabia 15, 91–156.

Kotowski, A.J., Cloos, M., Stockli, D.F., Bos Orent, E., 2021. Structural and thermal evolution of an infant subduction shear zone: Insights from sub-ophiolite metamorphic rocks recovered from Oman Drilling Project site BT-1B. J. Geophys. Res. Solid Earth 126. https://doi.org/10.1029/2021JB021702 e2021JB021702.

Lallemand, S., Arcay, D., 2021. Subduction initiation from the earliest stages to self-sustained subduction: Insights from the analysis of 70 Cenozoic sites. ESR 221, 103779.

Le Métour, J., De Gramont, X., Villey, M., 1986a. Geological Map of Quryat Sheet NF40-4D Scale 1:100,000. Directorate General of Minerals, Oman Ministry of Petroleum and Minerals, Muscat.

Le Métour, J., De Gramont, X., Villey, M., Beurrier, M., 1986b. Geological Map of Masqat Sheet NF40-4A Scale 1:100,000. Directorate General of Minerals, Oman Ministry of Petroleum and Minerals, Muscat.

Le Métour, J., Villey, M., De Gramont, X., 1986c. Geological Map of Masqat Sheet NF40-4A Scale 1:100,000 and Explanatory Notes. Directorate General of Minerals, Oman Ministry of Petroleum and Minerals, Muscat.

Liu, F.L., Gerdes, A., Xue, H.M., 2009. Differential subduction and exhumation of crustal slices in the Sulu HIGH-P-UHIGH-P metamorphic terrane: insights from mineral inclusions, trace elements, U-Pb and Lu-Hf isotope analyses of zircon in orthogneiss. J. Metamorph. Geol. 27, 805–825.

Lovelock, P., Potter, T.L., Walsworth Bell, E.B., Wiemer, W.M., 1981. Ordovician rocks in the Oman mountains: the Amdeh formation. Geol. Mijnb. 60, 487–495.

Mako, C.A., Caddick, M.J., 2018. Quantifying magnitudes of shear heating in metamorphic systems. Tectonophysics 744, 499–517.

Mann, A., Hanna, S.S., 1990. The tectonic evolution of pre-Permian rocks, Central and Southeastern Oman Mountains. Geol. Soc. Spec. Publ. 49, 307–325. https://doi.org/10.1144/GSL.SP.1992.049.01.19.

Mann, A., Hanna, S.S., Nolan, S.C., Mann, A., Hanna, S.S., 1990. The post-Campanian tectonic evolution of the central Oman Mountains: Tertiary extension of the eastern Arabian margin. Geological Society, London, Special Publications 49, 549–563.

Massonne, H.J., Opitz, J., Theye, T., Nasir, S., 2013. Evolution of a very deeply subducted metasediment from As Sifah, northeastern coast of Oman. Lithos 156–159, 171–185. https://doi.org/10.1016/j.lithos.2012.11.009.

Mattern, F., Scharf, A., 2018. Postobductional extension along and within the Frontal Range of the Eastern Oman Mountains. J. Asian Earth Sci. 154, 369–385. https://doi.org/10.1016/j.jseaes.2017.12.031.

Mattern, F., Scharf, A., Wang, P.-J., Callegari, I., Abbasi, I., Al-Wahaibi, S., Pracejus, B., Scharf, K., 2020. Deformation of the Cambro-Ordovician Amdeh Formation (members 1 and 2): Characteristics, Origins, and Stratigraphic significance (Wadi

Amdeh, Saih Hatat Dome, Oman Mountains). Geosciences 10, 1–23. https://doi.org/10.3390/geosciences10020048.
Mattern, F., Pracejus, B., Scharf, A., Frijia, G., Al-Salmani, M., 2022a. Microfacies and composition of ferruginous beds at the platform-foreland basin transition (late Albian to Turonian Natih Formation, Oman Mountains): forebulge dynamics and regional to global tectono-geochemical framework. Sediment. Geol. 429 https://doi.org/10.1016/j.sedgeo.2021.106074.
Mattern, F., Gallucio, L., Scharf, A., Frijia, G., Al-Salmani, M., Al-Mamari, Y., Pracejus, B., 2022b. The Ediacaran Hiyam Formation: a zoom through the diagenetic and structural complexity of the metamorphic Hi2 Member, Saih Hatat Dome, Oman Mountains. Mar. Pet. Geol. 147 https://doi.org/10.1016/j.marpetgeo.2022.106025.
Mattern, F., Scharf, A., Al-Sayigh, A.R., Al-Wahaibi, N., Gallucio, L., Frijia, G., Al-Salmani, M., 2023. Lagoonal Microfacies, Lithostratigraphy, Correlation and Shale Migration of the Basal Middle Eocene Seeb Formation (Rusayl Embayment, Sultanate of Oman) Geosciences 13. MDPI. https://doi.org/10.3390/geosciences13090254.
Métour, J., Villey, M., 1986. Geological Map of Masqat 1:100,00 Sheet NF40-41A with Explanatory Notes. Ministry of Petroleum and Mineral, Directorate General of Minerals, Muscat, Oman, p. 45.
Michard, A., Goffé, B., Saddiqi, O., Oberhänsli, R., Wendt, A., 1994. Late cretaceous exhumation of the Oman blueschists and eclogites: a two-stage process. Terra Nova 6, 404–413.
Miller, J.M., Gray, D.R., Gregory, R.T., 1998. Exhumation of high-pressure rocks in northeastern Oman. Geology 26, 235–238. https://doi.org/10.1130/0091-7613(1998)026<0235:EOHIGH-PRI>2.3.CO;2.
Miller, J.M., Gregory, R.T., Gray, D.R., Foster, D.A., 1999. Geological and geochronological constraints on the exhumation of a high-pressure metamorphic terrane, Oman. Geol. Soc. Lond. Spec. Publ. 154, 241–260. https://doi.org/10.1144/GSL.SP.1999.154.01.11.
Miller, J.M., Gray, D.R., Gregory, R.T., 2002. Geometry and significance of internal windows and regional isoclinal folds in northeast Saih Hatat, Sultanate of Oman. J. Struct. Geol. 24 (2), 359–386. https://doi.org/10.1016/S0191-8141(01)00061-X.
Minoux, L., Janjou, D., 1986. Explanatory Notes to the Geological Map of Ibri, Sheet NF 40-2F. In: Scale 1:100 000. Ministry of Petroleum and Minerals, Directorate of Minerals (BRGM), Orleans, France.
Montigny, R., Le Mer, O., Thuizat, R., Whitechi, H., 1988. K–Ar and 40Ar/39Ar study of metamorphic rocks associated with the Oman ophiolite: Tectonic implications. Tectonophysics 151, 345–362.
Morris, A., Meyer, M., Anderson, M.W., MacLeod, C.J., 2016. Clockwise rotation of the entire Oman ophiolite occurred in a suprasubduction zone setting. Geology 44, 1055–1058.
Müller, W., Mancktelow, N.S., Meier, M., 2000. Rb-Sr microchrons of synkinematic mica in mylonites: an example from the DAV fault of the Eastern Alps. Earth Planet. Sci. Lett. 180, 385–397.
Müller, R.D., Zahirovic, S., Williams, S.E., Cannon, J., Seton, M., Bower, D.J., Tetley, M. G., Heine, C., Le Breton, E., Liu, S., 2019. A global plate model including lithospheric deformation along major rifts and orogens since the Triassic. Tectonics 38. https://doi.org/10.1029/2018TC005462.
Nicolas, A., 1989. Structures of Ophiolites and Dynamics of Oceanic Lithosphere. Springer, Berlin.
Nikolaeva, K., Gerya, T.V., Marques, F.O., 2010. Subduction initiation at passive margins: Numerical modeling. J. Geophys. Res. 115, B03406. https://doi.org/10.1029/2009JB006549.
Nolan, S.C., Skelton, P.W., Clissold, B.P., Smewing, J.D., 1990. Maastrichtian to early tertiary stratigraphy and palaeogeography of the central and northern Oman Mountains. In: Robertson, A.H.F., Searle, M.P., Ries, A.C. (Eds.), The Geology and Tectonics of the Oman Region, Geological Society of London, Special Publications, 49, pp. 495–519. https://doi.org/10.1144/gsl. sp.1992.049.01.31.
Okamoto, K., Shinjoe, H., Katayama, I., Terada, K., Sano, Y., Johnson, S., 2004. SHRIMP U–Pb zircon dating of quartz-bearing eclogite from the Sanbagawa Belt, south- west Japan: implications for metamorphic evolution of subducted protolith. Terra Nova 16, 81–89.
Pacheco, J.F., Sykes, L.R., 1992. Seismic moment catalog of large shallow earthquakes, 1900 to 1989. Bull. Seismol. Soc. Am. 82, 1306–1349.
Peacock, S.M., 1990. Numerical simulation of metamorphic pressure–temperature– time paths and fluid production in subducting slabs. Tectonics 9, 1197–1211.
Penniston-Dorland, S.C., Kohn, M.J., Manning, C.E., 2015. The global range of subduction zone thermal structures from exhumed blueschists and eclogites: Rocks are hotter than models. Earth Planet. Sci. Lett. 428, 243–254.
Platt, J.P., Behr, W.M., 2011. Grainsize evolution in ductile shear zones: Implications for strain localization and the strength of the lithosphere. J. Struct. Geol. 33, 537–550.
Poupinet, G., Avouac, J.P., Jiang, M., Wei, S., Kissling, E., Herquel, G., Guilbert, J., Paul, A., Wittlinger, G., Su, H., Thomas, J.C., 2002. Intracontinental subduction and Paleozoic inheritance of the lithosphere suggested by a teleseismic experiment across the Chinese Tien Shan. Terra Nova 14, 18–24.
Rabu, D., Béchennec, F., Beurrier, M., Hutin, G., 1986. Geological Map of Nakhl Sheet NF40-3E Scale 1:100,000. Directorate General of Minerals, Oman Ministry of Petroleum and Minerals, Muscat.
Rabu, D., Nehlig, P., Roger, J., et al., 1993. Stratigraphy and structure of the Oman Mountains.Doc. B.R.G.M. 221, 1–122.
Ribeiro, B.V., Kirkland, C.L., Finch, M.A., Faleiros, F.M., Reddy, S.M., Rickard, W.D.A., Hartnady, M.I.H., 2023. Microstructures, geochemistry, and geochronology of mica fish: Review and advances. J. Struct. Geol. 175, 104947 https://doi.org/10.1016/j.jsg.2023.104947.
Ring, U., Kassem, O.M.K., 2007. The nappe rule: why does it work? J. Geol. Soc. Lond. 164, 1109–1112.
Ring, U., Layer, P.W., 2003. High-pressure metamorphism in the Aegean, eastern Mediterranean: Underplating and exhumation from the late cretaceous until the Miocene to recent above the retreating Hellenic subduction zone. Tectonics 22 (3), 1022. https://doi.org/10.1029/2001TC001350, 23p.
Ring, U., Brandon, M.T., Willett, S.D., Lister, G.S., 1999. Exhumation processes. Geol. Soc. Lond. Spec. Publ. 154, 1–27. https://doi.org/10.1144/GSL.SP.1999.154.01.01.
Ring, U., Glodny, J., Will, T., Thomson, S., 2010. The Hellenic subduction system: high-pressure metamorphism, exhumation, normal faulting, and large-scale extension. Annu. Rev. Earth Planet. Sci. 38, 45–76. https://doi.org/10.1146/annurev.earth.050708.170910.
Ring, U., Pantazides, H., Glodny, J., Skelton, A., 2020. Forced return flow deep in the subduction channel, Syros, Greece. Tectonics 39. https://doi.org/10.1029/2019TC005768.
Ring, U., Glondy, J., Scharf, A., Hansman, R., 2023. Some like it cold: the conudrum of Samail revisited. Tectonics 42. https://doi.org/10.1029/2022TC007531 e2022TC007531.
Rioux, M., et al., 2013. Tectonic development of the Samail ophiolite: High-precision U-Pb zircon geochronology and Sm-Nd isotopic constraints on crustal growth and emplacement. J. Geophys. Res. Solid Earth 118, 2085–2101. https://doi.org/10.1002/jgrb.50139.
Rioux, M., et al., 2016. Synchronous formation of the metamorphic sole and igneous crust of the Semail ophiolite: New constraints on the tectonic evolution during ophiolite formation from high-precision U–Pb zircon geochronology. Earth Planet. Sci. Lett. 451, 185–195.
Rioux, M., et al., 2021. High-precision U-Pb zircon dating of late magmatism in the Samail ophiolite: a record of subduction initiation. J. Geophys. Res. Solid Earth 126. https://doi.org/10.1029/2020JB020758 e2020JB020758.
Robertson, A.H.F., 1987. Upper cretaceous Multi formation: transition of a Mesozoic carbonate platform to a foreland basin in the Oman Mountains. Sedimentology 34, 1123–1142. https://doi.org/10.1111/j.1365-3091.1987.tb00596.x.
Rousseau, M., Dromart, G., Garcia, J.-P., Atrops, F., Guillocheau, F., 2005. Jurassic evolution of the Arabian carbonate platform edge in the Central Oman Mountains. J. Geol. Soc. Lond. 162, 349–362.
Rousseau, M., Dromart, G., Droste, H., Homewood, P., 2006. Stratigraphic organisation of the Jurassic sequence in Interior Oman, Arabian Peninsula. GeoArabia 11, 17–50.
Saddiqi, O., Michard, A., Goffe, B., Poupeau, G., Oberhänsli, R., 2006. Fission-track thermochronology of the Oman Mountains continental windows, and current problems of tectonic interpretation. Bull. Soc. Géol. France 177 (3), 127–134.
Scharf, A., Sudo, M., Pracejus, B., Mattern, F., Callegari, I., Bauer, W., Scharf, K., 2020. Late Lutetian (Eocene) mafic intrusion into shallow marine platform deposits north of the Oman Mountains (Rusayl Embayment) and its tectonic significance. J. Afr. Earth Sci. 170 https://doi.org/10.1016/j.jafrearsci.2020.103941.
Scharf, A., Mattern, F., Al-Wardi, M., Frijia, G., Moraetis, D., Pracejus, B., Bauer, W., Callegari, I., 2021. The geology and tectonics of the Jabal Akhdar and Saih Hatat domes, Oman Mountains. Geol. Soc. Lond. Mem. M54, 1–125. https://doi.org/10.1144/M54.
Searle, M.P., 2007. Structural geometry, style and timing of deformation in the Hawasina Window, Al Jabal al Akhdar and Saih Hatat culminations, Oman Mountains. Geoarabia 12, 311pp.
Searle, M.P., 2007. Structural geometry, style and timing of deformation in the Hawasina Window, Al Jabal al Akhdar and Saih Hatat culminations, Oman Mountains. Geoarabia 12, 311pp.
Searle, M., 2019. Geology of the Oman Mountains, Eastern Arabia. Tectonophysics. Searle, M. P. (2007). Structural geometry, style and timing of deformation in the Hawasina window, Al Jabal Al Akhdar and Saih Hatat culminations, Oman Mountains. GeoArabia 12, 99–130. https://doi.org/10.1016/0040-1951(77)90059-2.
Searle, M.P., Cox, J., 2002. Subduction zone metamorphism during formation and emplacement of the Semail ophiolite in the Oman Mountains. Geol. Mag. 139, 241–255.
Searle, M.P., Graham, G.M., 1982. "Oman Exotics" – Oceanic carbonate build-ups associated with the early stages of continental rifting. Geology 10, 43–49.
Searle, M.P., Malpas, J., 1980. Structure and metamorphism of rocks beneath the Semail ophiolite of Oman and their significance in ophiolite obduction. Trans. R. Soc. Edinb. Earth Sci. 71, 247–262. https://doi.org/10.1017/S0263593300013614.
Searle, M.P., Lippard, S.J., Smewing, J.D., Rex, D.C., 1980. Volcanic rocks beneath the Semail Ophiolite nappe in the northern Oman mountains and their significance in the Mesozoic evolution of Tethys. J. Geol. Soc. Lond. 137, 589–604. https://doi.org/10.1144/gsjgs.137.5.0589.
Searle, M.P., Waters, D.J., Martin, H.N., Rex, D.C., 1994. Structure and metamorphism of blueschist–eclogite facies rocks from the northeastern Oman Mountains. J. Geol. Soc. Lond. 151, 555–576. https://doi.org/10.1144/gsjgs.151.3.0555.
Searle, M.P., Warren, C.J., Waters, D.J., Parrish, R.R., 2003. Subduction zone polarity in the Oman mountains: implications for ophiolite emplacement. Geol. Soc. Spec. Publ. 218, 467–480. https://doi.org/10.1144/GSL.SP.2003.218.01.24.
Searle, M.P., Warren, C.J., Waters, D.J., Parrish, R.R., 2004. Structural evolution, metamorphism and restoration of the Arabian continental margin, Saih Hatat region, Oman Mountains. J. Struct. Geol. 26, 451–473. https://doi.org/10.1016/j.jsg.2003.08.005.
Searle, M., Rioux, M., Garber, J.M., 2022. One line on the map: a review of the geological history of the Semail Thrust, Oman-UAE mountains. J. Struct. Geol. 158, 104594.
Skelton, P.W., Nolan, S.C., Scott, R.W., 1990. The Maastrichtian transgression onto the northwestern flank of the Proto-Oman Mountains: sequences of rudist-bearing beach to open shelf facies. Geological Society, London, Special Publications 49, 521–547.
Soret, M., Bonnet, G., Agard, P., et al., 2022. Timescales of subduction initiation and evolution of subduction thermal regimes. Earth Planet. Sci. Lett. 584, 117521.

Stampfli, G.M., Borel, G., 2002. A plate tectonic model for the Paleozoic and Mesozoic constrained by dynamic plate boundaries and restored synthetic oceanic isochrons. Earth Planet. Sci. Lett. 196, 17–33.
Stern, R.J., 2018. The evolution of plate tectonics. Phil. Trans. R. Soc. A 376, 20170406. https://doi.org/10.1098/rsta.2017.0406.
Stern, R.J., Gerya, T., 2018. Subduction initiation in nature and models: a review. Tectonophysics. https://doi.org/10.1016/j.tecto.2017.10.014.
Stüwe, K., Schuster, R., 2010. Initiation of subduction in the Alps: continent or ocean? Geology 38, 175–178. https://doi.org/10.1130/G30528.1.
Tagami, T., Carter, A., Hurford, A.J., 1996. Natural long-term annealing of the zircon fission-track system in Vienna Basin deep borehole samples: constraints upon the partial annealing zone and closure temperature. Chem. Geol. 130, 147–157.
Takeshita, T., Imayama, T., Ando, M., Kimura, Y., Python, M., 2023. Pressure–temperature paths of tectonic blocks in mélange: Recording thermal evolution of a subduction channel at an initial stage of subduction. J. Metamorph. Geol. https://doi.org/10.1111/jmg.12718.
Tilton, G.R., Hopson, C.A., Wright, J.E., 1981. Uranium-lead isotopic ages of the Samail Ophiolite, Oman, with applications to Tethyan ocean ridge tectonics. J. Geophys. Res. Solid Earth 86, 2763–2775. https://doi.org/10.1029/JB086iB04p02763.
Vandeginste, V., John, C.M., Manning, C., 2013. Linking process, dimension, texture, and geochemistry in dolomite geobodies: a case study from Wadi Mistal (northern Oman). Am. Petrol. Geol. Bull. 97, 1181–1207.
Vandeginste, V., John, C.M., Becket, J., 2015. Diagenetic Geobodies: Fracture-controlled burial dolomite in outcrops from Northern Oman. SPE Reserv. Eval. Eng. 18, 84–93.
Villey, M., De Gramont, X., Le Métour, J., 1986a. Geological Map of Fanjah Sheet NF40-3F Scale 1:100,000. Directorate General of Minerals, Oman Ministry of Petroleum and Minerals, Muscat.
Villey, M., De Gramont, X., Le Métour, J., 1986b. Geological Map of Seeb Sheet NF40-3C Scale 1:100,000 and Explanatory Notes. Directorate General of Minerals, Oman Ministry of Petroleum and Minerals, Muscat.
Vitale Brovarone, A., Herwartz, D., 2013. Timing of high-P metamorphism in the Schistes Lustrés of Alpine Corsica: New Lu–Hf garnet and lawsonite ages. Lithos 172, 175–191.
Warburton, J., Burnhill, T.J., Graham, R.H., Isaac, K.P., 1990. The evolution of the Oman Mountains Foreland Basin. In: Robertson, A.H.F., Searle, M.P., Poes, A.C. (Eds.), The Geology and Tectonics of the Oman Region, 49. Geological Society Special Publication, pp. 419–427.
Warren, C.J., Waters, D.J., 2006. Oxidized eclogites and garnet-blueschists from Oman: P-T path modelling in the NCFMASHO system. J. Metamorph. Geol. 24, 783–802. https://doi.org/10.1111/j.1525-1314.2006.00668.x.
Warren, C.J., Parrish, R.R., Searle, M.P., Waters, D.J., 2003. Dating the subduction of the Arabian continental margin beneath the Semail Ophiolite, Oman. Geology 31, 889–892.
Warren, C.J., Parrish, R.R., Waters, D.J., Searle, M.P., 2005. Dating the geologic history of Oman's Semail Ophiolite: insights from U-Pb geochronology. Contrib. Mineral. Petrol. 150, 403–422.
Warren, C.J., Sherlock, S.C., Kelley, S.P., 2011. Interpreting high pressure phengite 40Ar/39Ar laserprobe ages: an example from Saih Hatat, NE Oman. Contrib. Mineral. Petrol. 161, 991–1009. https://doi.org/10.1007/s00410-010-0576-1.
Warren, C.J., Hanke, F., Kelley, S.P., 2012. When can muscovite 40Ar/39Ar dating constrain the timing of metamorphic exhumation? Chem. Geol. 291, 79–86.
Weidle, C., Wiesenberg, L., El-Sharkawy, A., Krüger, F., Scharf, A., Agard, P., Meier, T., 2022. A 3-D crustal shear wave velocity model and Moho map below the Semail Ophiolite, eastern Arabia. Geophys. J. Int. 231, 817–834. https://doi.org/10.1093/gji/ggac223.
Weidle, C., Wiesenberg, L., Scharf, A., Agard, P., El-Sharkawy, A., Krüger, F., Meier, T., 2023. Lithospheric evolution of eastern Arabia based on surface wave and receiver function analyses. Earth Planet. Sci. Lett. 611, 118145 https://doi.org/10.1016/j.epsl.2023.118145.
Wright, V.P., Burchette, T.P., 1996. Shallow-water carbonate environments. In: Reading, H.G. (Ed.), Sedimentary Environments: Processes, Facies and Stratigraphy, 3rd ed. Blackwell, pp. 325–394.
Yamato, P., Agard, P., Goffé, B., De Andrade, V., Vidal, O., Jolivet, L., 2007. New, high-precision P-T estimates for Oman blueschists: implications for obduction, nappe stacking and exhumation processes. J. Metamorph. Geol. 25, 657–682. https://doi.org/10.1111/j.1525-1314.2007.00722.x.